AD-A073 144 HONEYWELL ELECTRO-OPTICS CENTER LEXINGTON MA F/G 17/5
STUDY OF TEMPERATURE /MOISTURE RETRIEVAL CAPABILITIES OF DMSP /--ETC(U)
SEP 78 A S ZACHOR F19628-77-C-0184
UNCLASSIFIED 7809-4 AFGL-TR-78-0279 NL

1 OF 2
AD
A073144

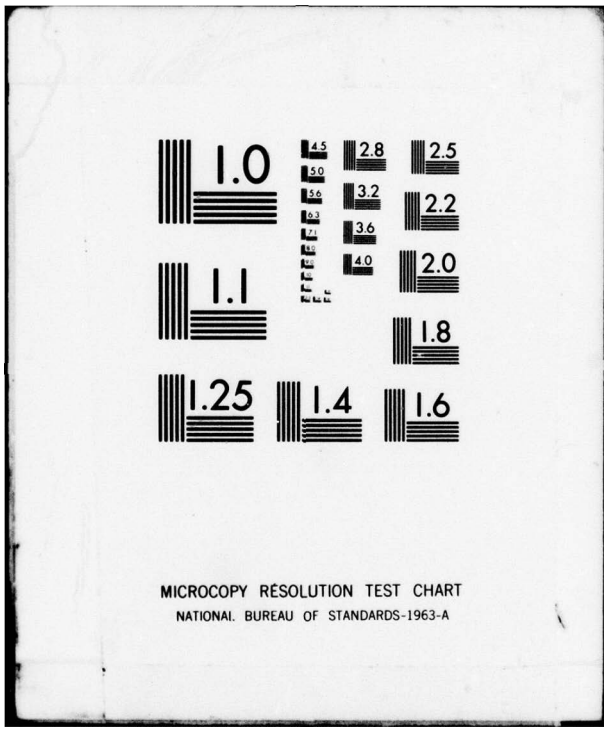
1.0
1.1
1.25
1.4
1.6
1.8
2.0
2.2
2.5
2.8
3.2
3.6
4.0
4.5
5.0
5.6
6.3
MICROCOPY RESOLUTION TEST CHART
NATIONAL BUREAU OF STANDARDS-1963-A

AFGL-TR-78-0279

LEVEL II

STUDY OF TEMPERATURE/MOISTURE RETRIEVAL CAPABILITIES OF DMSP/SSH SENSOR CHANNELS

Alexander S. Zachor

Honeywell
Electro-Optics Center
2 Forbes Road
Lexington, Massachusetts 02173

September 1978

Final Report
22 August 1977 to 22 August 1978

Approved for public release; distribution unlimited.

AIR FORCE GEOPHYSICS LABORATORY
AIR FORCE SYSTEMS COMMAND
UNITED STATES AIR FORCE
HANSCOM AFB, MASSACHUSETTS 01731

Unclassified

SECURITY CLASSIFICATION OF THIS PAGE (When Data Entered)

(19) REPORT DOCUMENTATION PAGE	READ INSTRUCTIONS BEFORE COMPLETING FORM
(18) 1. REPORT NUMBER: AFGL-TR-78-0279	2. GOVT ACCESSION NO. / 3. RECIPIENT'S CATALOG NUMBER
(6) 4. TITLE (and Subtitle): Study of Temperature/Moisture Retrieval Capabilities of DMSP/SSH Sensor Channels	5. TYPE OF REPORT & PERIOD COVERED: FINAL; Aug 22, 1977 to Aug 22, 1978
(14)	6. PERFORMING ORG. REPORT NUMBER: 7809-4
(10) 7. AUTHOR(s): Alexander S. Zachor	(15) 8. CONTRACT OR GRANT NUMBER(s): F19628-77-C-0184
9. PERFORMING ORGANIZATION NAME AND ADDRESS: HONEYWELL Electro-Optics Center, 2 Forbes Road, Lexington, MA 02173	10. PROGRAM ELEMENT, PROJECT, TASK AREA & WORK UNIT NUMBERS: 62101F (17) 99; (16) 767009AK
11. CONTROLLING OFFICE NAME AND ADDRESS: Air Force Geophysics Laboratory(OPI), Hanscom AFB, MA 02173, Contract Monitor: J.I.King (OPI) (11)	12. REPORT DATE: 25 Sept [redacted]978
	13. NUMBER OF PAGES: 143
14. MONITORING AGENCY NAME & ADDRESS(if different from Controlling Office) (12) 148 p.	15. SECURITY CLASS. (of this report): UNCLASSIFIED
	15a. DECLASSIFICATION/DOWNGRADING SCHEDULE

16. DISTRIBUTION STATEMENT (of this Report)

Approved for public release; distribution unlimited

17. DISTRIBUTION STATEMENT (of the abstract entered in Block 20, if different from Report)

(9) Final rept. 22 Aug 77 – 22 Aug 78

18. SUPPLEMENTARY NOTES

19. KEY WORDS (Continue on reverse side if necessary and identify by block number)

Infrared Remote Sensing, Temperature, Water Vapor, Temperature Retrievals, Water Vapor Retrievals

20. ABSTRACT (Continue on reverse side if necessary and identify by block number)

A number of retrieval algorithms were examined for efficacy in inferring atmospheric temperature and humidity structure from upwelling Earth-atmospheric radiances measured in the sensing bands of DMSP/SSH. Inversions of synthetic radiances for cloud-free conditions were performed to determine the limits on retrievable information. It is shown that the CO_2 channels yield fairly accurate temperature retrievals, especially when statistical data are used in constructing a guess profile and in regularizing the solutions. Maximum errors below the →next page

DD FORM 1 JAN 73 1473 EDITION OF 1 NOV 65 IS OBSOLETE

Unclassified

SECURITY CLASSIFICATION OF THIS PAGE (When Data Entered)

393776

70 mb pressure level are typically 3 to 4°C at middle-to-high latitudes, and 4 to 5°C in the tropics. The analysis used noise-free synthetic radiances, but regularization parameter values were assigned on the basis of measured DMSP noise-equivalent spectral radiances. The humidity retrieval capabilities of the six SSH H_2O channels are marginal because three of the channels are redundant, and because the channels are too strongly absorbing to infer low-level moisture except under moderately dry conditions. It was found that substitute "window" channels near 795 and 900/cm^{-1} are too opaque to provide an independent determination of total precipitable water, although they are probably good candidates as sounding channels to replace the redundant DMSP channels. Several other topics of investigation are suggested for potentially improving the humidity sensing capabilities of DMSP.

ACKNOWLEDGMENT

I am grateful to Jean King, Robert McClatchey and Vincent Falcone of the Air Force Geophysics Laboratory for their helpful suggestions. James Chetwynd of AFGL assisted in the utilization of AFGL computer codes, transmittance calculations and radiosonde data. Robin Williams of Honeywell coded the algorithms for temperature and moisture retrieval. Mary Corkery typed the final report.

TABLE OF CONTENTS

SECTION	TITLE	PAGE
1	**INTRODUCTION AND SUMMARY**	1
1.1	STUDY PLAN	2
2	**STUDY OF TEMPERATURE RETRIEVAL TECHNIQUES**	4
2.1	SELECTION OF RETRIEVAL TECHNIQUES	4
2.2	DEFINITION OF ALGORITHMS	6
	2.2.1 Direct Nonlinear Methods	6
	2.2.2 Linear, Inverse Methods	13
2.3	QUADRATURE GRID AND WEIGHTING FUNCTIONS	15
2.4	RESULTS OF TEMPERATURE RETRIEVALS BY THE NONSTATISTICAL, NONLINEAR METHODS	17
2.5	PROPERTIES OF THE C-MATRICES	32
2.6	COMPARISON OF TEMPERATURE RETRIEVALS BY FOUR CLASSES OF RETRIEVAL TECHNIQUE	47
	2.6.1 Artic Cases	48
	2.6.2 Midlatitude Cases	55
	2.6.3 Tropical Cases	55
	2.6.4 Relative Capabilities of the Retrieval Methods	74
3	**STUDY OF WATER VAPOR RETRIEVAL**	83
3.1	SELECTION AND DEFINITION OF ALGORITHMS	83
	3.1.1 Linear Inverse Methods	85
	3.1.2 Smith Iterative Technique	86
	3.1.3 Fleming Statistical Method	87
3.2	TRANSMISSION FUNCTIONS FOR THE DMSP WATER VAPOR CHANNELS	88
	3.2.1 Transmission Functions for Alternate Channels	94
3.3	C-MATRICES FOR H_2O RETRIEVAL	97
3.4	RESULTS OF H_2O RETRIEVALS	100
	3.4.1 Nature of Solutions for Tropical Cases (Minimum-Information Solution)	100
	3.4.2 Channel Redundancies	105
	3.4.3 Solutions Obtained by the Full-Statistics Method	108
	3.4.4 Effects of Temperature Retrieval Errors	115
3.5	INFORMATION RETRIEVABLE FROM WINDOW CHANNELS AT 795 cm^{-1} AND 900 cm^{-1}	118
4	**CONCLUSIONS AND RECOMMENDATIONS**	132
4.1	TEMPERATURE RETRIEVAL CAPABILITY	132
4.2	HUMIDITY RETRIEVAL CAPABILITY	133
4.3	RECOMMENDATIONS	135
APPENDIXES		
A	DERIVATION OF EQUATION 22	138
B	AVERAGE WEIGHTING FUNCTIONS FOR THE DMSP TEMPERATURE SENSING CHANNELS, AND EMPIRICAL FUNCTIONS $\tilde{\tau}(u_s)$, $\tilde{N}(u_s)$ FOR THE WINDOW CHANNELS AT 795 AND 900 cm^{-1}	140

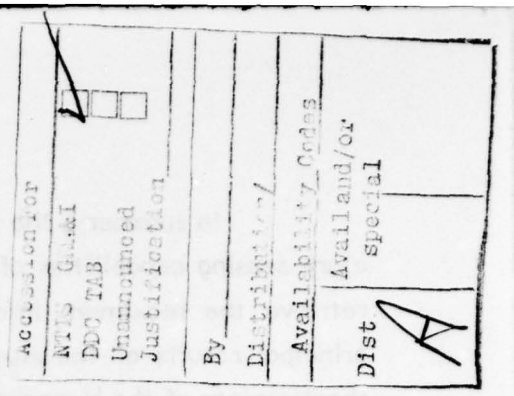

SECTION I
INTRODUCTION AND SUMMARY

This final report describes a study of mathematical algorithms for inferring atmospheric temperature and humidity structure from remotely-sensed radiances. The primary objectives were to determine the efficacy of these algorithms when applied to the sensing channels of the DMSP E– and H–packages, to select those which retrieve maximal information consistent with limitations set by instrument noise, and to implement the selected algorithms as computer codes suitable for inverting real DMSP data.

The study succeeded in defining the capabilities of the DMSP E– and H–packages, which proved to be quite good with respect to temperature retrieval, but marginal, at best, with respect to humidity retrieval.

Three of the six humidity channels were found to be redundant, and the remaining three too strongly absorbing to infer low-level moisture except for relatively dry atmospheres. Because of this outcome it was decided (with approval from the Contract Monitor) to de-emphasize some of the planned study tasks and adopt the additional task of determining how the humidity sensing performance could be improved by the addition of two window channels.

The added window channels (at 795 cm^{-1} and 900 cm^{-1}) were analyzed to determine their effectiveness in inferring the total water vapor column thickness of the atmosphere and the effective surface temperature. When the window channels are used in this way, the remaining three (non-redundant DMSP) humidity channels are required only to distribute the total water in altitude. It was found that the selected window channels are too opaque to accurately infer total water in most cases; consequently, the augmented set of five channels yielded no more information than the three non-redundant DMSP channels. However, it is likely that improved results can be obtained by incorporating these same channels as additional sounding channels, that is, by performing a simultaneous five-channel inversion, since the window channel weighting functions are large near the surface.

In summary, the study provides a comprehensive analysis of the remote temperature sensing capabilities of the DMSP E– and H–packages, and a computer code that will retrieve the maximum information available on vertical temperature structure. The principal results of the study relative to humidity retrieval are an identification of the shortcomings of the H–package, and suggested approaches to be followed in future research to improve the capabilities of DMSP. Some of the by–products of the study, for example the empirical transmittance functions developed for the DMSP humidity channels, are useful in themselves. Also, the comparisons of different temperature retrieval techniques, although based on inversions of synthetic DMSP band radiances, are applicable in a qualitative sense to all remote vertical temperature sounders.

1.1 STUDY PLAN

A plan of study was adopted early in the contract, which defined the specific tasks to be performed, the basis of selection of candidate retrieval algorithms, and the key questions to be addressed in evaluations of the candidate algorithms. The plan, in some respects, was more ambitious than the contract work statement, and was not followed in every detail. However, it is worth presenting the plan because it defines the scope of the study, the context of discussions in the following sections, and the motivation for some of analyses and comparisons.

Table 1 lists the planned major tasks of the study. The purpose of the first two tasks is to identify a 2–by–2 matrix of specific candidate algorithms judged to be the best representatives of linear and nonlinear methods, used with and without a priori statistical data. The two algorithms in the "statistical" class use empirical covariances to regularize (stabilize) the retrieval solutions; statistical regression methods were excluded from consideration. Tasks 3 and 4 compare the capabilities of the four candidates, as demonstrated in inversions of synthetic radiances, and select the "best" one as the recommended procedure.

The questions addressed in evaluating and comparing the candidate retrieval techniques are listed in Table 2. All of the questions applicable to temperature inversions were answered, except the one dealing with instrument noise. That is, we did not add pseudo–random noise values to the synthetic radiances used in the retrievals, although we chose values for regularization parameters which should effectively damp any instabilities

resulting from the noise equivalent radiances of the DMSP channels. In studying the H_2O retrieval capabilities of DMSP-H and the two window channels, we addressed parts of the first four questions, but the answers obtained are mostly qualitative.

Table 1 MAJOR TASKS OF DMSP RETRIEVAL ANALYSIS PROGRAM

1.	Comprehensive Testing of Known Retrieval Techniques Applied to SSH Temperature and Humidity Channels
2.	Selection of "Best" Technique in Each Class of Retrieval Method
3.	Simulation of Retrievals via "Best" Techniques, to Obtain Statistical Measures of Accuracy and Information Content
4.	Definition of Recommended Procedure for SSH Retrieval of Temperature and Humidity Profiles
5.	Coding of Recommended Retrieval Algorithms

Table 2 QUESTIONS ADDRESSED IN THE STUDY OF SPECIFIC RETRIEVAL ALGORITHMS

1.	Overall Accuracy
2.	Maximum Achievable Resolution in Vertical Structure (Temperature and Humidity)
3.	Dependence of Solutions of Initial Guesses
	- Magnitude, Variance and Shape of Residuals
4.	Effects of Statistical Constraints (Covariances)
	- Effects of Using "Bad" Statistics
5.	Effects of Noise
6.	Optimal Method for Selecting Guess Humidity Profile
	- Effects of Using Statistics

SECTION 2
STUDY OF TEMPERATURE RETRIEVAL TECHNIQUES

2.1 SELECTION OF RETRIEVAL TECHNIQUES

We initially selected ten candidate techniques to be studied with respect to temperature retrieval. These are listed in Table 3. Note that the techniques are grouped into four classes, according to whether they are linear or nonlinear, and whether or not they use statistical data in the regularization of solutions. Each class is represented by one technique except the nonlinear, nonstatistical class. The study first examined the nonlinear, nonstatistical methods except the one due to King, since it was being studied independently by Dr. King at AFGL. After extensive retrievals of synthetic radiances, we selected the "best" of these methods, which reduced the number of candidates to four; i.e., one in each class. The procedure was then repeated to determine the "best" of the four.

J. I. F. King's nonlinear technique[5] obtains an inverse solution of the radiative transfer equation. With this exception the selected nonlinear techniques are direct methods: they solve the radiative transfer equation in the forward direction, initially for a guess profile, then iteratively for revised guesses determined by differences between the computed and measured radiances. The direct methods differ from each other only in the relaxation formulas used to revise the temperature profile at each stage of iteration. We regard the Chow method as a generalized and improved version of the well-known Chahine method, which is why the latter is not listed as one of the selected methods.

The linear methods use inverse solutions. These are generally regularized least-squares solutions of an equation set consisting of a linearized form of the radiative transfer equation written out for each of the sounding channels. The names in the last column of Table 3 identify two well-known matrix solutions: the "minimum-information" solution obtained by Foster[6] and independently by Twomey[7], and the more general statistical form derived in different fashions by Foster[6], by Strand and Westwater[8], and by Rodgers[9]. These formal solutions, however, can be implemented in different ways. Usually one solves for a highly over-specified temperature profile (defined at many more levels than these are

Table 3 RETRIEVAL TECHNIQUES TO BE COMPARED

	NONLINEAR	LINEAR, INVERSE
NON-STATISTICAL	**Direct** SMITH[1] CHOW[2] FLEMING[3] <- - - (ANALOGS) - - -> NEW (MODIFIED TWOMEY[4]) AND VARIANTS (2) **Inverse** KING[5]	**Regularized Least-Squares** FOSTER[6], TWOMEY[7]
STATISTICAL	**Direct** FLEMING STATISTICAL[3] <- - - - - ->	**Statistically-Regularized Least-Squares** FOSTER[6], STRAND & WESTWATER[8]

spectral bands) or for the coefficients in an expansion of the temperature (Planck function) profile in empirical orthogonal functions; both techniques avoid preselection of pressure levels, which would restrict the form of the retrieved profiles. One also can choose among several methods of linearizing the radiative transfer equation, and whether or not to represent the transfer equation in perturbation form (use the method with iteration). Details of how the two linear retrieval methods were implemented are given below.

Note that the two nonlinear methods attributed to H. E. Fleming in Table 3 are identified as analogs of the two selected linear methods. The Fleming methods use linear relaxation equations derived from the requirement that the mean-square error in Planck function change (as prescribed by the relaxation formula) be a minimum. As a result, the relaxation formulae are simple algebraic analogs of the corresponding matrix solutions of the linear methods; this mathematical relationship is noted on page 14.

2.2 DEFINITION OF ALGORITHMS

2.2.1 Direct Nonlinear Methods

The direct nonlinear methods start with a guess temperature profile which is used to compute corresponding Planck radiance profiles B_{ij}, where i denotes the spectral channel and j the atmospheric pressure level. The radiative transfer equation in quadrature form,

$$I_i = \sum_{j=1}^{J} B_{ij} W_{ij}; \quad i = 1, 2, \ldots M,$$

is used to obtain the radiances I_i corresponding to the guess profile. In the present study, M is equal to 6, but J can be as large as desired. In our retrieval simulations, the atmospheric temperature is defined at 100 levels; the value j = J = 101 corresponds to the boundary term of the radiative transfer equation (the surface temperature).

In the selected direct nonlinear methods, either the difference

$$\Delta I_i \equiv I_i \text{ (meas)} - I_i$$

between the measured and computed radiances, or their ratio

$$R_i \equiv I_i\,(\text{meas})/I_i$$

is substituted into a relaxation equation to obtain an adjustment ΔB_{ij} to the computed Planck radiance profiles B_{ij}. This gives M new Planck radiance profiles, one for each value of i.

The next step in the procedure is to apply the inverse of Planck's equation to the revised radiance profiles to obtain M corresponding temperature profiles. Finally, the M different temperature profiles are averaged in some fashion to obtain a single temperature profile. This profile replaces the initial guess, and the entire procedure is repeated until an appropriate convergence criterion is satisfied.

The following is a summary of the different relaxation equations used by the selected methods, and their origins. The simplest formula, due to Smith[1],

$$\Delta B_{ij} = \Delta I_i, \tag{1}$$

increments the Planck radiances equally at all altitudes. Twomey[4] proposed a general relaxation formula for directly solving the linear Fredholm equation; if we modify it to deal with the radiative transfer equation in its actual nonlinear form, the result is

$$\Delta B_{ij} = \frac{W_{ij}}{\max_j [W_{ij}]} \frac{\Delta I_i}{I_i} B_{ij} \tag{2}$$

where the first factor in the right hand side is the usual weighting function W_{ij} normalized to its maximum value. Fleming's "new nonlinear" technique[3] uses the formula

$$\Delta B_{ij} = \frac{W_{ij}}{\sum_{j=1}^{J} W_{ij}^2 + \alpha} \Delta I_i; \qquad \alpha = \text{constant} \tag{3}$$

which is the result of requiring a linear relaxation equation that minimizes the mean-square error in ΔB_{ij}, and making simplifying assumptions about the statistics of the atmospheric

temperature profile (the same ones leading to Foster's minimum information solution). The Chow method uses the formula

$$\Delta B_{ij} = (R_i^K - 1)\, B_{ij}; \qquad K = \text{constant} \tag{4}$$

For K = 1, this reduces to the simplest ratio-type (Chahine-type) relaxation formula

$$\frac{B_{ij} + \Delta B_{ij}}{B_{ij}} = R_i. \tag{4a}$$

However, in the Chahine method each j (level) is associated with a particular i (channel), and the number of levels equals the number of channels.

The Smith, Fleming and Chow nonlinear methods all prescribe Smith's temperature profile averaging scheme:

$$T_j = \sum_{i=1}^{M} T_{ij} W_{ij} \Big/ \sum_{i=1}^{M} W_{ij}, \tag{5}$$

where T_{ij} are the temperature profiles obtained by solving the inverse Planck equation for the new radiance profile estimates B_{ij}. It seemed reasonable, therefore, to use the same scheme in the method adapted from Twomey[4]. Note that approximating the radiative transfer equation by a linear Fredholm equation is symbolically equivalent to replacing B_{ij} by a function b_j which depends only on j; i.e., the case treated by Twomey does not require averaging over the spectral channels.

Note that both the Fleming method and our modified Twomey method (Equations 3 and 2), prescribe a ΔB_{ij} which has the same vertical distribution as the weighting function W_{ij}. This would seem to be a desirable feature, since according to the radiative transfer equation the desired ΔB_{ij} information contained in a change ΔI is distributed as W_{ij}. That is, we should vary B more at altitudes where a unit change will produce a large change in computed radiance, than at altitudes where a unit change would have a relatively

small effect on I. However, if this weighting is used in the relaxation equation, should it be used again in the averaging formula? It is conceivable that this "double-weighting" will produce undesirable biases in the retrieved temperature profile. Hence, we chose to also study the effects of using the alternate (unweighted) temperature average

$$T_j' = \frac{1}{M} \sum_{i=1}^{M} T_{ij} \qquad (6)$$

with the Fleming and modified Twomey methods.

Table 4 lists the combinations of relaxation and averaging formulas used in studying the direct, nonlinear, nonstatistical techniques.

Table 4 ALGORITHMS FOR THE DIRECT NONLINEAR, NONSTATISTICAL METHODS

NAME	GRAPHICS SYMBOL	RELAXATION FORMULA	AVERAGING FORMULA
SMITH	SMH	Eq. 1	Eq. 5
TWOMEY-LIKE	TWM	Eq. 2	Eq. 5
ALTERNATE TWOMEY-LIKE	TW2	Eq. 2	Eq. 6
FLEMING NEW NONLINEAR	FLM	Eq. 3	Eq. 5
NEW	NEW	Eq. 3	Eq. 6
CHOW	CHW	Eq. 4	Eq. 5

It is interesting to note that Fleming's result (Eq. 3) without the parameter α can be derived in a very simple manner: Apply the identity

$$\Delta B_{ij} W_{ij} = \left(\frac{\Delta B_{ij}}{W_{ij}}\right) W_{ij}^2$$

to the radiative transfer equation in quadrature-perturbation form, and require that the factor $\Delta B_{ij}/W_{ij}$ equal a constant. The transfer equation is then identical to Equation 3 with $\alpha = 0$. In fact, it is questionable whether a non-zero value of α (which has exactly the same meaning as the single regularization parameter in Foster's minimum information solution) is required, since it is generally not necessary to regularize the direct nonlinear methods. They are inherently more stable because they are direct and also because the temperature averaging operation tends to reduce the effects of noise.

2.2.1.1 **Statistical Direct Nonlinear Method (Fleming Statistical)**

We include a derivation of the relaxation formula for this case, since we do not know if one exists in the literature. The method seeks a linear formula

$$\Delta B_{ij} = C_{ij}\, \Delta I_i; \quad i = 1, 2, \ldots M; \quad j = 1, 2, \ldots J \tag{7}$$

giving the least-squares best fit to an ensemble of data $\Delta B_{ijk} = B_{ijk} - \langle B_{ij} \rangle$ and $\Delta I_{ik} = I_{ik} - \langle I_i \rangle$. These represent a set of actual (in situ, measured) Planck function profiles and the corresponding computed or measured upwelling radiances; k denotes the ensemble members and $\langle\ \rangle$ a mean over the ensemble. Hence, it is required to find the matrix C which minimizes the error

$$\xi\,(C) = \sum_{k=1}^{K} (\Delta B_{ijk} - C_{ij}\, \Delta I_{ik})^2 \tag{8}$$

Differentiating ξ with respect to the matrix element C_{ij} and setting the result equal to zero gives

$$\sum_{k=1}^{K} 2\Delta I_{ik}\, (\Delta B_{ijk} - C_{ij}\, \Delta I_{ik}) = 0 \tag{9}$$

or

$$C_{ij} = \sum_{k=1}^{K} \Delta B_{ijk} \, \Delta I_{ik} \Big/ \sum_{k=1}^{K} (\Delta I_{ik})^2. \qquad (10)$$

The ΔI's and ΔB's are related by the radiative transfer equation. If we acknowledge that the I_{ik} contain random noise E_{ik}, the relationship is

$$\Delta I_{ik} = \sum_{n=1}^{J} W_{in} \, \Delta B_{ink} + E_{ik} \qquad (11)$$

Substitution of Equation 11 into the denominator of Equation 10 gives

$$\begin{aligned} \sum_{k=1}^{K} (\Delta I_{ik})^2 &= \sum_{j=1}^{J} W_{ij} \sum_{n=1}^{J} W_{in} \sum_{k=1}^{K} \Delta B_{ijk} \, \Delta B_{ink} + \sum_{k=1}^{K} E_{ik}^{\,2} \\ &= K \sum_{j=1}^{J} W_{ij} \sum_{n=1}^{J} S_{ijn} \, W_{in} + K \sigma_{E_i}^{\,2} \end{aligned} \qquad (12)$$

where S_{ijn} denotes, for channel i, the covariance of the vertical Planck radiance profile, and $\sigma_{E_i}^{\,2}$ the mean-square noise in channel i. We have assumed no correlation between the noise and the Planck radiance deviations for any channel. Similarly, substitution of Equation 11 into the numerator of Equation 10 gives

$$\sum_{k=1}^{K} \Delta B_{ijk} \, \Delta I_{ik} = K \sum_{n=1}^{J} S_{ijn} \, W_{in} \qquad (13)$$

assuming the noise has zero mean. From Equations 7, 10, 12, and 13, the relaxation formula is

$$\Delta B_{ij} = \Delta I_i \left[\frac{\sum_{n=1}^{J} S_{ijn} W_{in}}{\sum_{j=1}^{J} W_{ij} \sum_{n=1}^{J} S_{ijn} W_{in} + \sigma_{E_i}^2} \right] \qquad (14)$$

Fleming proposed to use this equation together with Smith's channel averaging scheme.

Note that the Fleming statistical relaxation formula revises B_{ij} at a particular frequency i and level j according to the weights W for <u>all levels</u>, but the weight for level n is scaled in proportion to the expected correlation between ΔB_{in} and ΔB_{ij}. This will tend to introduce expected structural features to the retrieved profiles, which tends to increase their average accuracy while sacrificing the ability to recover unusual or anomalous profiles; of course, this statement needs to be quantified.

If we have no knowledge of temperature correlations or the vertical distribution of Planck function variance (or choose to reject the use of a priori information) then the matrix S_{ijk} becomes the identity matrix times $\sigma_{B_i}^2$, the variance of B_{ij}. Then Equation 14 reduces to Equation 3 with

$$\alpha = \sigma_{E_i}^2 / \sigma_{B_i}^2, \qquad (15)$$

which may be called the ratio of noise to "signal" power. This is the minimum information case, analogous to Foster's minimum information linear inverse solution.

2.2.2 Linear, Inverse Methods

The linear methods require that we first put the radiative transfer equation

$$I(\nu) = B\ [T(p_o)]\ \tau_\nu(p_o) - \int_0^{p_o} B_\nu [T(p)] \frac{d\tau_\nu(p)}{dx(p)}\ dx(p) \qquad (16)$$

into a linear form; here B_ν denotes Planck's function, T(p) the temperature profile, $\tau_\nu(p)$ the transmittance of the atmosphere above level p, and x is any convenient single-valued function of pressure. We will use the linearization scheme suggested by Smith, Woolf and Fleming[10]. In this method, the measured radiances I(ν) are used to find their equivalents at a single reference frequency $\nu = r$ through the operations

$$\begin{aligned} T_B(\nu) &= B_\nu^{-1}\ [I(\nu)], \\ I_r(\nu) &= B_r\ [T_B(\nu)], \end{aligned} \qquad (17)$$

i.e., we convert the measured radiances to brightness temperatures via the inverse Planck equation, and then from the brightness temperatures determine the corresponding radiances at $\nu = r$. (The reference frequency should be near the median frequency of the sounding channels.) An approximate radiative transfer equation is obtained by writing (17) for the reference frequency (except that the τ_ν's are unchanged):

$$I_r(\nu) \simeq B_r\ [T(p_o)]\ \tau_\nu(p_o) - \int_0^{p_o} B_r [T(p)] \frac{d\tau_\nu(p)}{dx(p)}\ dx(p) \qquad (18)$$

which is linear in $B_r\ [T(p)]$. (In fact, it is a linear Fredholm equation.) Once we solve for $B_r\ [T(p)]$ it is a simple matter to obtain the temperature profile.

Fleming[3] has shown that spectral radiance errors resulting from the linearization (17) is typically less than 0.3 percent over the spectral range 668 cm^{-1} to 747 cm^{-1}.

Writing Equation 18 in quadrature-perturbation form we obtain

$$\Delta I_r(\nu_i) = \sum_{j=1}^{J} W_{ij} (\Delta B_r)_j; \quad i = 1, 2, \ldots M, \tag{19}$$

which in matrix notation is

$$\underset{\sim}{\Delta I}_r = W \underset{\sim}{\Delta B}_r. \tag{20}$$

Solutions of this equation are non-unique, if J > M, and are also unstable because of the ill-conditioned nature of the weighting function matrix W. A regularized solution of the form

$$\underset{\sim}{\Delta B}_r = C \underset{\sim}{\Delta I}_r \tag{21}$$

may be obtained by requiring that Equation 21 represent a least-squares best fit to an ensemble of data, and acknowledging that the measurement vector components ΔI_{r_i} contain noise E_i. The least-squares minimization procedure (determination of C) is completely analogous to the derivation of Equation 14, and leads to the well-known matrix solution

$$\underset{\sim}{\Delta B}_r = SW^T \left[WSW^T + S_E \right]^{-1} \underset{\sim}{\Delta I}_r \tag{22}$$

where S is the covariance of $\underset{\sim}{B}_r$, and S_E is the M by M noise covariance matrix, or, if the channel noises are uncorrelated, the diagonal matrix of mean-square channel noise values; $(\ )^T$ and $(\ )^{-1}$ denote matrix transpose and inverse, respectively. Equation 22 is derived in Appendix A.

Not surprisingly, there is close similarity between Equation 22 and Equation 14, the relaxation formula for the Fleming statistical method. In fact, if we truncate $\underset{\sim}{\Delta I}_r$ to a single component ΔI_m, replace S by the matrix with components S_{mjk}, and envision W as a row vector of components W_{mj}, the two results are identical expressions for ΔB_{mj}; that is, Equation 22 becomes a relaxation formula suitable in a direct nonlinear retrieval method.

The minimum information equivalent of Equation 22 is obtained by assuming there is no correlation between temperatures at different levels, and that the reference-frequency Planck function variance is constant with altitude; i.e., $S = \sigma_{B_r}^2 I$, where I is the identity matrix. If we also assume equal mean square noise σ_E^2 in the different sounding channels, the Foster minimum information solution is

$$\underset{\sim}{\Delta B}_r = W^T \left[WW^T + \alpha I \right]^{-1} \underset{\sim}{\Delta I}_r; \quad \alpha = \sigma_E^2 / \sigma_{B_r}^2 \tag{23}$$

Equation 23 has the same analogy to Equation 3 as Equation 22 has to Equation 14.

In the present study, Equations 22 and 23 are used to obtain highly over-specified retrieval solutions; that is $\underset{\sim}{\Delta B}_r$ is a vector of 101 components, S is a 101 by 101 matrix, W is 6 by 101, and the matrix

$$C \equiv SW^T \left[WSW^T + S_E \right]^{-1} \tag{24}$$

is 101 by 6. The selected reference frequency is 707 cm^{-1}, representing the fourth sounding channel. The corresponding S matrix is a subset of the data S_{ijk} required by the Fleming statistical method, since we also use 101-point solutions in its evaluation.

2.3 GRADRATURE GRID AND WEIGHTING FUNCTIONS

The 101-point grid that we are using to represent the temperature profile and to integrate the radiative transfer equation corresponds to 100 atmospheric pressure levels spaced equally in $p^{2/7}$, and to the surface temperature. The weighting functions W_{ij} were determined using McClatchey's[11] computed transmittance profiles. We interpolated these to the 100 atmospheric levels and then averaged over the nine different sets provided by McClatchey (representing nine different temperature profiles) to insure that the weighting functions would not have any noticeable slope discontinuities. In this study the weights are assumed invariant with atmospheric temperature.

Figure 1 shows our weighting functions presented in the conventional form, pressure versus $-d\tau_\nu / d \log p$. (In our computations, the weights are defined as transmittance change between successive gradrature grid points; these are given in tabular form in Appendix B.)

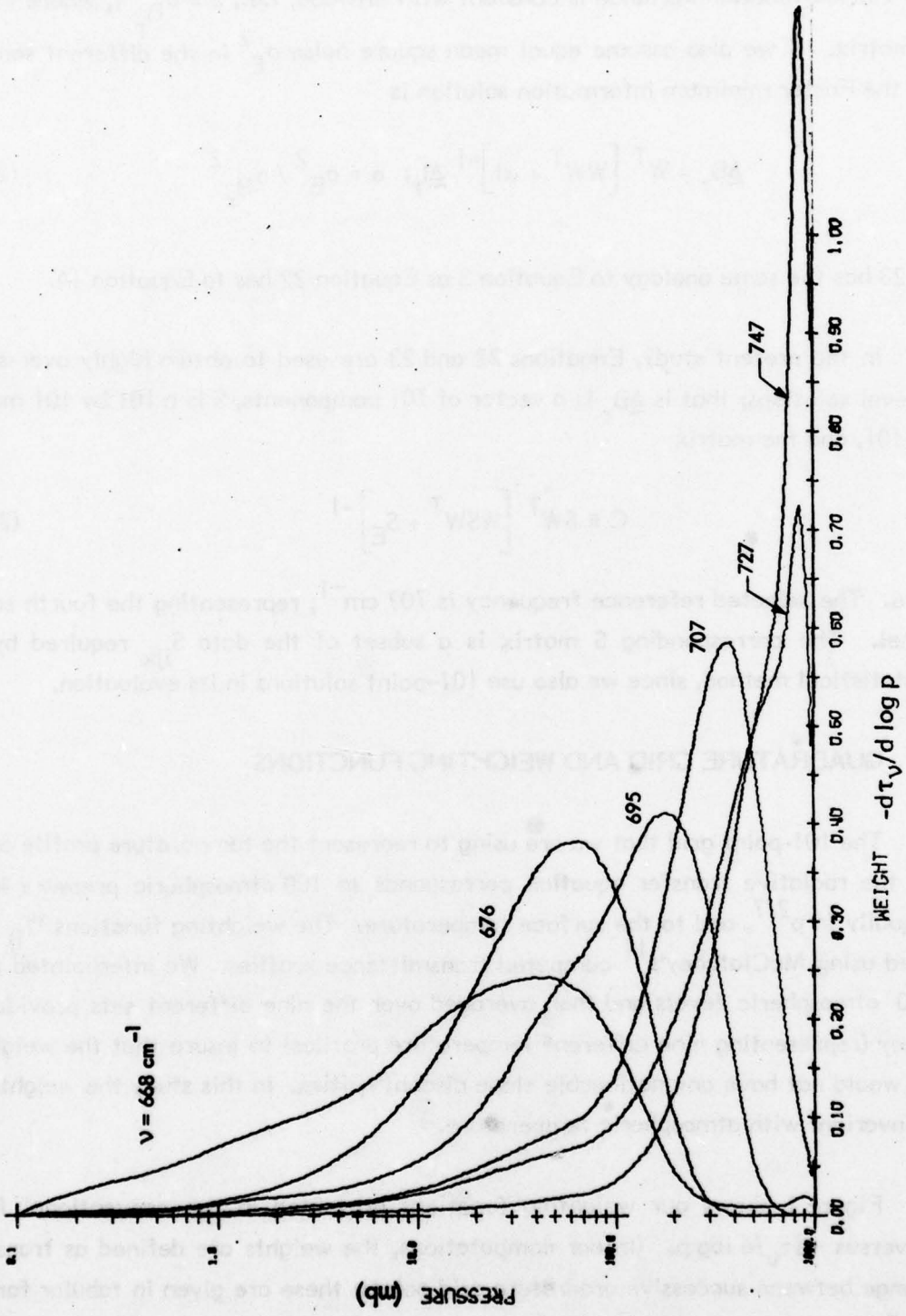

Figure 1 DMSP Weighting Functions Used for Temperature Retrieval

7809-4

To a very rough approximation, the direct nonlinear methods obtain the retrieved temperature profile as a superposition of weighting functions, when an unbiased (isothermal) first guess is used. Thus, the retrieved profiles would generally not be expected to contain any structure sharper than the weighting functions themselves, unless the structure is introduced via the initial guess. Figure 2 shows attempts to construct tropopause-like features as sums of two and three weighting functions. The three-function sum gives an indication of the achievable vertical resolution at tropopause levels.

Figure 3 shows the nine radiosonde temperature profiles on which our weighting functions are based. Except for the Point Mugu mid-latitude profile, the profiles are representative of the tropics. The very high degree of correlation exhibited by the tropical profiles suggests that the statistical retrieval methods may be quite useful, at least within a given climatological class.

2.4 RESULTS OF TEMPERATURE RETRIEVALS BY THE NONSTATISTICAL, NONLINEAR METHODS

Figures 4 through 7 show retrievals obtained using synthetic radiances and Smith's direct nonlinear technique. In these tests we selected the "actual" profile and the initial guess from among three different cases: the Point Mugu profile in Figure 3, the tropical profile in Figure 3 with the sharpest tropopause, and an isothermal (240 K) profile. We did not include instrument noise in the simulation. Figure 4 shows that the method cannot retrieve a sharp tropopause feature, starting from an isothermal guess; the error at the tropopause is almost 9 degrees C. Similar errors result when the actual profile is the Point Mugu case (Figure 5), because of the somewhat irregular feature near the 100 mb level. Figures 6 and 7 illustrate the effects of the initial guess. Note that the retrieved profile retains the character of the guess profile except at the lowest levels, where the weighting functions are relatively large. Of course, the guesses used in these last two examples represent the wrong climatology and, therefore, are not fair tests of the accuracy of the Smith method.

Figures 8, 9 and 10 show results obtained by the Fleming nonlinear (FLM)*, the alternate Fleming (NEW)*, and the Chow (CHW)** algorithms***. In each case the actual

* In all simulations using FLM and NEW, the parameter α was set to zero.
** We used K = 1 in the simulations.
*** Note that in the error plots, positive errors appear to the right of the reference line, which is a different convention than used in Figures 4 through 7.

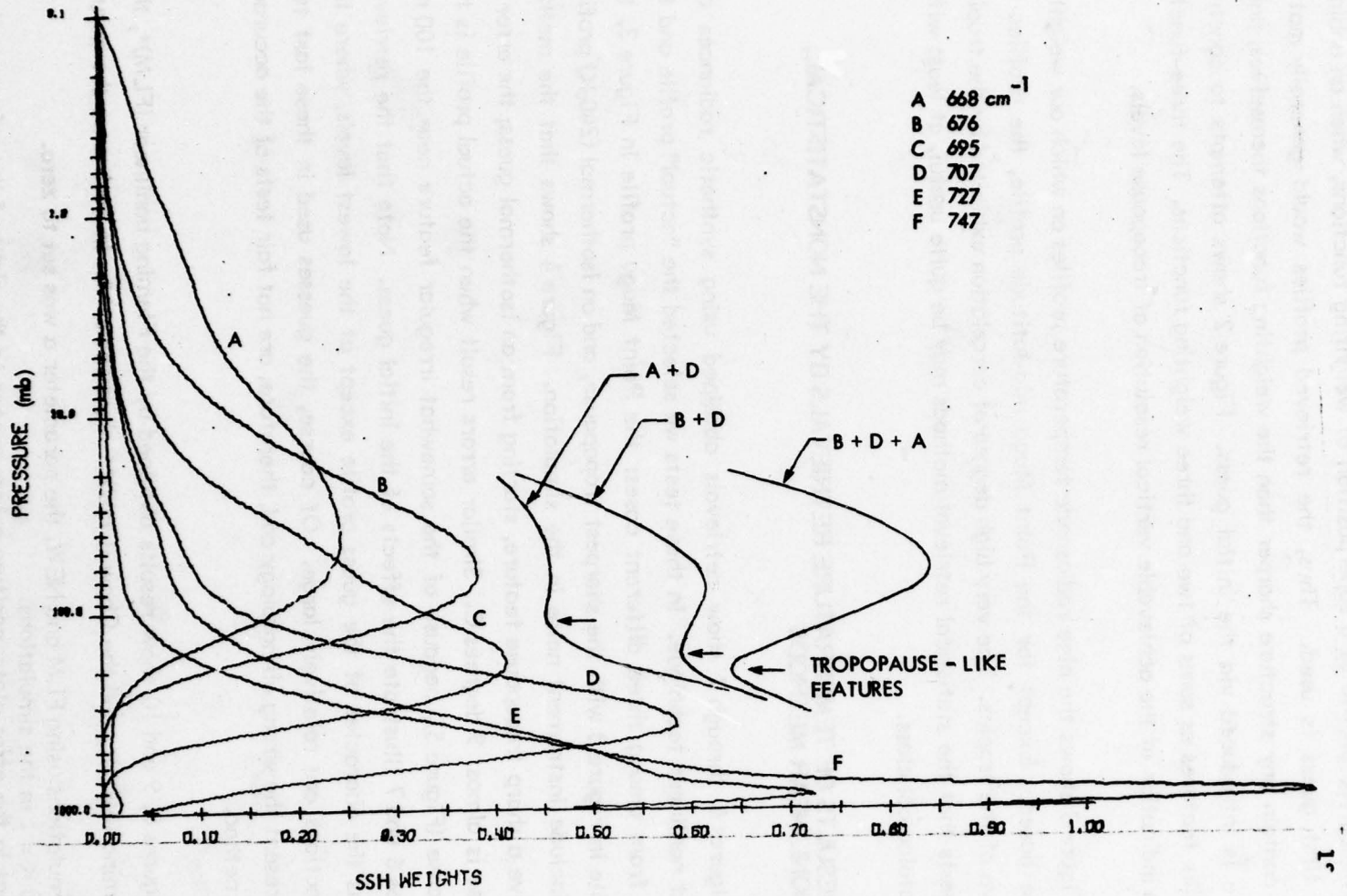

Figure 2 Construction of Tropopause-like Features Using Sums of Weighting Functions

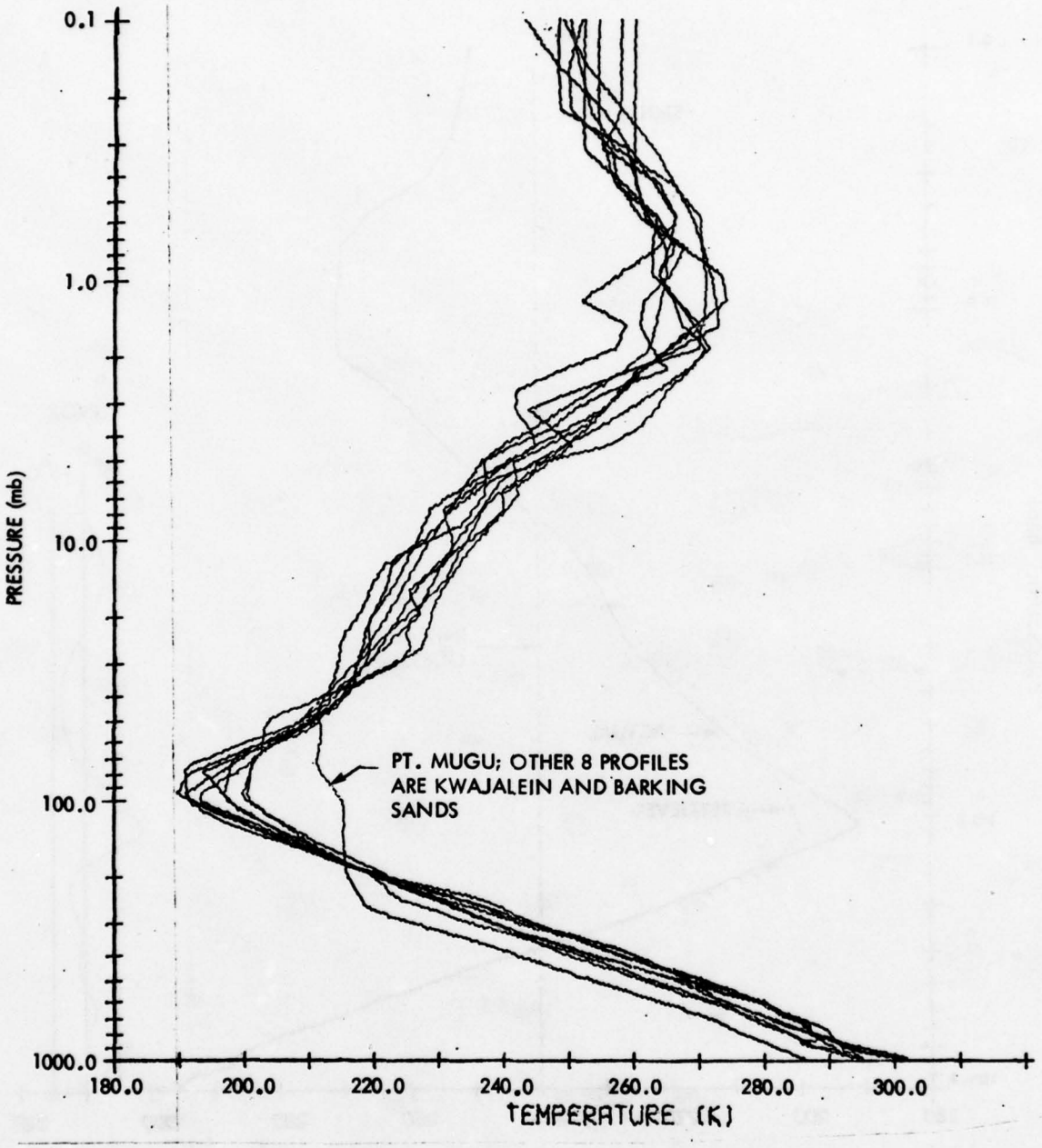

Figure 3 The Nine Temperature Profiles Used by McClatchey[11] in Computing Vertical Transmittance Profiles

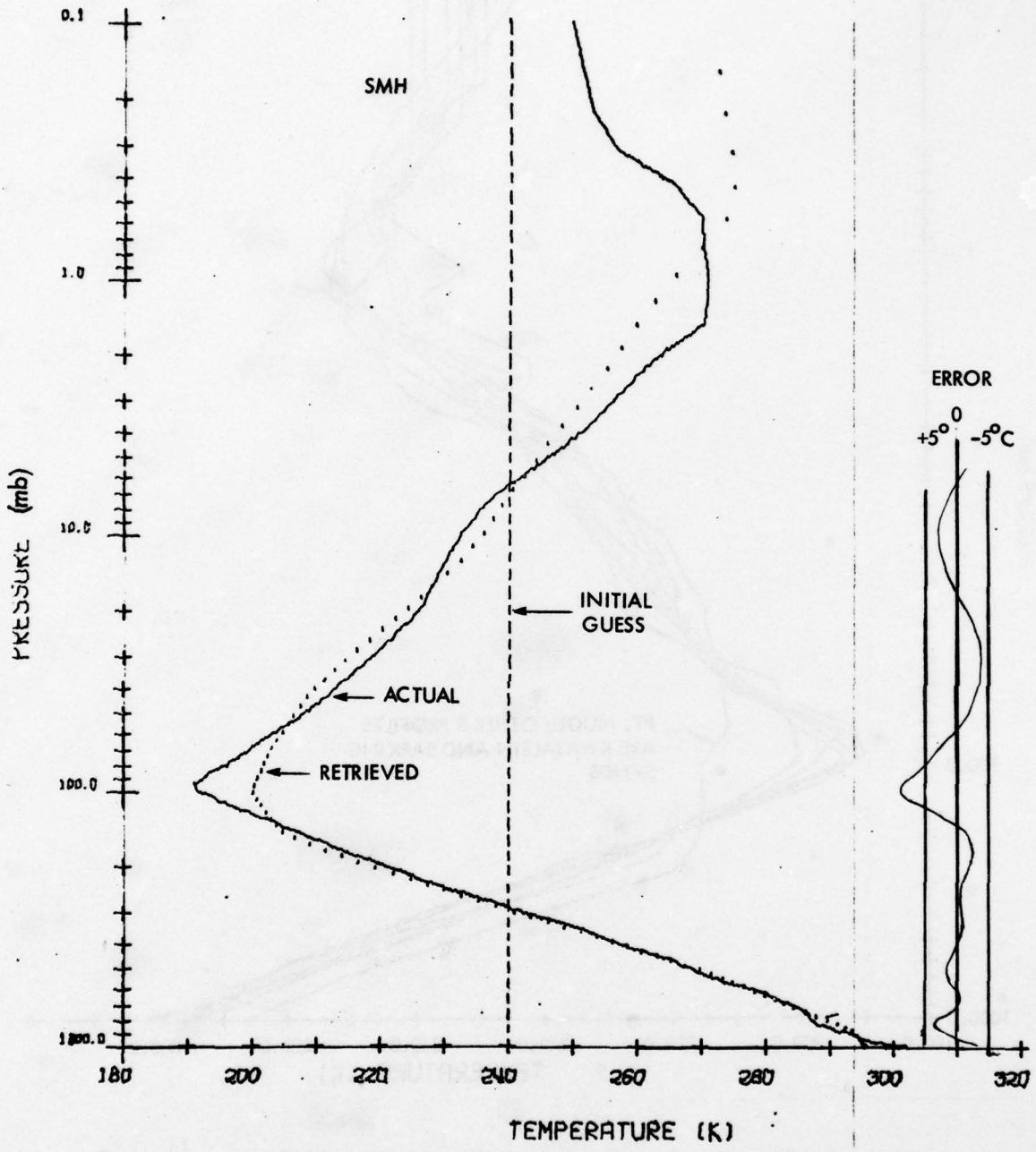

Figure 4 Temperature Retrieval Using the Smith Method

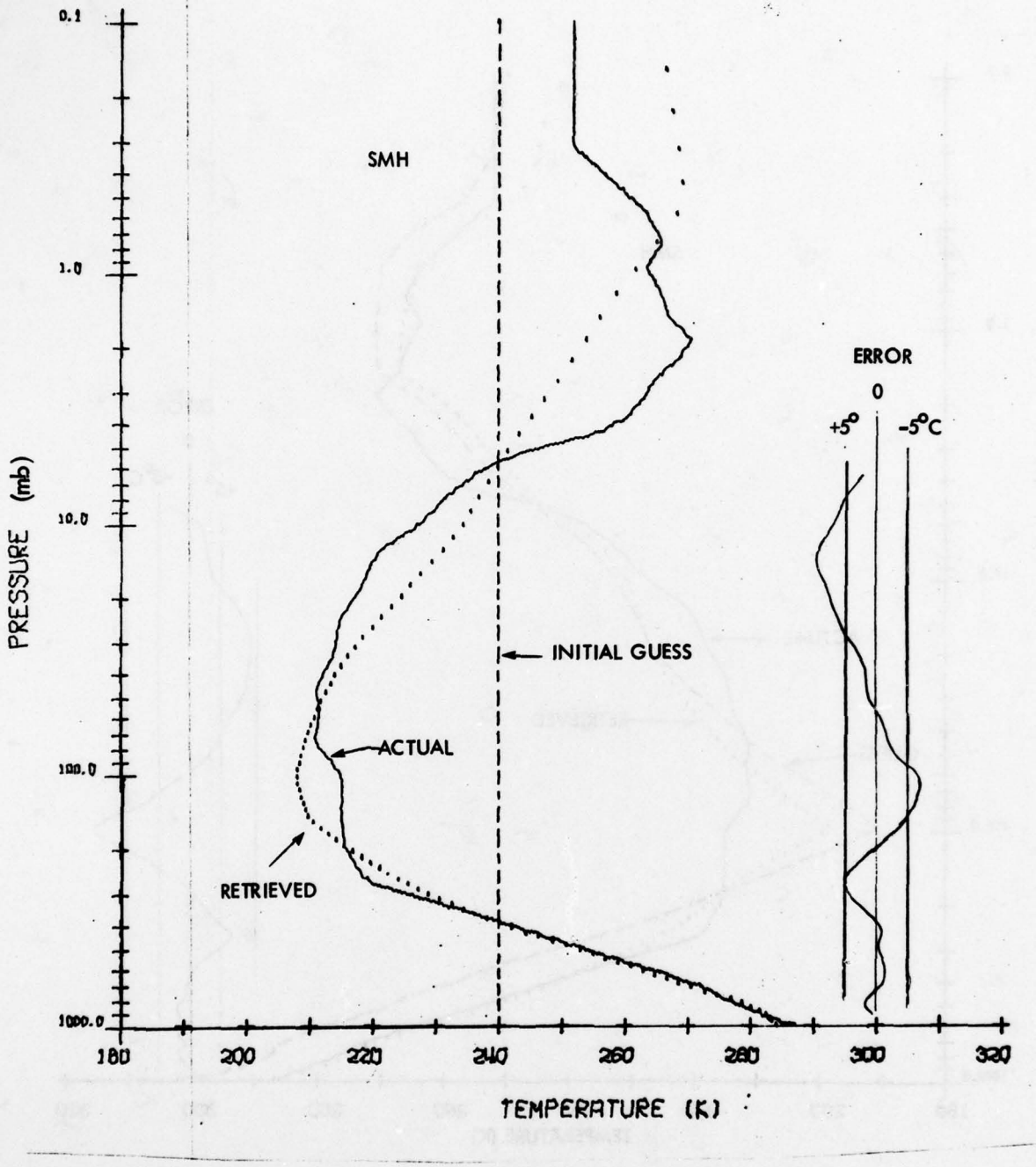

Figure 5 Temperature Retrieval Using the Smith Method

7809-4

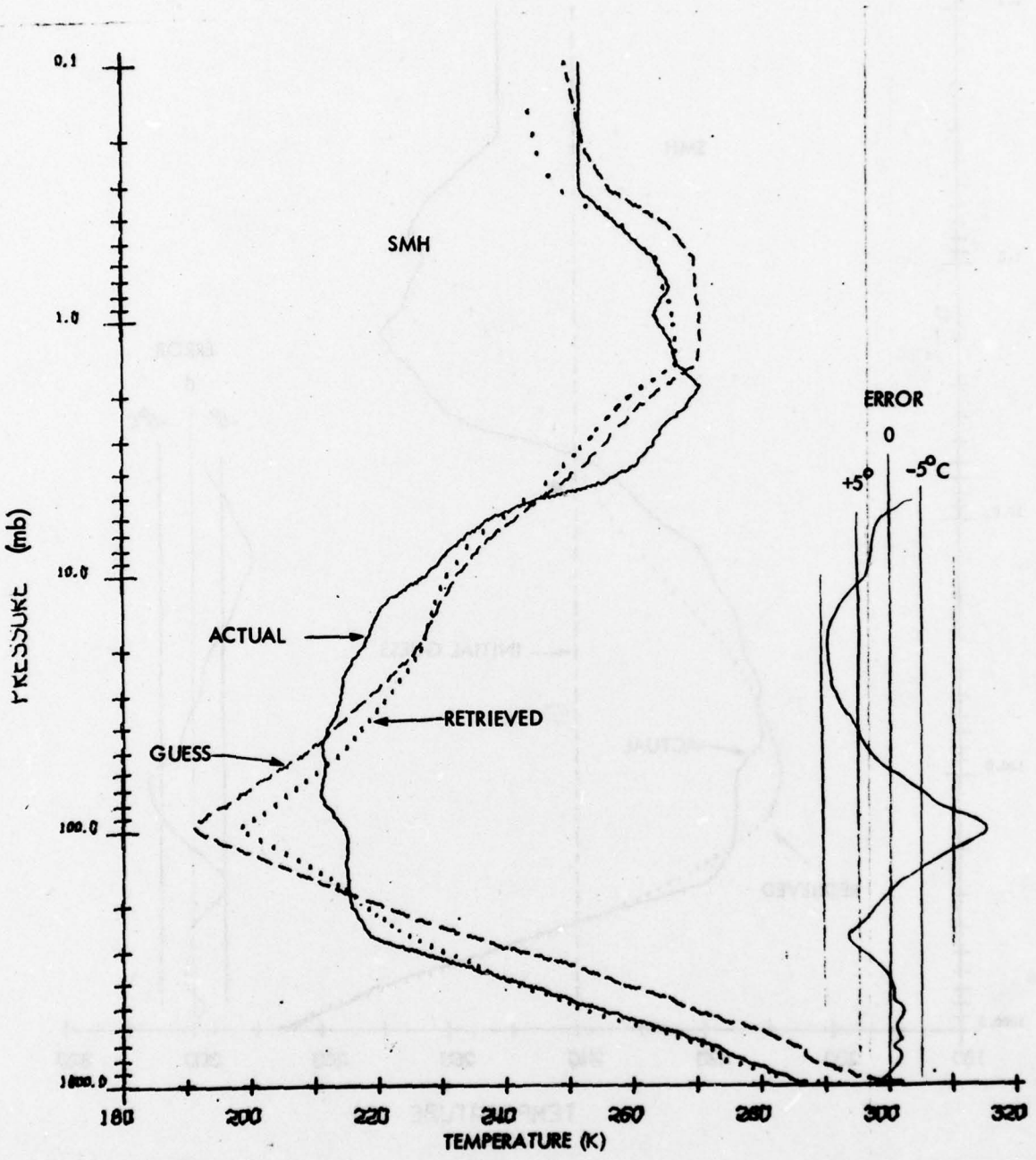

Figure 6 Temperature Retrieval Using the Smith Method

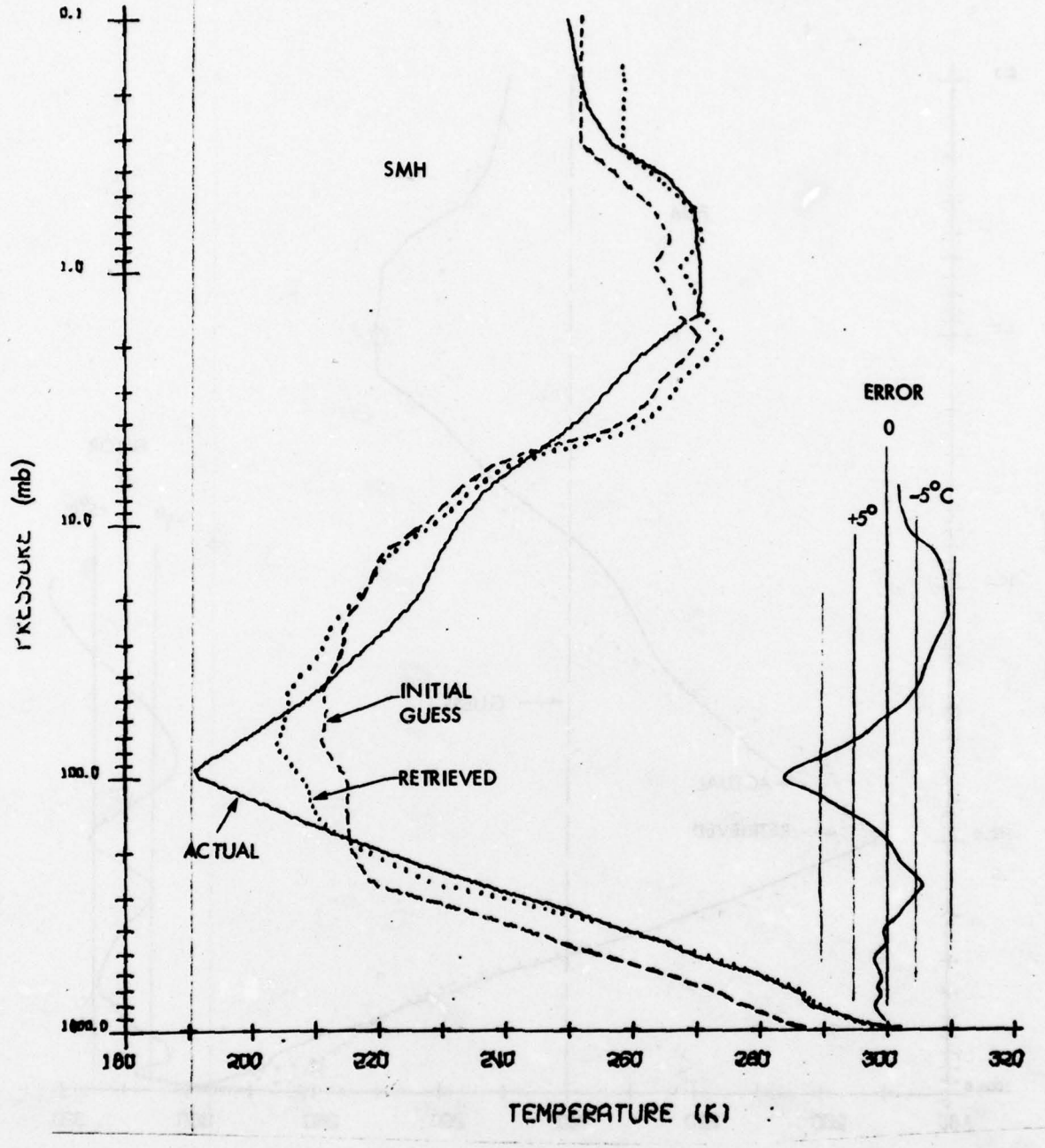

Figure 7 Temperature Retrieval Using the Smith Method

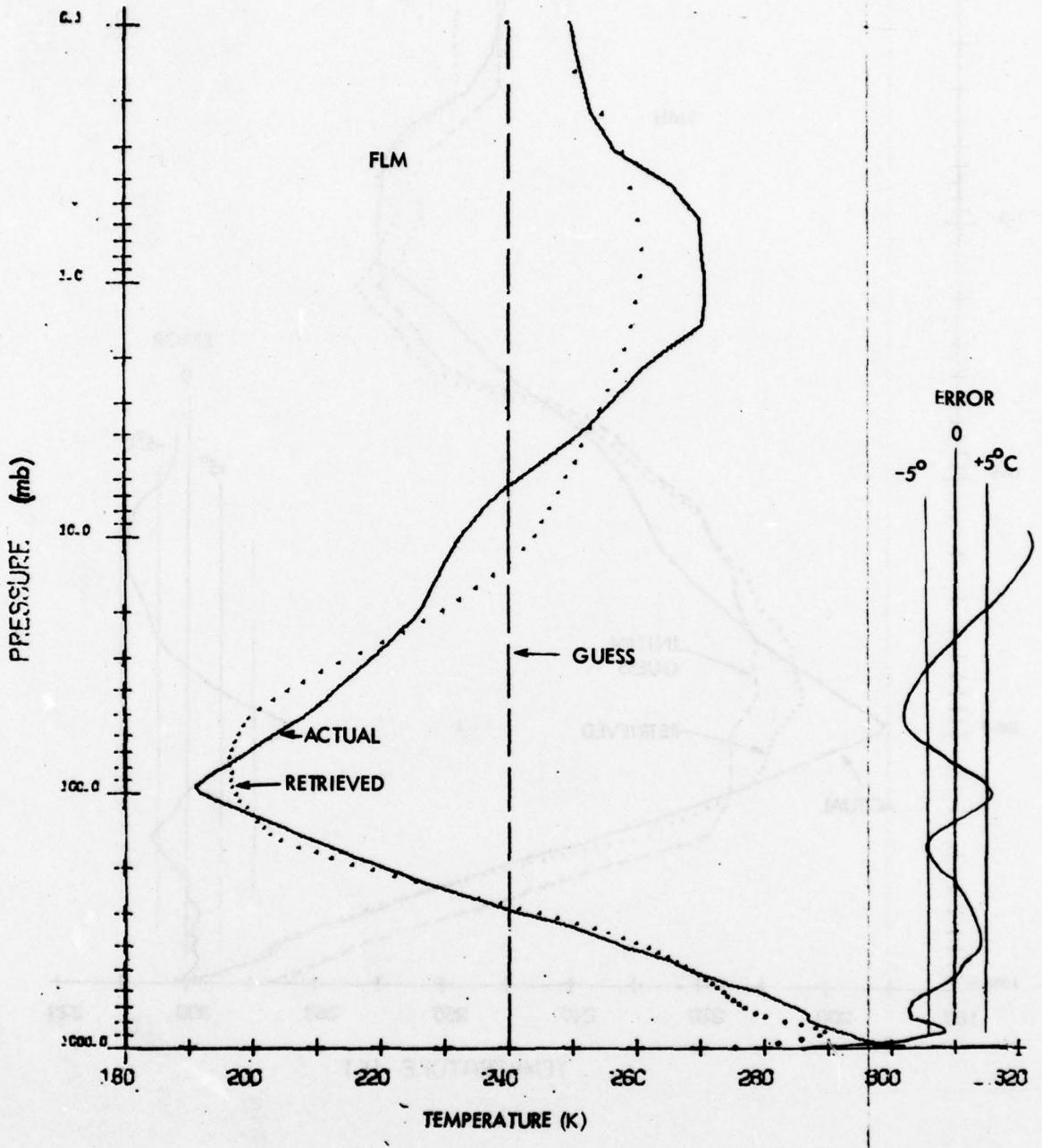

Figure 8 Temperature Retrieval Using the Fleming Nonlinear Method

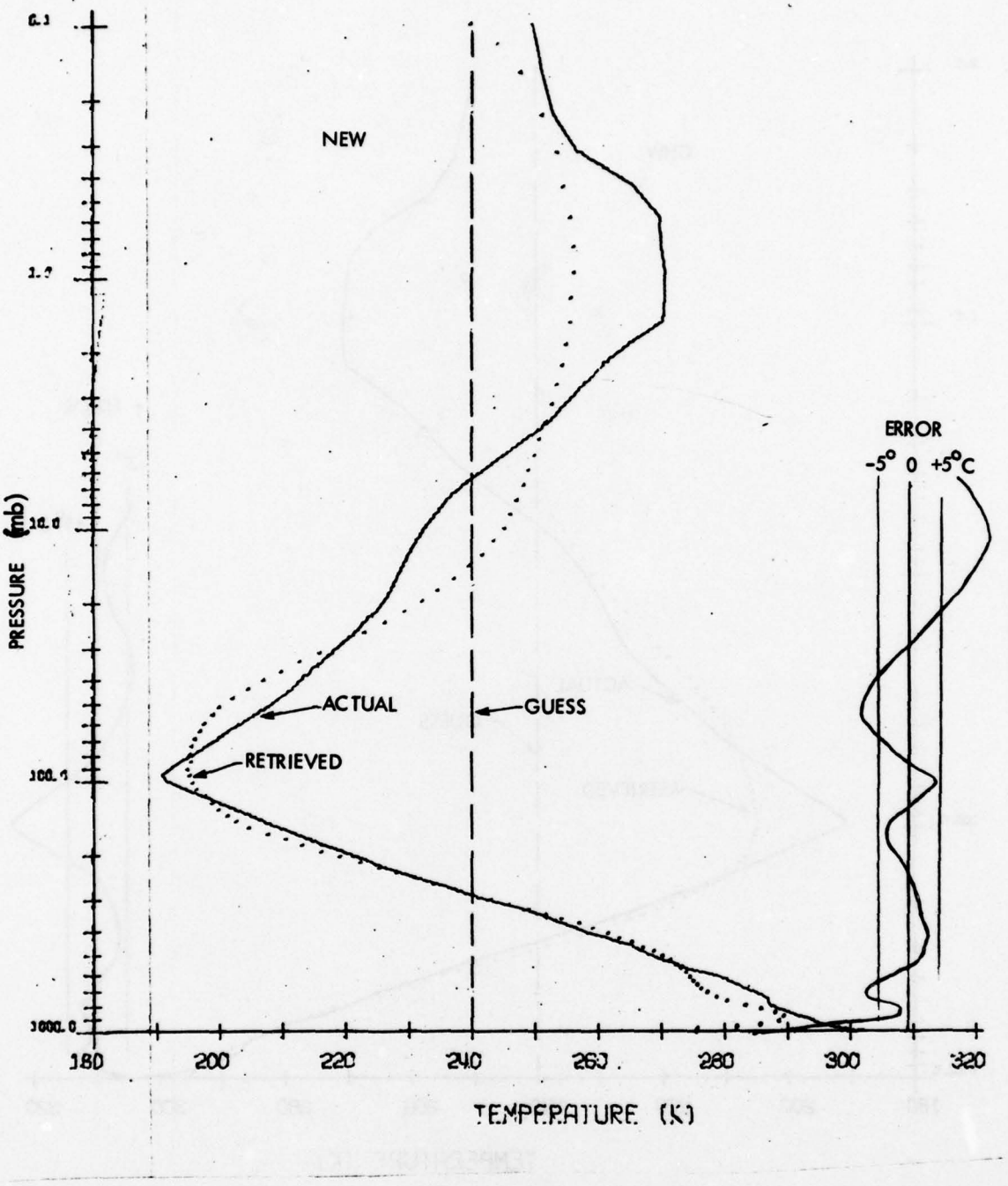

Figure 9 Temperature Retrieval Using the Alternate Fleming Nonlinear (NEW) Method

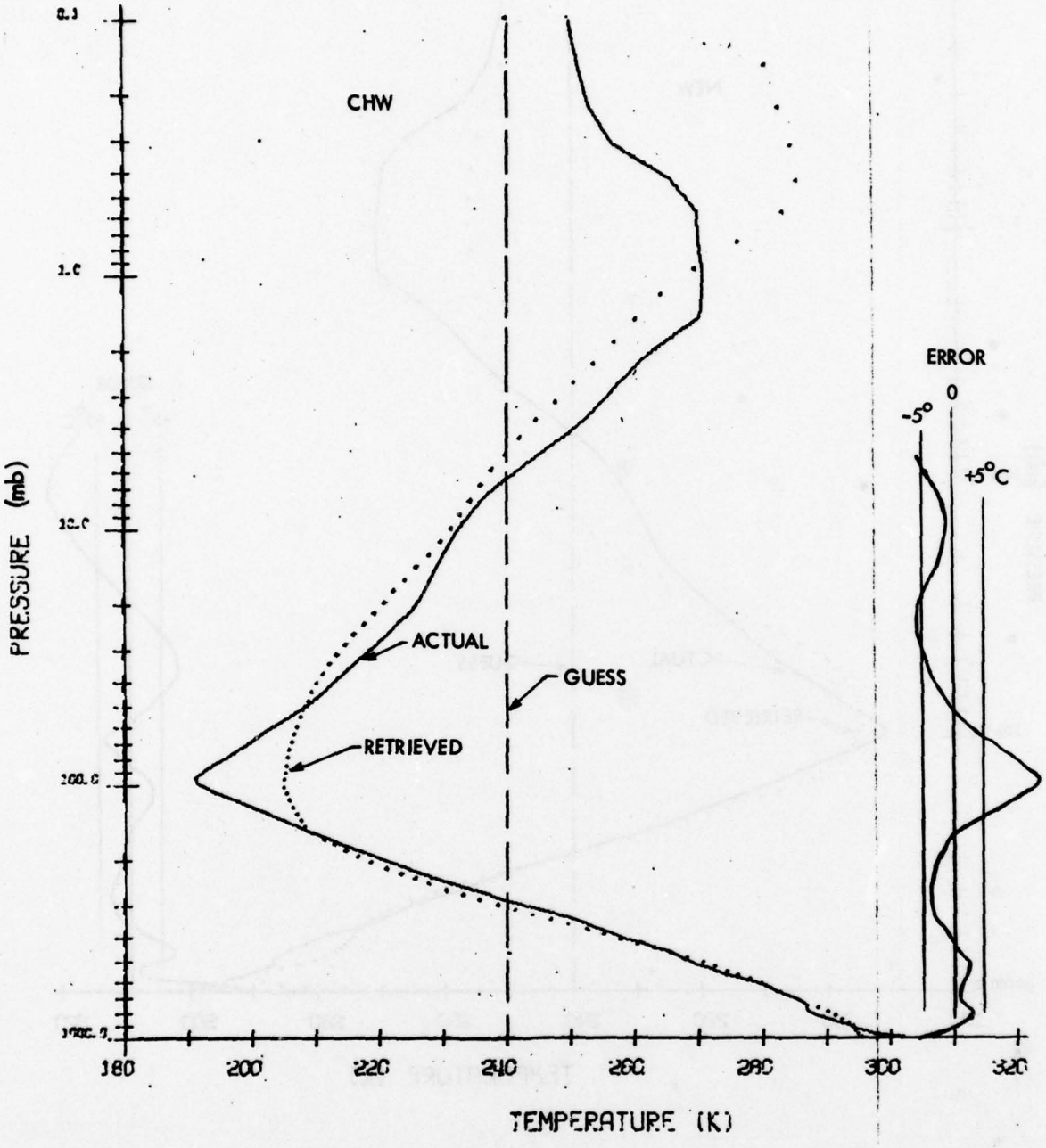

Figure 10 Temperature Retrieval Using the Chow Method

7809-4

profile is the tropical case, and the guess is isothermal. A noticeable feature of the FLM and NEW retrieved profiles is their shapes in the lower troposphere, which closely resemble the 727 cm^{-1} and/or 747 cm^{-1} weighting functions. It appears that incorporating the weighting functions in the relaxation formulas can introduce a significant bias to the solutions and resultant large errors between the 600 mb level and the surface. On the other hand the maximum error near the tropopause is smaller for the two versions of the Fleming method than for the Smith method. The Chow method yields a solution similar to the one obtained from the Smith method, with slightly greater error at all levels.

Figures 8 and 9 show that the retrieved profile obtained by NEW is slightly better than the one obtained by FLM, indicating that the alternate temperature averaging method may yield a somewhat less biased result.

Figure 11 shows the profile retrieved by method FLM when the actual profile is the tropical case, and the guess is the Point Mugu profile (same as Figure 7 except FLM is used in place of the Smith method SMH). Note that the bias due to the 727 cm^{-1} and 747 cm^{-1} weighting functions is much less than when an isothermal guess is used (Figure 8), which is apparently the result of using a much more accurate guess in the lower troposphere (i.e., correct lapse rate but 20-degree temperature difference compared to a 40 to 60-degree difference for the isothermal guess). Note that the initial guess imposes a significant bias above the 200 mb level, which is true of all the direct nonlinear methods.

Figure 12 illustrates how the accuracy of the retrieved profile increases as the actual profile becomes smoother: using one of the smoother tropical cases as the actual profile, and starting from an isothermal guess, the Smith method achieves a retrieval accuracy of approximately 3 degrees or better, except at the surface and tropopause levels, where the error is about 5 degrees.

Figures 13 and 14 show retrieval results from the Twomey-like method TWM and its alternate TW2. Note that the retrieved profiles are similar to those from the FLM and NEW methods, but the errors are generally larger. TW2 gives better retrievals than TWM below the 200-mb level, but TWM does better near the tropopause.

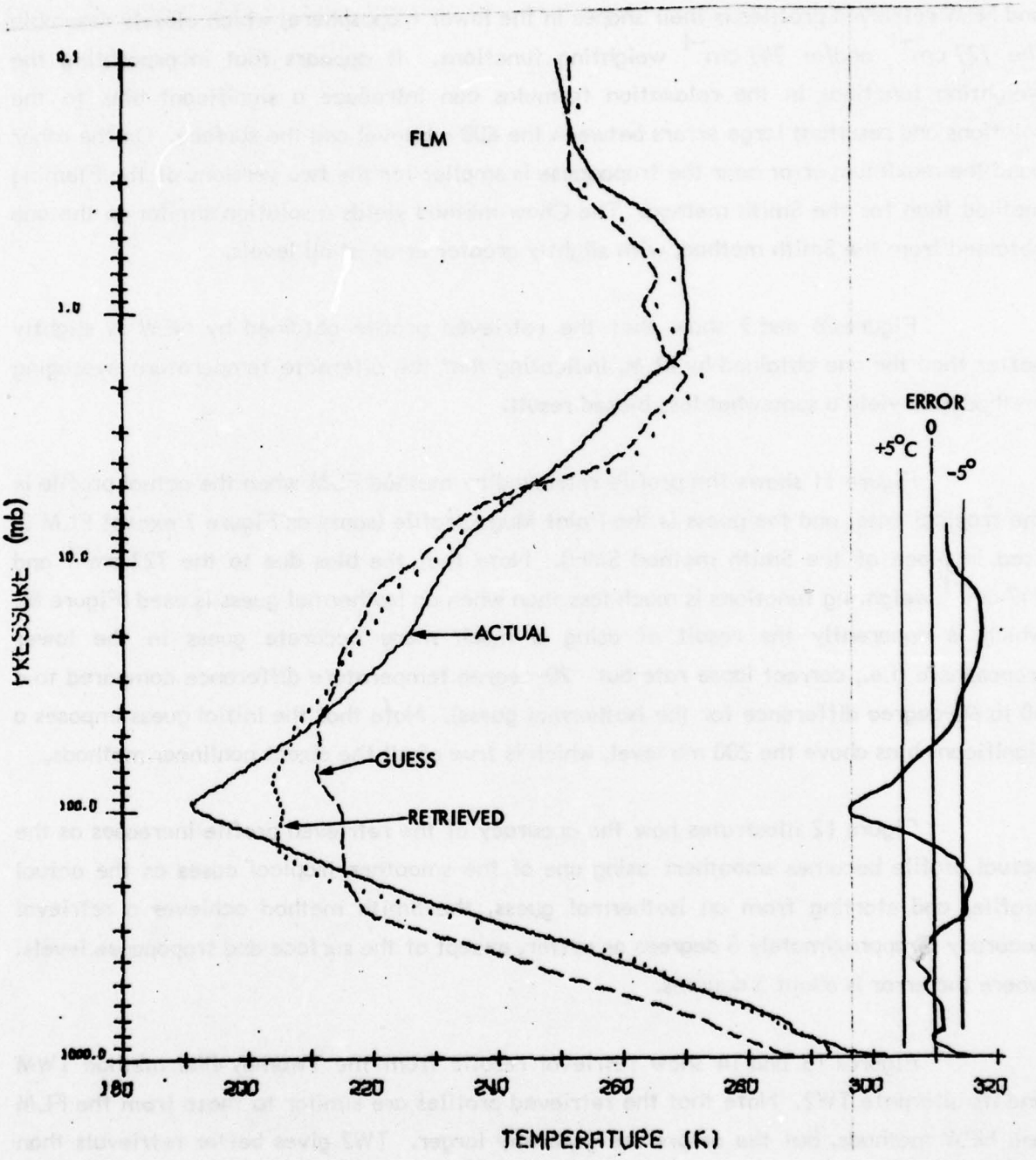

Figure 11 Temperature Retrieval Using the Fleming Nonlinear Method

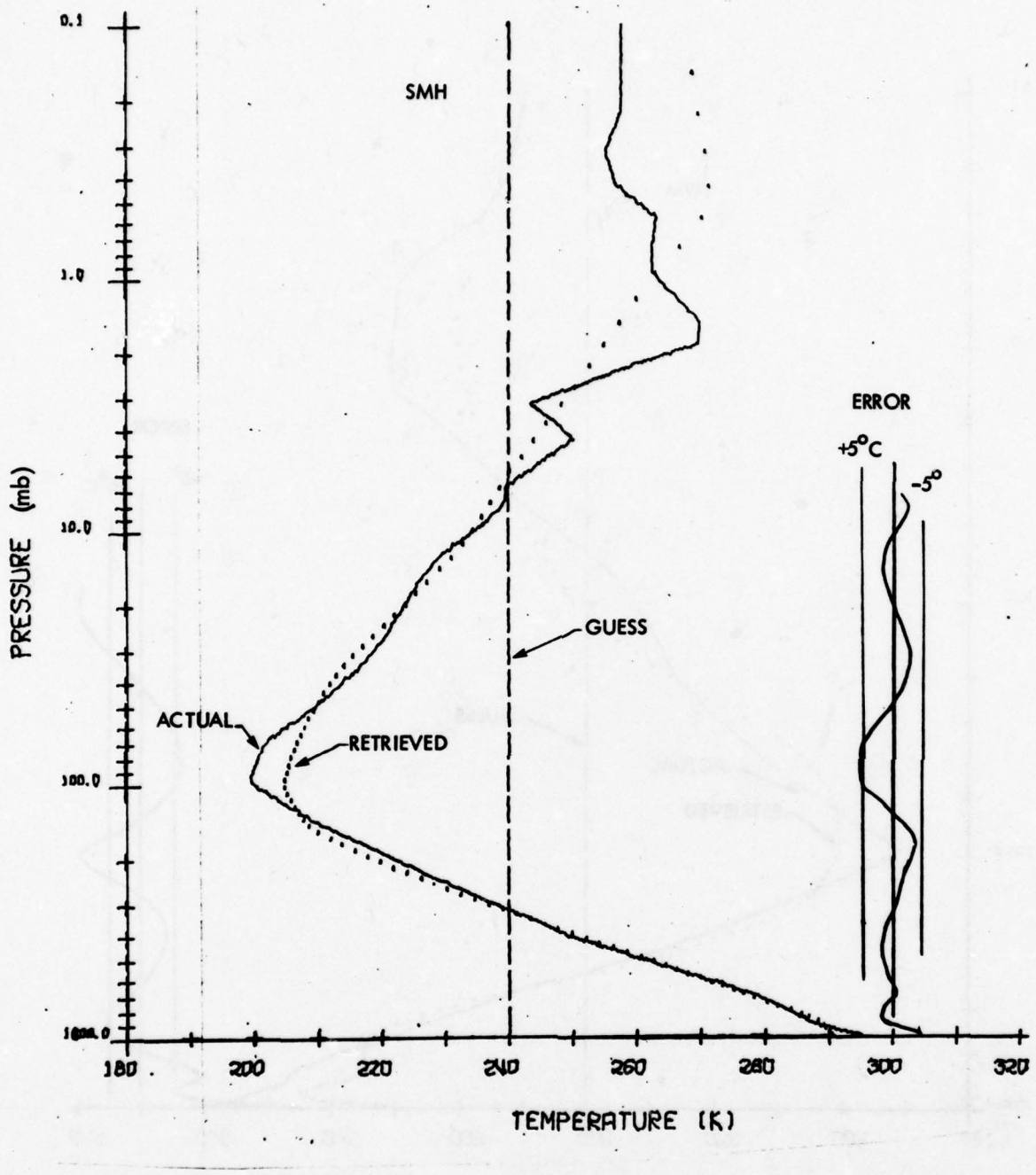

Figure 12 Temperature Retrieval Using the Smith Method

7809-4

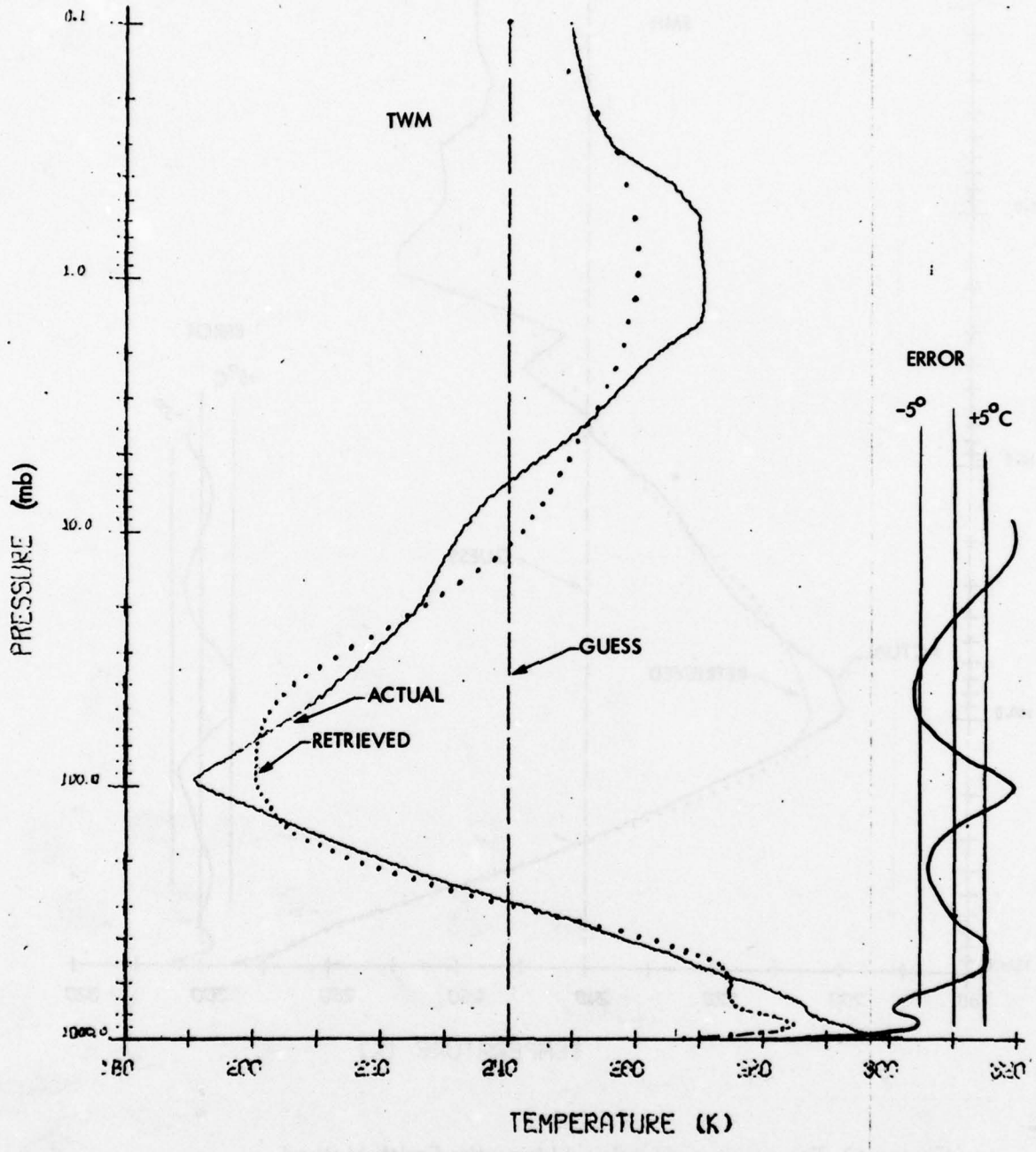

Figure 13 Temperature Retrieval Using the Twomey-like Method

7809-4

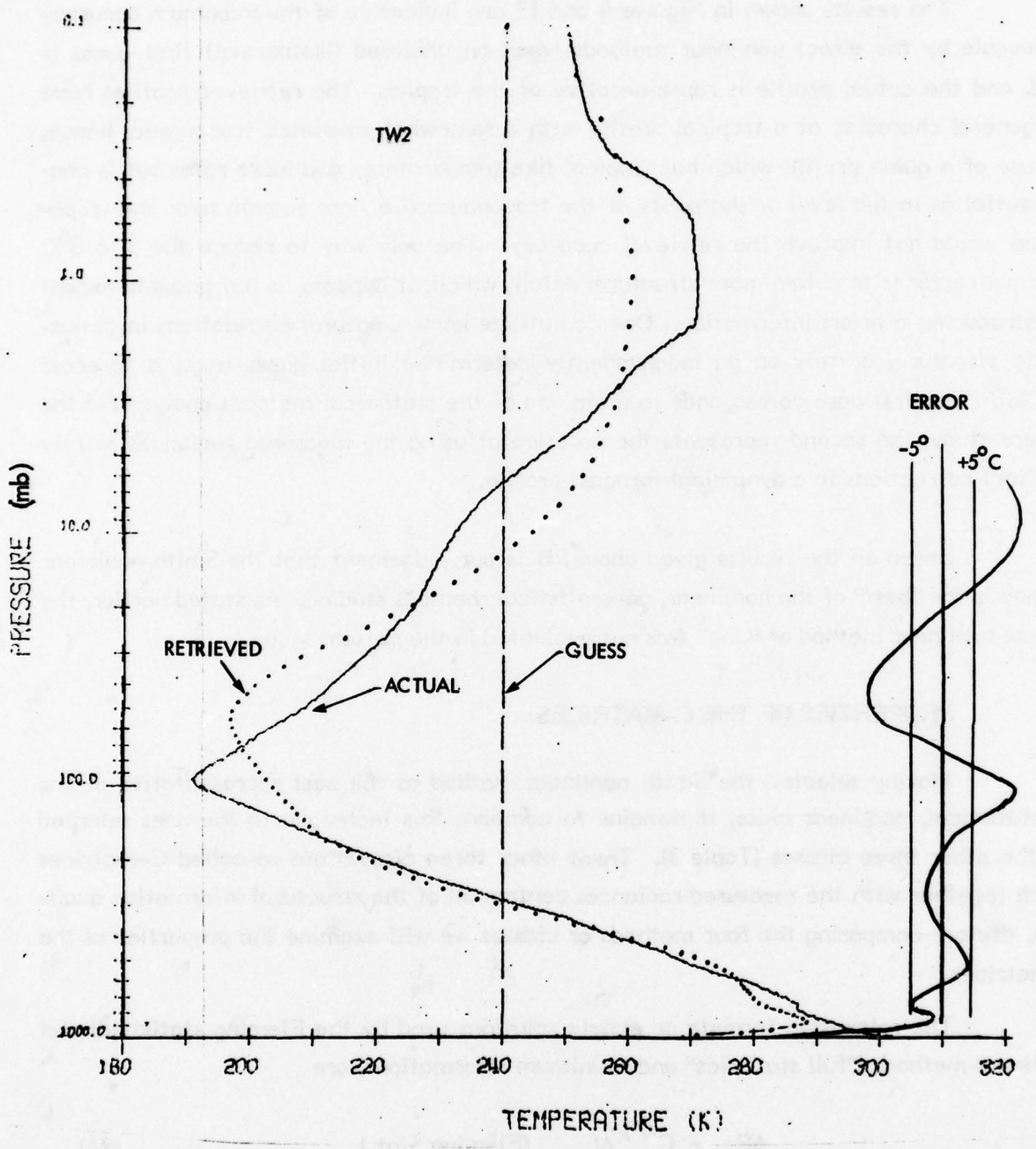

Figure 14 Temperature Retrieval Using the Alternate Twomey-like Method

The results shown in Figures 4 and 12 are indicative of the maximum accuracy achievable by the direct nonlinear methods when an unbiased (isothermal) first guess is used, and the actual profile is representative of the tropics. The retrieved profiles have the general character of a tropical profile with a somewhat smoothed tropopause; hence, the use of a guess profile which has tropical-like temperatures and lapse rates but is non-committal as to the level or sharpness of the tropopause (i.e., are smooth near the tropopause) would not improve the retrieval accuracy. The only way to reduce the 5 to 8°C maximum error is to obtain more structural detail, which, it appears, is not possible except by introducing a priori information. One can utilize known, natural correlations in atmospheric structure, or rely on an independently determined initial guess (e.g., a forecast profile). The first case corresponds to using one of the statistical methods analyzed in the present study; the second represents the practice of using the measured radiances merely to effect corrections to a dynamical forecast profile.

Based on the results given above, it is our judgement that the Smith nonlinear method is the "best" of the nonlinear, nonstatistical methods studied. As stated earlier, the inverse nonlinear method of King[5] was not evaluated in the present study.

2.5 PROPERTIES OF THE C-MATRICES

Having selected the Smith nonlinear method as the best representative of the nonstatistical, nonlinear class, it remains to compare this technique to the ones selected for the other three classes (Table 3). These other three classes use so-called C-matrices which together with the measured radiances contain all of the structural information available. Before comparing the four methods or classes we will examine the properties of the C-matrices.

The relaxation formula or matrix solutions used by the Fleming statistical and the linear methods ("full statistics" and "minimum information") are

$$\Delta B_{ij} = C_{ji}^{(F)} \Delta I_i \qquad \text{(Fleming Stat.)} \qquad (25)$$

$$\underset{\sim}{\Delta B}_r = C^{(FS)} \underset{\sim}{\Delta I}_r \qquad \text{(Full Stat.)} \qquad (26)$$

$$\underset{\sim}{\Delta B}_r = C^{(MI)} \underset{\sim}{\Delta I}_r \qquad \text{(Min. Info.)} \qquad (27)$$

where the matrices $C^{(F)}$, $C^{(MI)}$ and $C^{(FS)}$ are, from Equations 14, 23 and 22,

$$C_{ji}^{(F)} = \sum_{n=1}^{J} S_{ijn} W_{in} \left[\sum_{j=1}^{J} W_{ij} \sum_{n=1}^{J} S_{ijn} W_{in} + \sigma_E^2 \right]^{-1}; \qquad (28)$$

$$C^{(MI)} = W^T \left[WW^T + \alpha I \right]^{-1}, \quad \alpha = \sigma_E^2 / \sigma_{B_r}^2; \qquad (29)$$

$$C^{(FS)} = SW^T \left[WSW^T + S_E \right]^{-1}. \qquad (30)$$

In Equation 28 the factor $[\,]^{-1}$ is the denominator of the expression, while in Equations 29 and 30 these factors are matrix inverses. W is the weighting function matrix and S is the atmospheric radiance covariance matrix (for channel i in Equation 28, and for the reference or channel 4 frequency, $\nu = 707\ cm^{-1}$, in Equation 30). Note that the C-matrices given by Equations 28 through 30 are constant throughout the iterative temperature retrieval, since W is assumed independent of temperature. In this study we also assume that the channel noises are equal and uncorrelated, i.e., that $S_E = \sigma_E^2\, I$, where I is the six-by-six identity matrix. We used the nominal noise equivalent radiance $\sigma_E = 2.5 \times 10^{-8}$ $W/cm^2\text{-sr-}cm^{-1}$ = 0.25 $ergs/s\text{-}cm^2\text{-sr-}cm^{-1}$ for the DMSP temperature sensing channels.

The tropical temperature profile is distinctive in two respects: its very sharp tropopause is difficult to reproduce in the retrieved profiles, and the profile as a whole is much less variable than extratropical temperature profiles. For this reason we computed one S-matrix using data obtained at all latitudes, and another using only tropical data (actually, the tropics was somewhat under-represented in the global data set, so that the former matrix may be regarded as extratropical). It is also appropriate to use different values for α (in Equation 29) for the tropics and extratropics. The corresponding C-matrices, therefore, are dually defined and number six in total.

The average variance in the global or extratropical reference-frequency Planck radiance profile, obtained by averaging the diagonal elements of the corresponding S-matrix, is $\sigma_{B_r}^2 = 1.98 \times 10^{-12}$ $(W/cm^2\text{-sr-}cm^{-1})^2$, which means that the assumed noise-equivalent radiance corresponds to a "signal-to-noise" of $\sigma_{B_r}/\sigma_E \simeq 56$ for the global case. For the tropics the average variance of the radiance profile is only 1.42×10^{-13} $(W/cm^2\text{-sr-}cm^{-1})^2$, corresponding to a "signal-to-noise" of approximately 15. The corresponding values of α are

$$\alpha \equiv \sigma_E^2/\sigma_{B_r}^2 = 3.2 \times 10^{-4} \text{(Extratropical)} \qquad (31)$$
$$= 4.4 \times 10^{-3} \text{ (Tropics).}$$

We note that the retrieved corrections to the guess temperature profile are constrained to be smoother for the tropical case, but the guess (mean) profile has sharper structure; hence, the final retrieved profiles are not necessarily smoother in the tropical case.

Equations 26 and 27 show that in the two linear methods the solution vector $\underset{\sim}{\Delta B}_r$ at each stage of iteration is a linear superposition of the columns of $C^{(FS)}$ or $C^{(MI)}$; i.e.,

$$(\Delta B_r)_j = \sum_{i=1}^{6} C_{ji}\, \Delta I_r(\nu_i), \qquad (32)$$
$$C_{ji} = C_{ji}^{(FS)} \text{ or } C_{ji}^{(MI)}$$

Moreover, since C is treated as a constant matrix in this study, the ΔI_r's in Equation 32 may be regarded as having been summed over iteration number, and therefore $\underset{\sim}{\Delta B}_r$ can represent the total correction to the initial guess Planck function profile $\underset{\sim}{B}_r$. In other words the final reference-frequency Planck function profile is equal to the guess profile plus a linear superposition of the columns of C. Therefore, a large set of temperature retrievals belonging to a given climatological class can be economically stored or archived in terms of

one C–matrix, the single initial guess profile, and six numbers per retrieved profile, equal to the six $\Delta I_r(\nu_i)$ summed over iteration number. In this representation the summed $\underset{\sim}{\Delta I}_r$ vectors are the "solutions", and the columns of C play the role of basis vectors.

Although the influence of temperature in the weighting function is ignored in the present study, it should probably be included in the routine reduction of satellite radiance data. This would require recomputing the W and C–matrices in each iteration, and would result in retrieved profiles that must be represented by 101 values (the number of quadrature points) rather than six.

In the Fleming nonlinear statistical method, the Smith channel averaging scheme is applied to the ΔB_{ij} obtained from Equation 25. That is, the columns of $C^{(F)}$ are combined in a nonlinear fashion to obtain the temperature profile, which means that $C^{(F)}$ is not directly comparable to $C^{(FS)}$ and $C^{(MI)}$. However, the following first-order analysis of the operations performed on $C^{(F)}$ leads to a related matrix, K, whose columns are approximate linear bases for the solution profiles.

The iterate temperature profile T_j obtained by evaluating the relaxation Equation 25 and then averaging over channels is

$$T_j = \frac{\sum_{i=1}^{6} W_{ij}\ T_i \left[\bar{B}_{ij} + C_{ij}^{(F)}\ \Delta I_i\right]}{\sum_{i=1}^{6} W_{ij}}, \qquad (33)$$

where $T_i(B)$ denotes the inverse Planck function applied at frequency i, and $\bar{B}_{ij}$ are the vertical Planck function profiles corresponding to the guess temperature profile (or previous iterate) $\bar{T}_j$. To first order, the effect of a change ΔB_{ij} in the argument of the inverse Planck may be represented by

$$T_i\,(B_{ij} + \Delta B_{ij}) \simeq T_j + \Delta B_{ij}\,(dB_{ij}/dT)^{-1}, \qquad (34)$$

which, when applied to Equation 23 gives

$$T_j = \bar{T}_j + \frac{\sum_{i=1}^{6} W_{ij}\, C_{ji}^{(F)}\, (dB_{ij}/dT)^{-1}\, \Delta I_i}{\sum_{i=1}^{6} W_{ij}} \qquad (35)$$

The effect of a temperature change in the direct Planck function applied at the reference frequency $\nu_r = 707\ cm^{-1}$ is, to first order,

$$B_{rj}(T_j + \Delta T_j) = B_{rj}(T_j) + \Delta T_j\, dB_{rj}/dT. \qquad (36)$$

Applying Equation 36 to Equation 35, we obtain the reference-frequency Planck function solution profile as

$$B_{rj} = \bar{B}_{rj} + \frac{d\bar{B}_{rj}}{dT} \frac{\sum_{i=1}^{6} W_{ij}\, C_{ji}^{(F)}\, (d\bar{B}_{ij}/dT)^{-1}\, \Delta I_i}{\sum_{i=1}^{6} W_{ij}}, \qquad (37a)$$

or in matrix notation

$$\underset{\sim}{B}_r = \bar{\underset{\sim}{B}}_r + K\underset{\sim}{\Delta I} \qquad (37b)$$

By analytically evaluating the Planck function derivatives in Equation 37a we find that the elements of matrix K can be written

$$K_{ij} = \left[\frac{\nu_r}{\nu_i}\right]^4 \frac{\cosh(c_2\, \nu_i/\bar{T}_j) - 1}{\cosh(c_2\, \nu_r/\bar{T}_j) - 1} \frac{W_{ij}\, C_{ji}^{(F)}}{\sum_{i=1}^{6} W_{ij}} \qquad (38)$$

where $c_2 = 1.4389\ cm^{\circ}K$ is the second radiation constant.

We see from Equation 37b that matrix K plays the same role as the matrices $C^{(FS)}$ or $C^{(MI)}$ in the linear methods. Of course the K-matrix and Equation 37b are an accurate representation of solutions obtained by the Fleming statistical method only when the actual temperature profile is close to the mean profile $\bar{T}_j$ used for the initial guess.

It is evident that plots of the columns of C in the form C_{ji} versus p_j represent a complete display of the structural temperature information available in the radiance measurements, for the two linear methods. Similar plots of the K-matrices are an approximate representation of this information for the Fleming statistical method. The matrix columns computed for the three methods using both tropical and extratropical statistics are shown in Figures 15 through 20. For completeness we also show the C-matrices for the Fleming statistical model (Figures 21 and 22), and the mean reference-frequency Planck radiance profiles for the tropics and extratropics (Figure 23).

Figure 15 shows the C-matrix columns computed for the full-statistics case using global (extratropical) statistics. A noteworthy feature, which is common to all of the different C-matrices, is the channel-to-channel change in vertical distribution of structure (information), which of course, is due to the influence of the weighting functions. Figure 16 shows the minimum information C-matrix for extratropical latitudes. Differences between these two cases are attributable to statistical temperature correlations between different pressure levels. Note, in particular, that the full statistics method can retrieve more information than the minimum information method above the 10-mb level. (Note the different scale factors in Figures 15 and 16.) The differences at the lower levels is essentially in small-scale structure. Some of the structural detail in the full statistics matrix columns may be artificial, since we used only 100 radiosonde profiles in generating the covariance matrix. However, at least some of the structure exhibited near the 300-mb level is probably real, since there is typically an abrupt change in temperature lapse rate near this level at extratropical latitudes (see, Figure 23, showing the mean Planck radiance profile). Correlated variations in the lapse rates just above and below 300 millibars, or variations in the altitude of the tropopause lower boundary, would be expected to produce the sharp features displayed in Figure 15.

The discontinuities on the C-matrix columns at the lowest pressure level (the surface) arise from the discontinuity in the weighting functions at the surface (corresponding to the boundary term of the radiative transfer equation, which is represented in the last

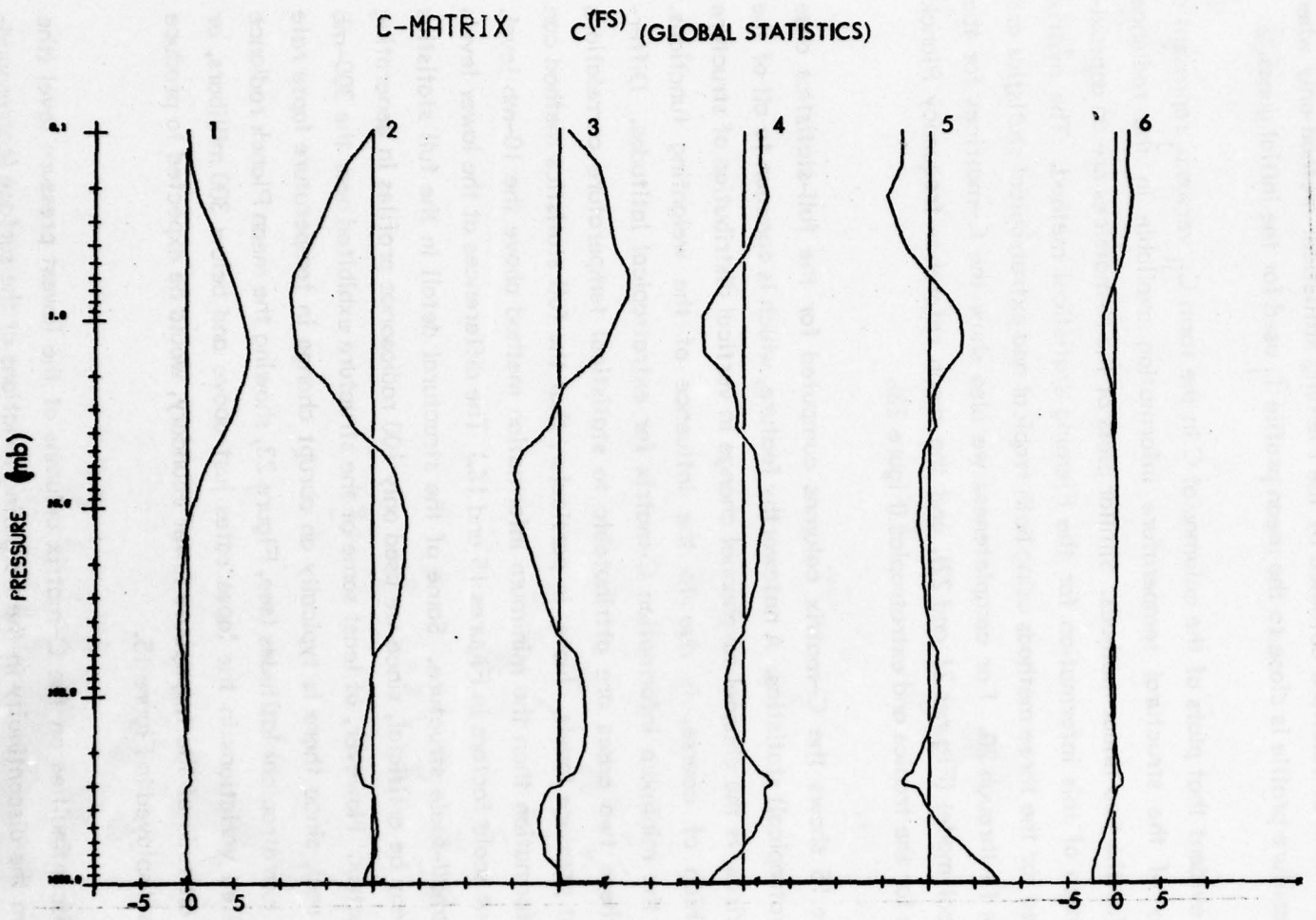

Figure 15 C-Matrix Columns For The Full-Statistics Method Using Global (Extratropical) Statistics

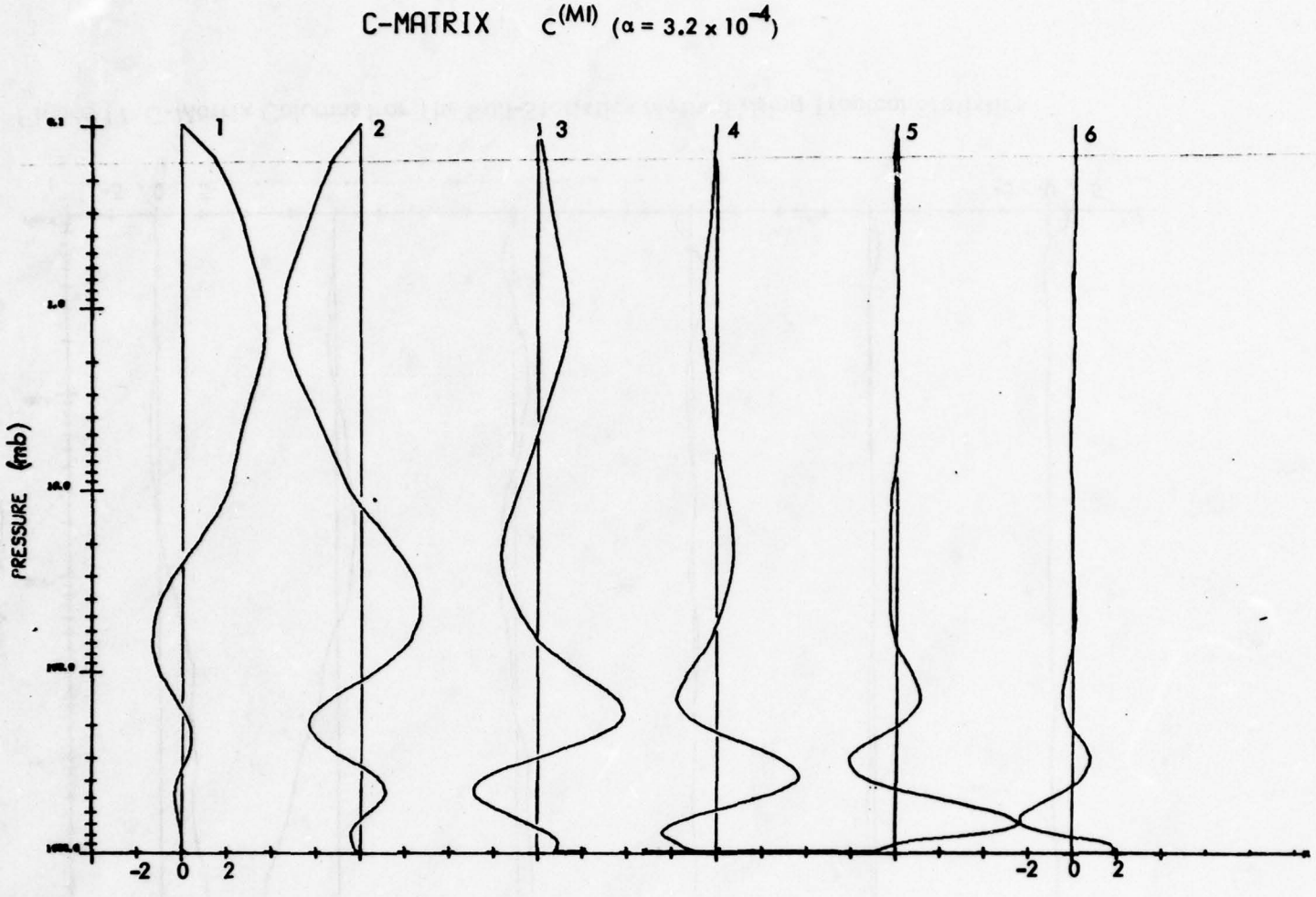

Figure 16 C-Matrix Columns For The Minimum-Information Method, Global Case ($\alpha = 3.2 \times 10^{-4}$)

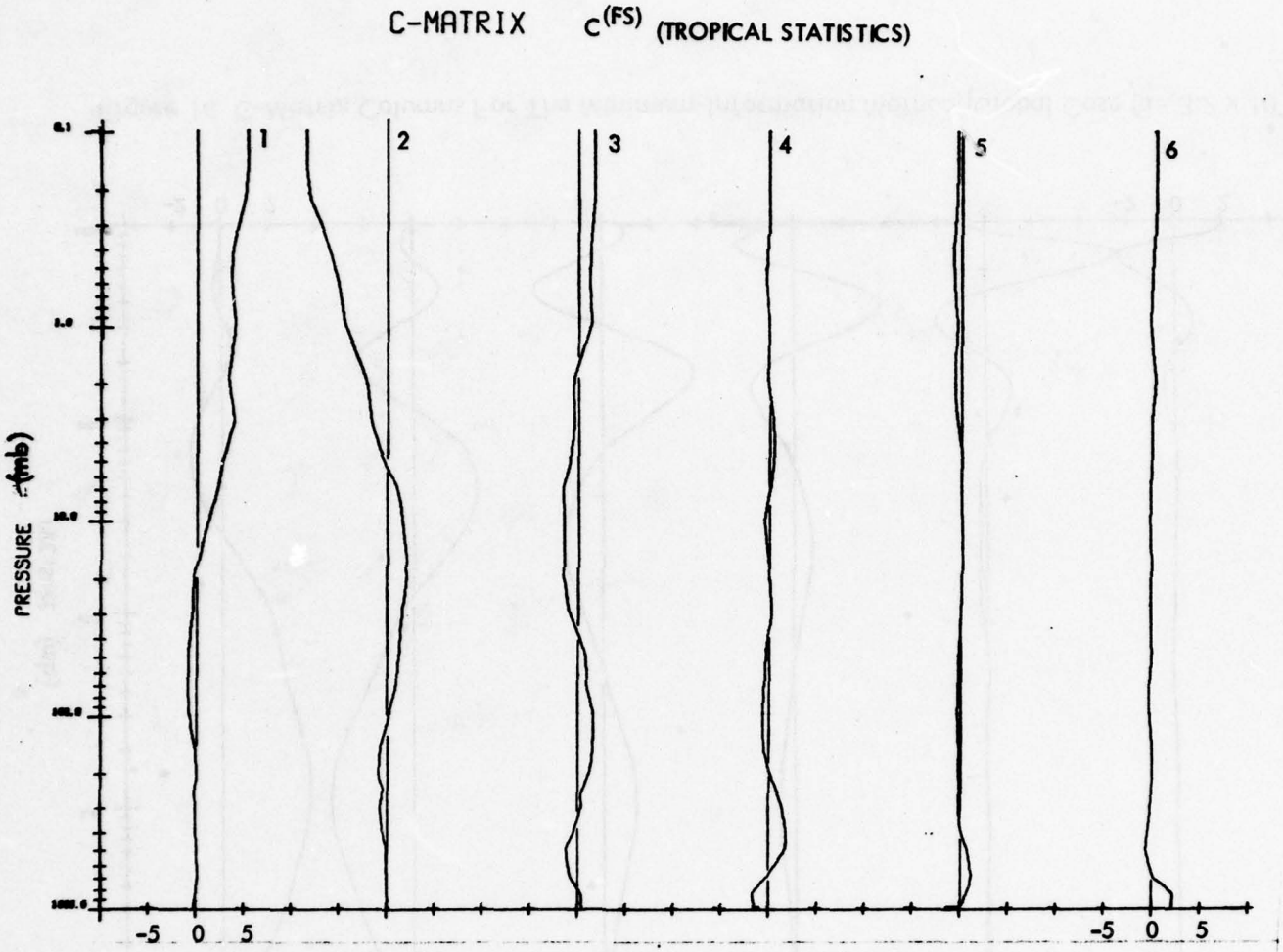

Figure 17 C-Matrix Columns For The Full-Statistics Method Using Tropical Statistics

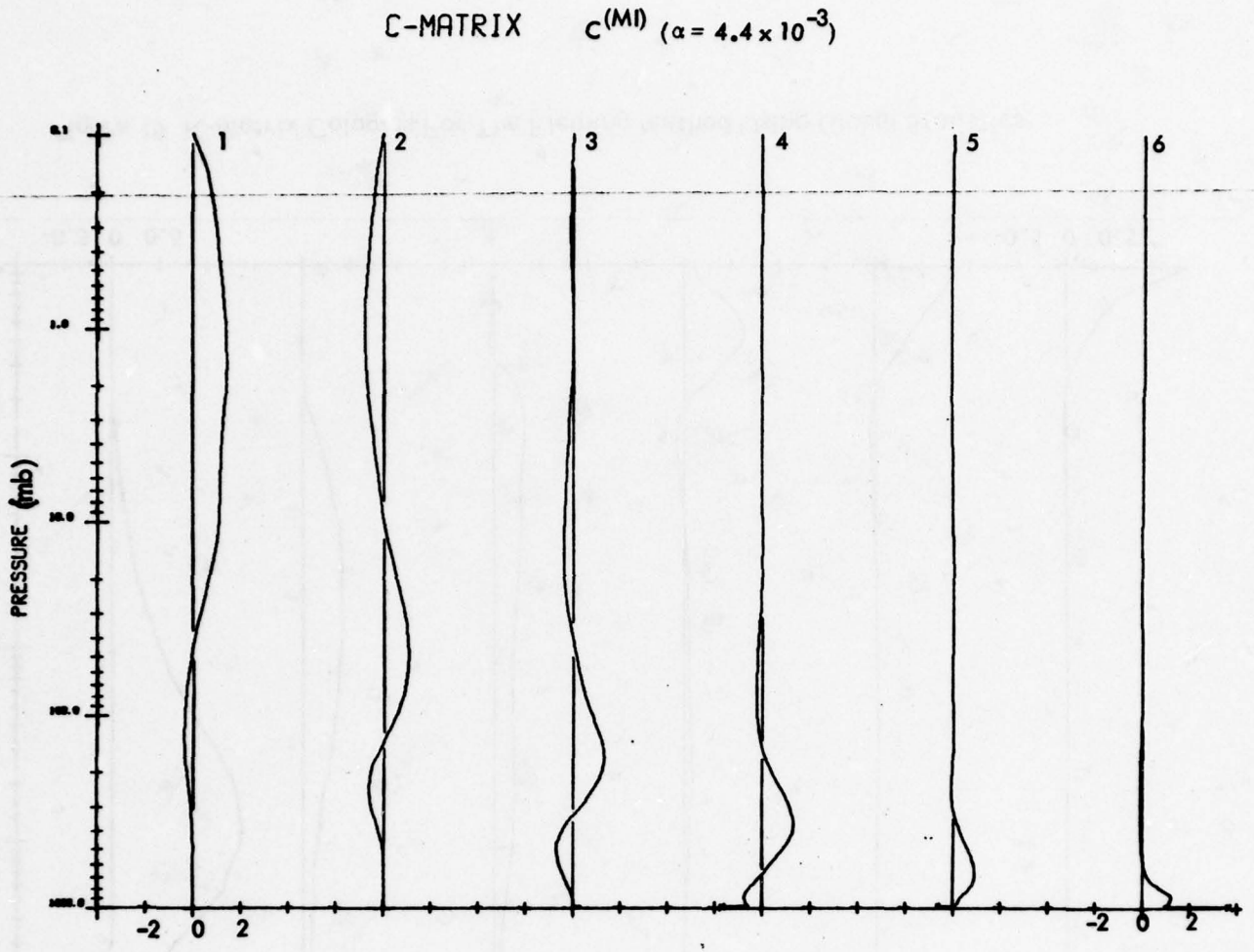

Figure 18 C-Matrix Columns For The Minimum-Information Method, Tropical Case ($\alpha = 4.4 \times 10^{-3}$)

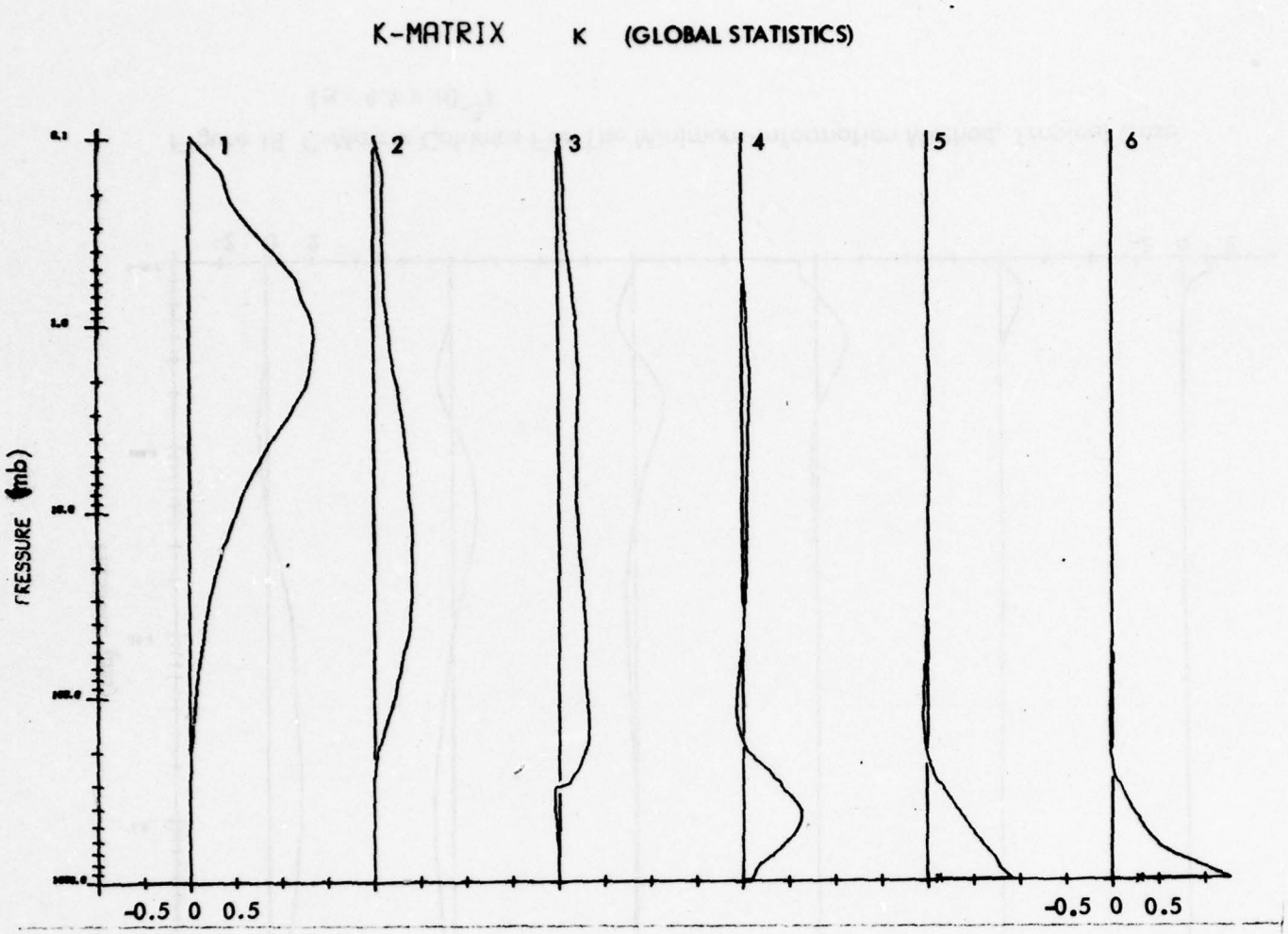

Figure 19 K-Matrix Columns For The Fleming Method Using Global Statistics

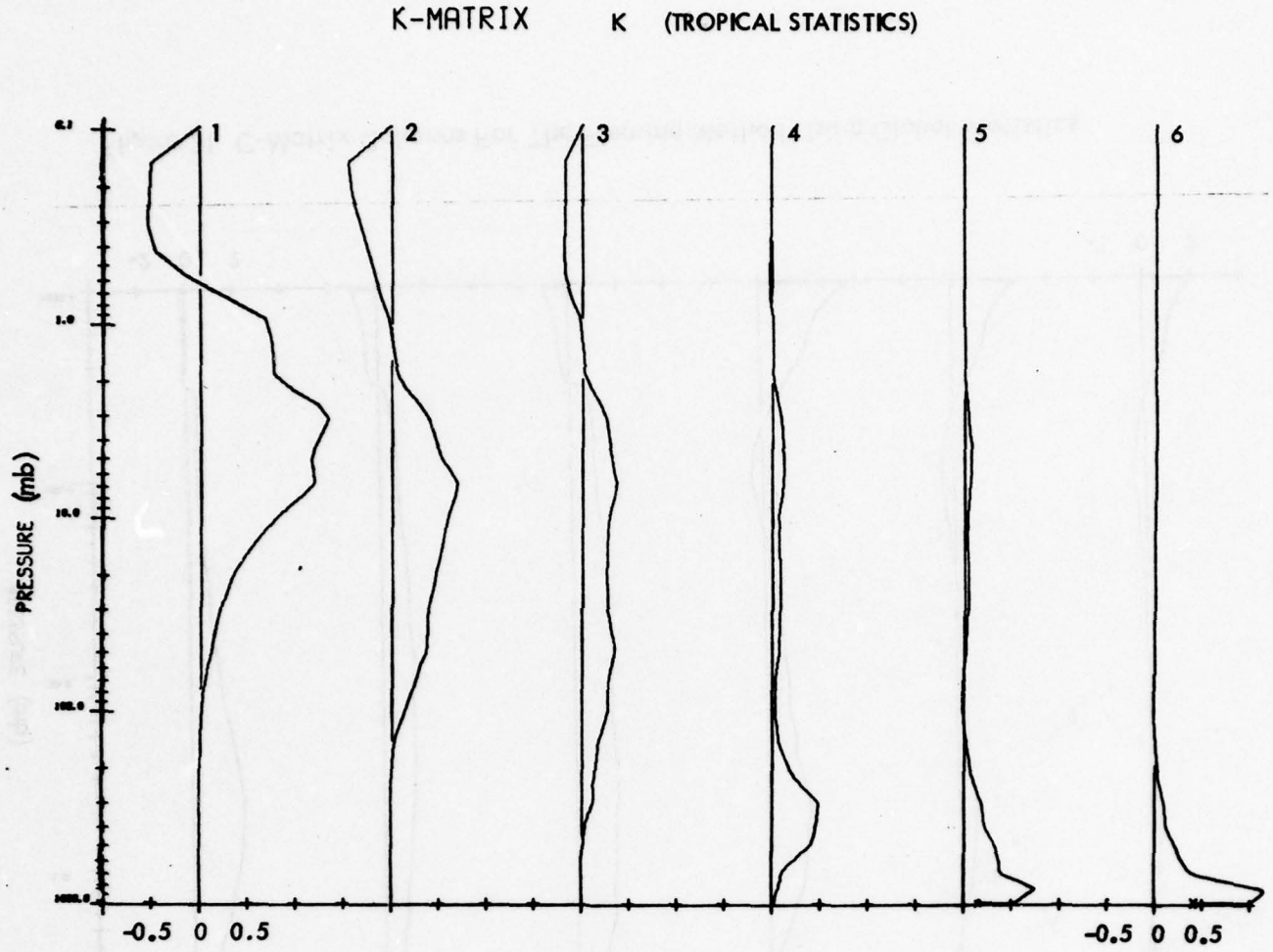

Figure 20 K-Matrix Columns For The Fleming Method Using Tropical Statistics

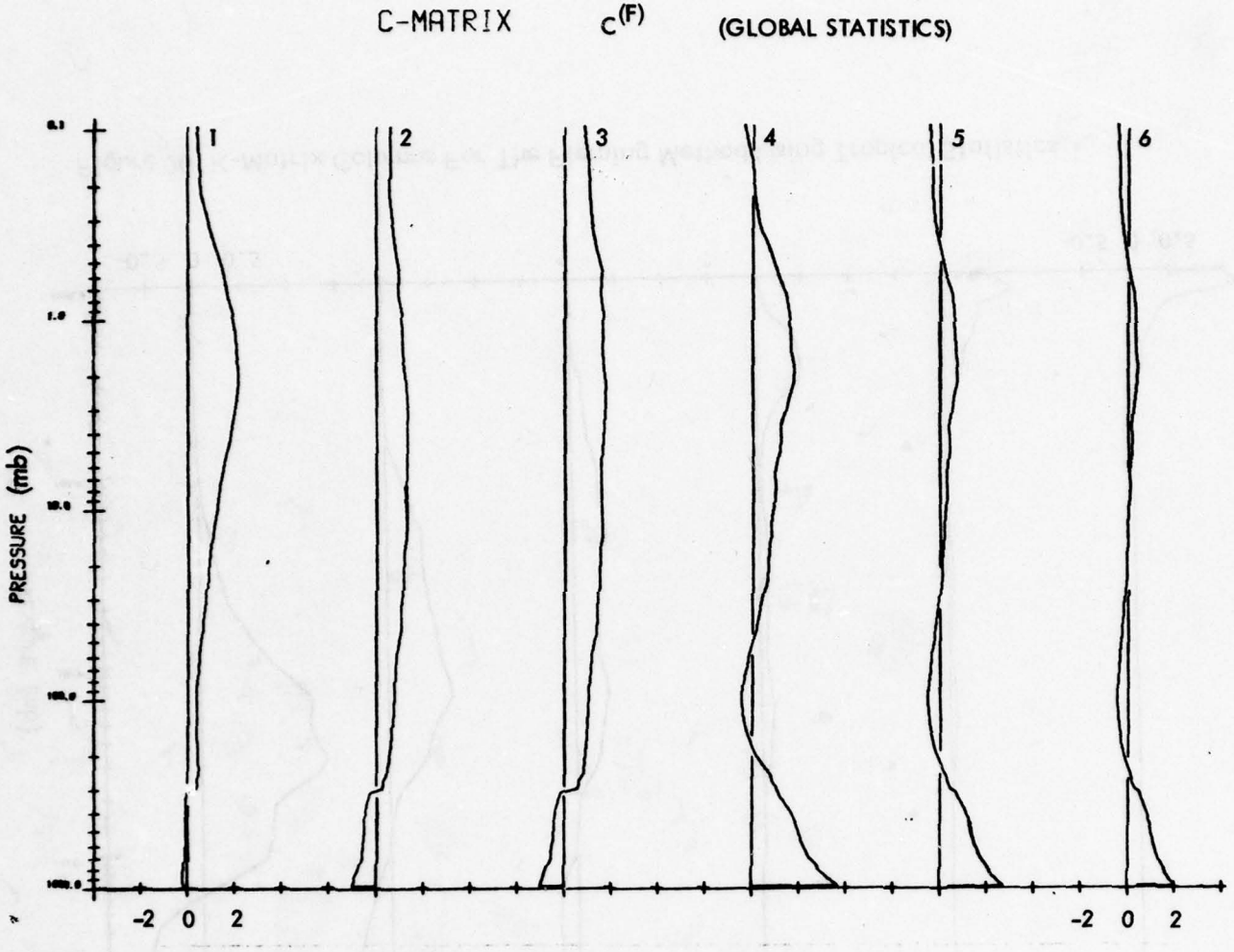

Figure 21 C-Matrix Columns For The Fleming Method Using Global Statistics

Figure 22 C-Matrix Columns For The Fleming Method Using Tropical Statistics

7809-4

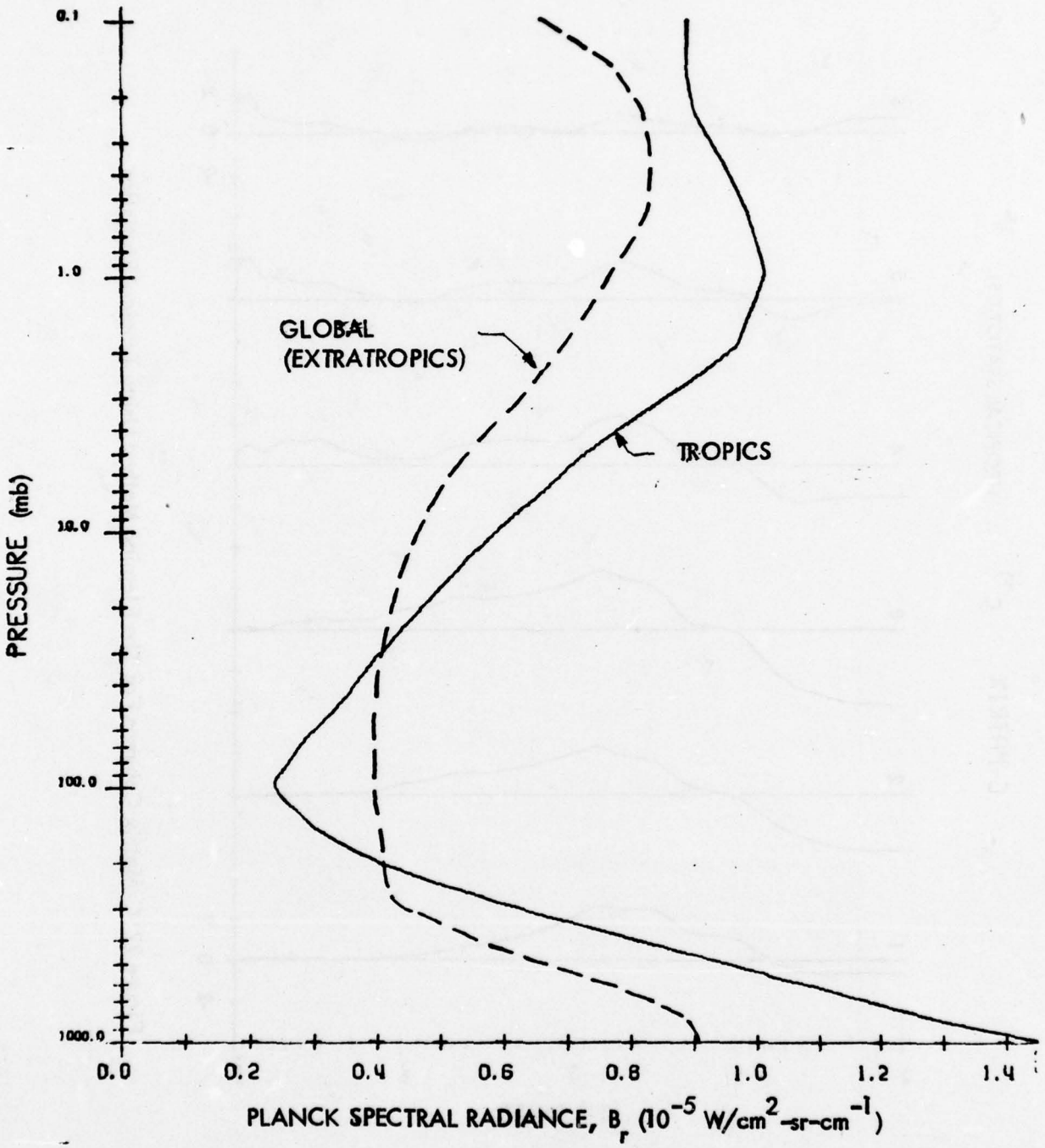

Figure 23 Mean Reference-Frequency Planck Radiance Profiles For The Tropics and Extratropics

column of W or last row of W^T). It may be noted that the C–matrix surface discontinuities would be considerably reduced in the full statistics case if the S matrix exhibited strong correlation between the surface temperature and low-level air temperature, i.e., if S(100, 101) ≅ S(101, 101). However, since surface temperature data was not available with the radiosonde data, we assumed no correlation between the surface and any other level. That is, we set S(k, 101) = 0; k = 1, 2, . . . 100 and S(101, 101) = S (100, 100).

Figure 17 applies to the full-statistics model, tropical case, and Figure 18 to the minimum information model, tropical case. As expected, the C–matrix columns are smoother (and display smaller amplitude modes) than in the extratropical cases. It is interesting that the C–matrix for the full-statistics tropical case (Figure 17), which was computed from 175 radiosonde profiles, does not display any sharp structure near the tropopause (100–mb) level. Apparently, it is the gradients in the Channel 1 and Channel 2 columns and the modal peak in the Channel 3 column near 100 mb that can effect a sharpening or blunting of the mean tropical guess profile, shown in Figure 23. The sharpness of the 100–mb tropopause in the mean profile and the lack of sharp features in the C–matrix columns near 100–mb (in both the full-statistics and minimum information cases) shows that the tropopause will always occur at the 100-mb level in the retrieved profiles.

Figures 19 and 20 show the K-matrices computed for the Fleming statistical model using global statistics and tropical statistics, respectively. Note that the matrix columns are 5 to 10 times smaller in amplitude than for the other methods. This is consistent with our observation that the iterative retrieval requires roughly five to ten times more iterations before convergence is achieved. Note also that the K–matrix columns have fewer oscillations than the C–matrix columns of the other methods. This suggests (and simulated retrievals confirm) that the Fleming statistical method is not able to accurately retrieve profiles belonging to a different climatological class than the covariance matrix and the mean profile. On the other hand the method is found to give extremely good results when appropriate statistics are used.

2.6 COMPARISON OF TEMPERATURE RETRIEVALS BY FOUR CLASSES OF RETRIEVAL TECHNIQUE

In this section we compare temperature retrieval errors for the Smith nonlinear method, Fleming statistical method, full-statistics method and minimum information

method. Comparisons are made separately for arctic, midlatitude and tropical cases. When using the last three methods for either arctic or midlatitude cases, we used the mean profile, C–matrices and α value computed from global (extratropical) data; the tropical versions of these quantities were used in tropical retrievals, except where noted. The same guess profiles (global or tropical mean) were used in retrievals by the Smith method. The surface temperature is approximately equal to the air temperature just above the surface in all cases (in both "actual" and guess profiles).

2.6.1 Arctic Cases

The first arctic case (actual temperature profile) is a 7/22/69 radiosonde at Thule. Figures 24 through 27 show the retrieval results, and Figure 28 compares the errors for the four methods. The Smith and Fleming statistical methods give the best overall temperature retrievals; the latter yields smaller error over the tropopause region, but introduces a small amount of false structure at the bottom of the tropopause and results in a much larger error in surface temperature. Agreement between the Fleming solution and the actual profile between 0.5 mb and 10 mb is fortuitous.

A portion of the surface temperature error in the Fleming and full-statistics methods may be attributed to the fact that we could not obtain data representing the correlation between surface temperature and the temperature at different atmospheric levels. To examine the effects of possible correlations we recomputed the S– and C–matrices for the F and FS methods using the assumption that the surface temperature is equal to the air temperature just above the surface, (i.e., we set the last row and last column of S equal to the 100th row and 100th column). This assumption eliminates the surface discontinuity in the full-statistics solution and reduces it in the Fleming method. The corresponding temperature retrievals contained the errors shown by the second and third curves in Figure 29 (the first and fourth curves are the same as Figure 28). Note that the error at the surface is now roughly the average of the previously calculated errors at the surface and just above the surface. A similar averaging effect extends up to approximately 800 mb. Note also that the Fleming solution is now slightly better than the Smith solution, i.e., is the best of the four retrievals.

One can generalize on the results shown in Figures 28 and 29: errors in inferred surface temperature generally have compensating errors at some slightly higher altitude

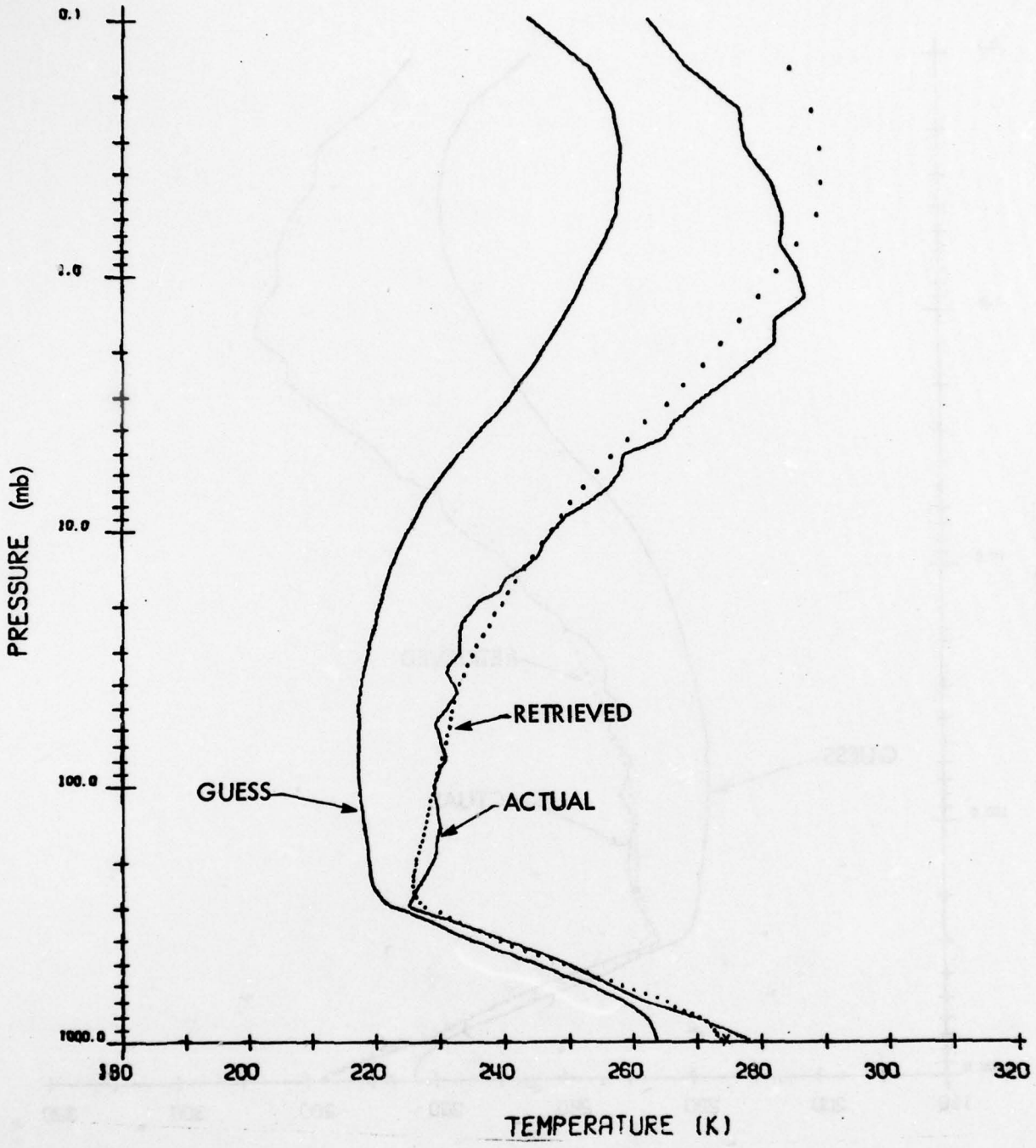

Figure 24 Simulated Retrieval by the Smith Method. Actual Profile is Thule 7/22/69 Radiosonde.

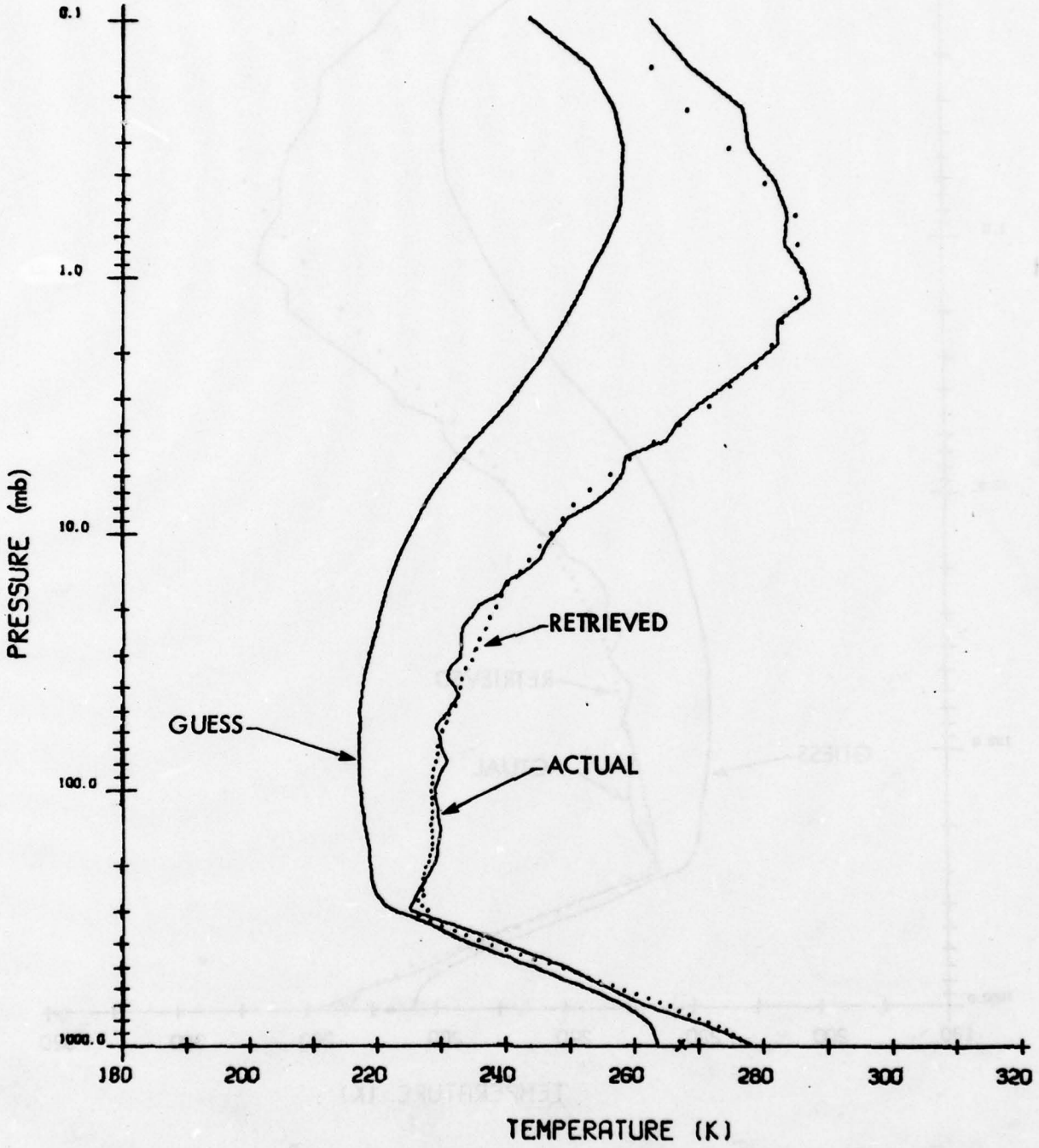

Figure 25 Simulated Retrieval by the Fleming Method. Actual Profile is Thule 7/22/69 Radiosonde.

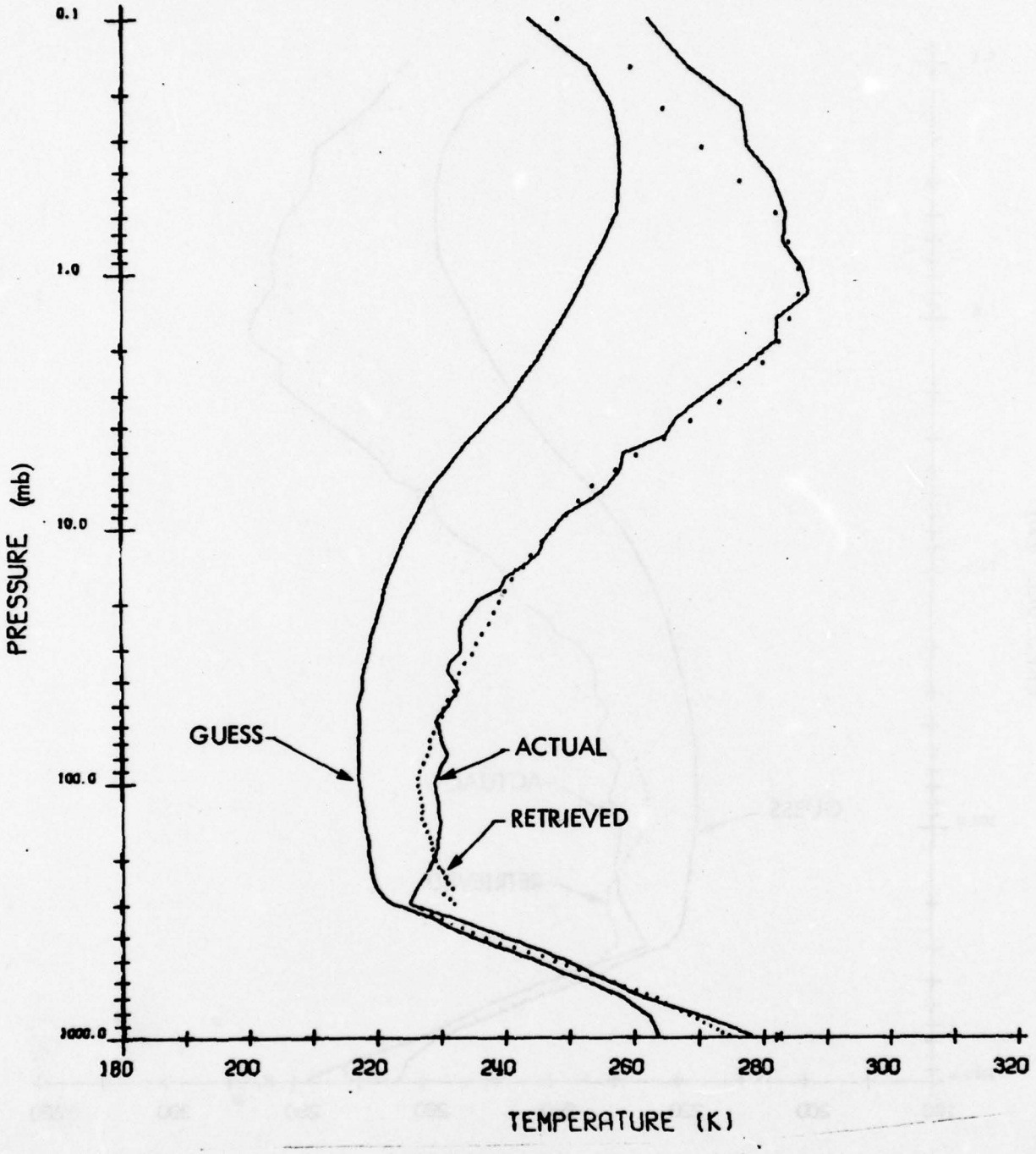

Figure 26 Simulated Retrieval by the Full Statistics Method. Actual Profile is Thule 7/22/69 Radiosonde.

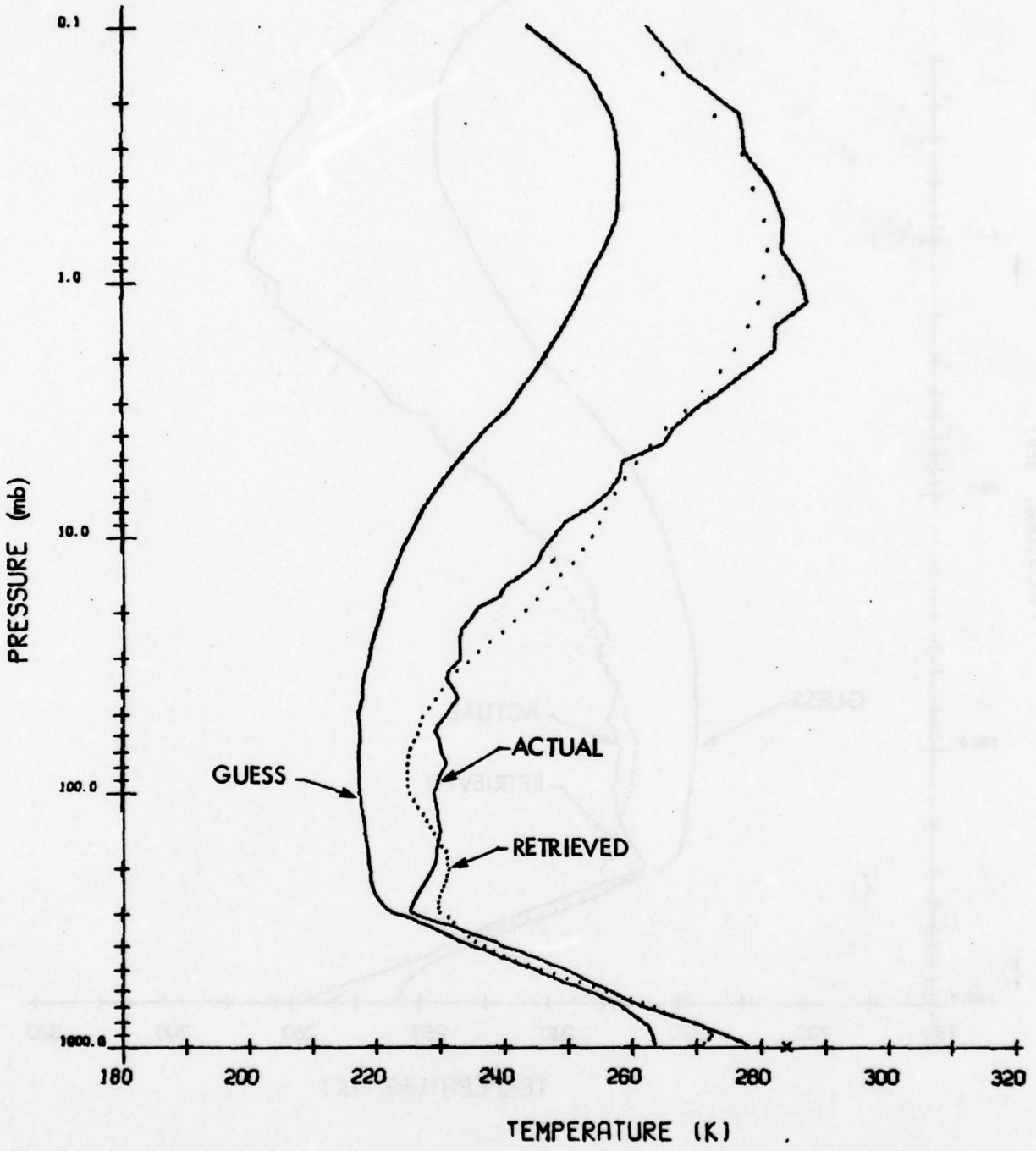

Figure 27 Simulated Retrieval by the Minimum-Information Method. Actual Profile is Thule 7/22/69 Radiosonde.

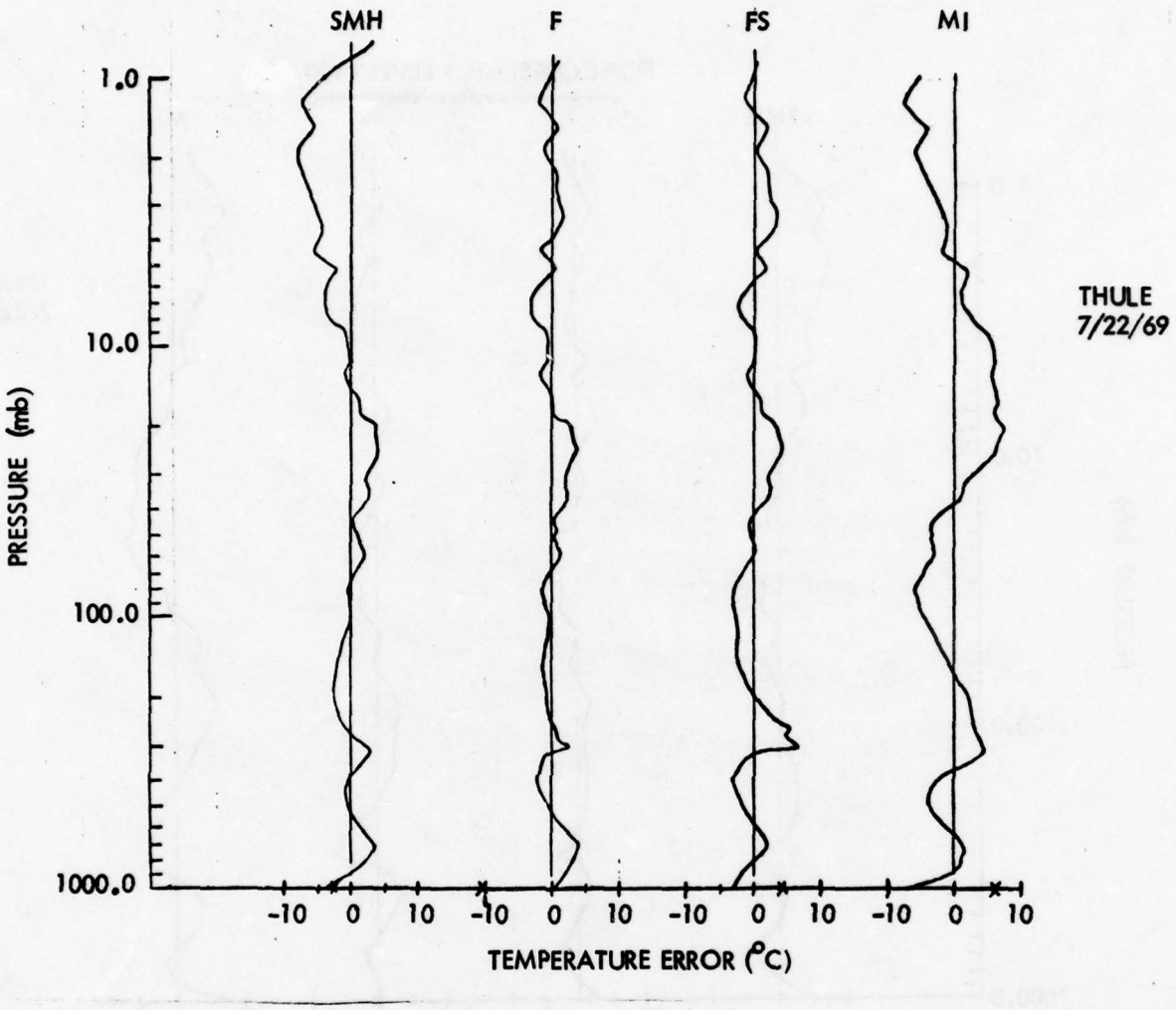

Figure 28 Compariosn of Retrieval Errors for the Four Methods.
Thule 7/22/69.

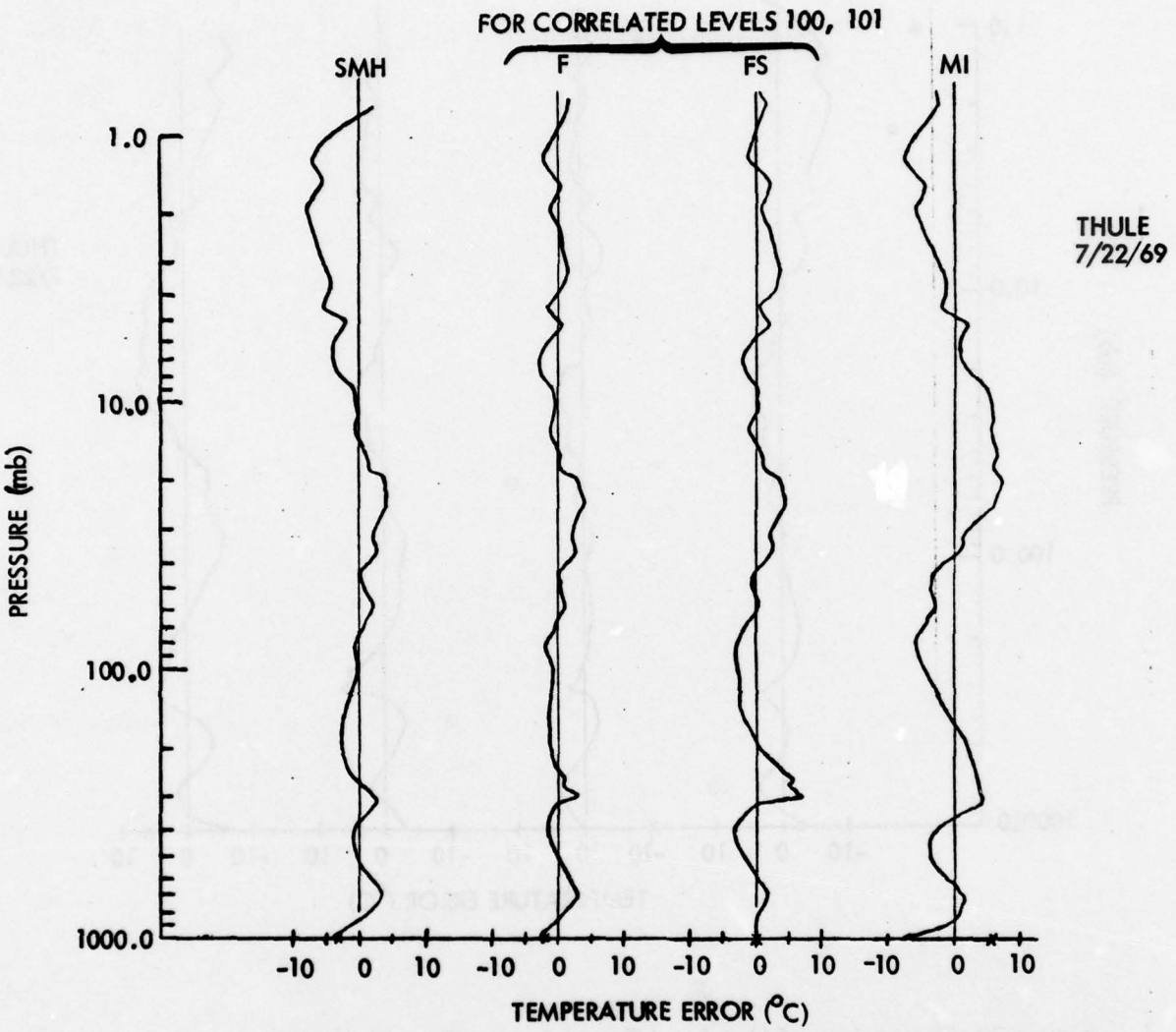

Figure 29 Comparison of Retrieval Errors When Levels 100, 101 are Assumed Correlated in the F and FS Methods. Thule 7/22/69.

between the surface and approximately 700 mb. The use of additional very transparent channels to accurately determine the surface temperature would improve considerably the accuracy of the retrieved profiles below 700 mb, especially if there are statistical correlations between the surface temperature and low-level air temperature. To the extent that data is available for defining these correlations, it should be used in computing the S– and C–matrices.

The second arctic case is a 11/16/65 radiosonde at Heiss Island (latitude 81° North). Figures 30 through 33 show the retrieval results, and Figure 34 compares the errors for the four methods. The Smith and full-statistics methods give the best results for this case. If the temperatures corresponding to levels 100 and 101 are assumed perfectly correlated, the errors in the retrieved profiles are as shown in Figure 35. Then the Fleming method gives the best result in our judgment, but it is only marginally better than the Smith or minimum-information solutions.

2.6.2 Midlatitude Cases

The first midlatitude case is a 2/17/75 radiosonde at Point Mugu. Figures 36 through 39 show the retrieval results, and Figure 40 compares the errors for the four methods. In this case the full-statistics method gives the best result, with the Smith solution running a close second. Figure 41 shows that when the surface temperature is assumed correlated with the above-surface air temperature, the Fleming solution is best and the full-statistics solution is second best.

The second midlatitude case is a 10/22/66 radiosonde at West Geirinish (latitude 57° North). Figures 42 through 45 show the retrieval results, and Figure 46 compares the errors of the four methods. The errors obtained assuming no surface discontinuity are shown in Figure 47. The full-statistics method gives the best retrieval in the first case. It also gives the best retrieval in the second case, but then it is only slightly better than the Fleming method.

2.6.3 Tropical Cases

The two tropical cases are a 2/27/75 radiosonde at Kwajalein and a 5/8/67 radiosonde at Fort Sherman. In both cases the four methods give nearly identical retrievals, and those obtained by the Fleming and full-statistics methods are virtually unaffected

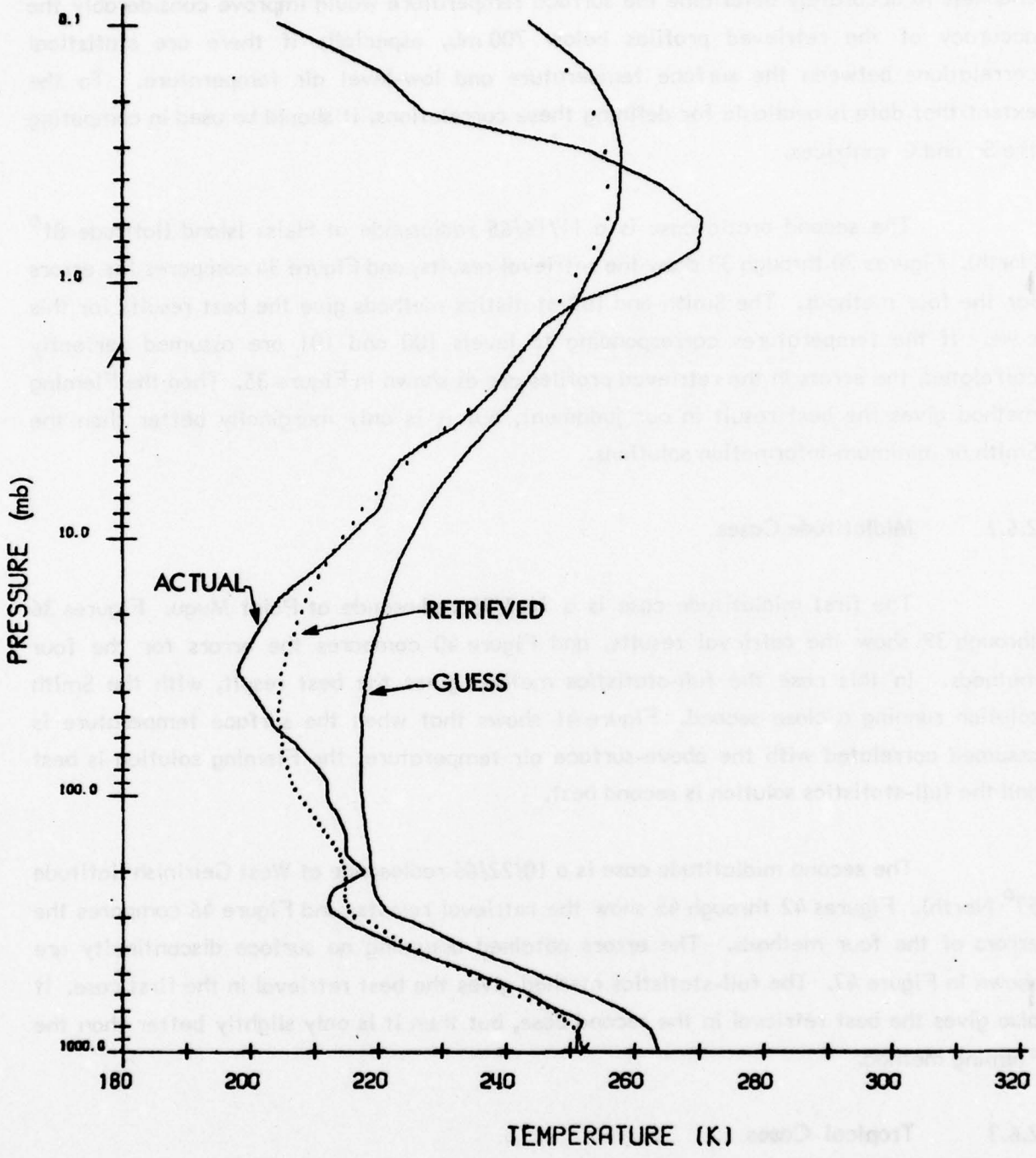

Figure 30 Simulated Retrieval by the Smith Method. Actual Profile is Heiss Island 11/16/65 Radiosonde.

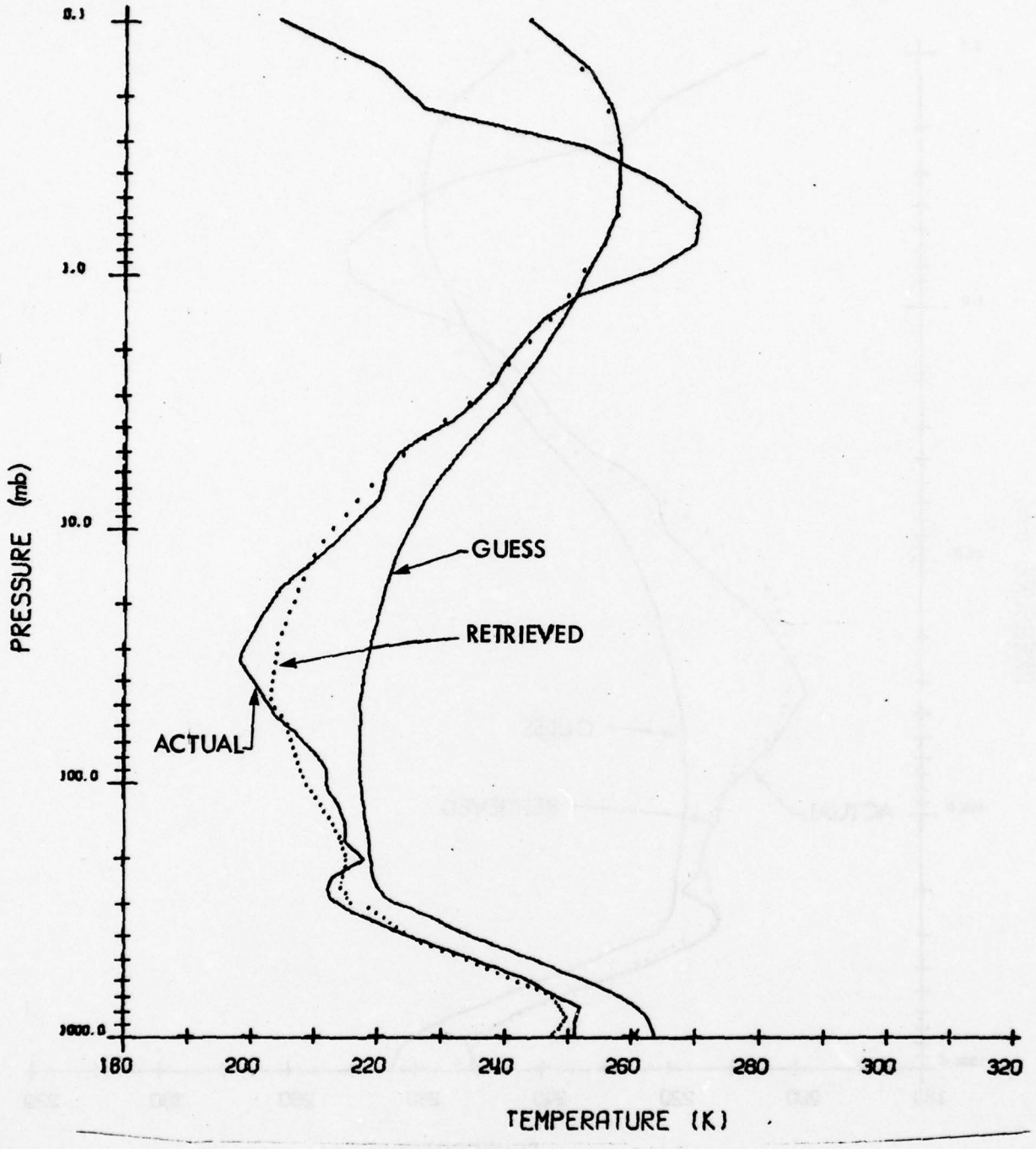

Figure 31 Simulated Retrieval by the Fleming Method. Actual Profile is Heiss Island 11/16/65 Radiosonde.

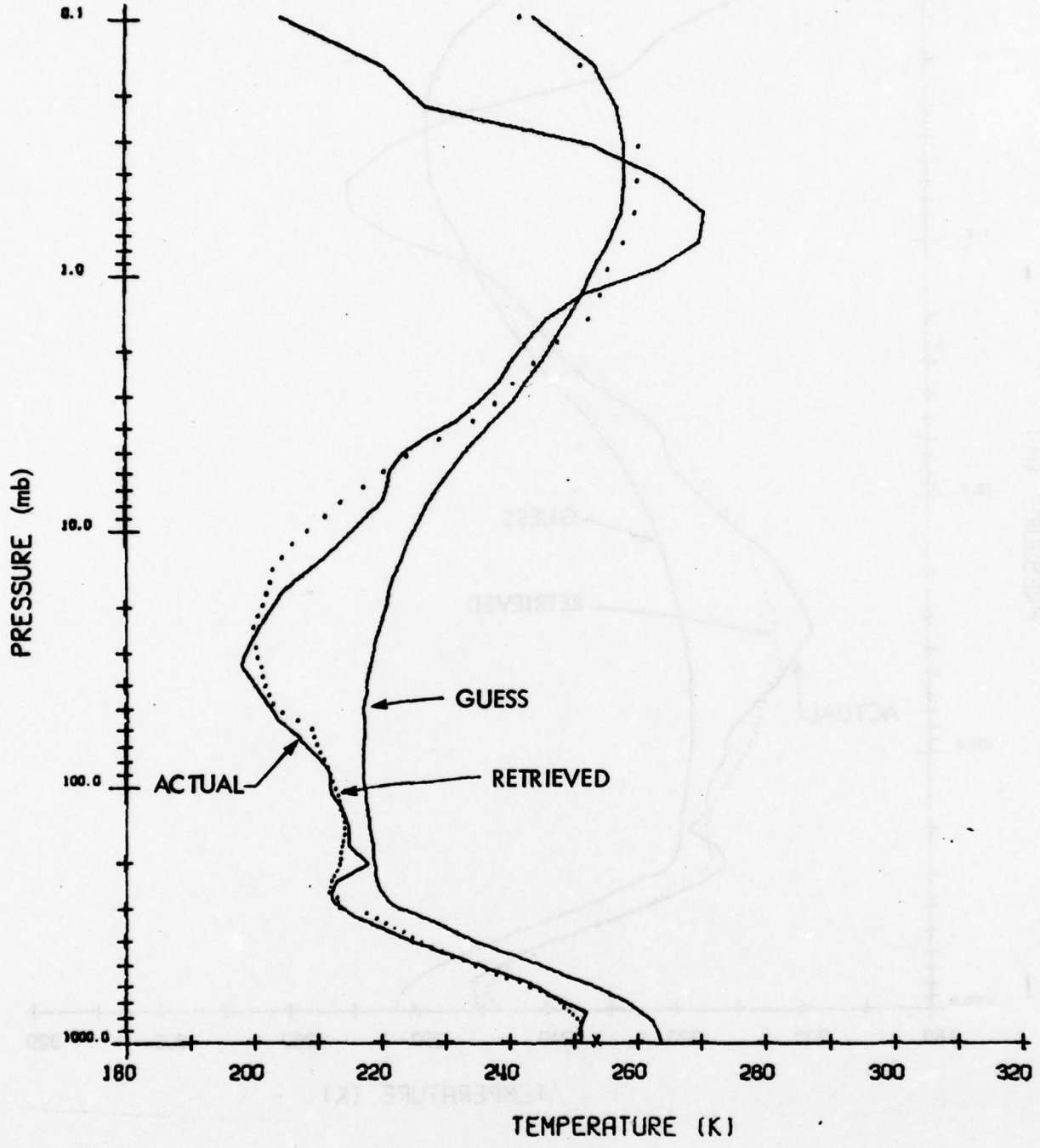

Figure 32 Simulated Retrieval by the Full-Statistics Method. Actual Profile is Heiss Island 11/16/65 Radiosonde.

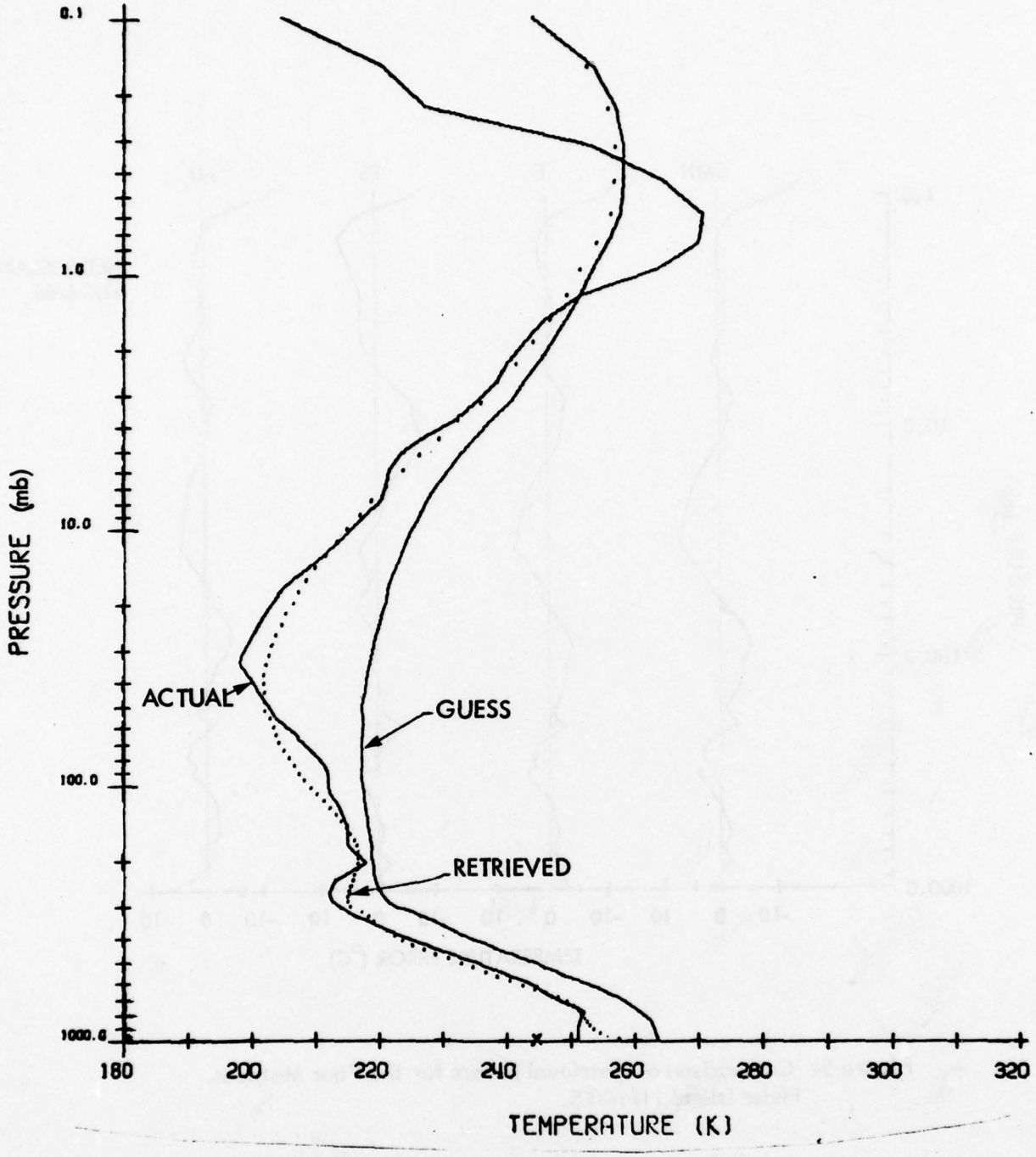

Figure 33 Simulated Retrieval by the Minimum-Information Method.
Actual Profile is Heiss Island 11/16/65 Radiosonde.

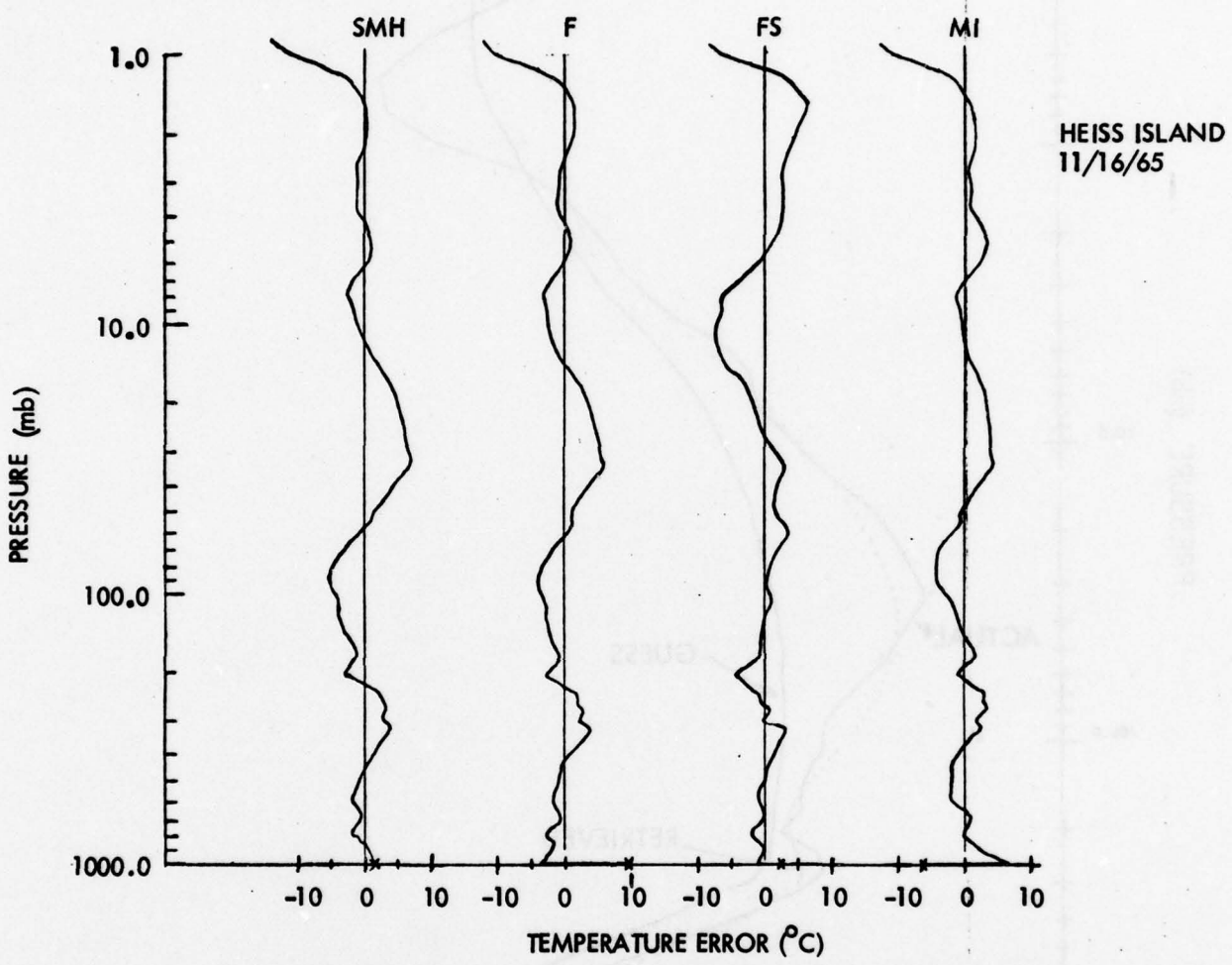

Figure 34 Comparison of Retrieval Errors for the Four Methods. Heiss Island 11/16/65.

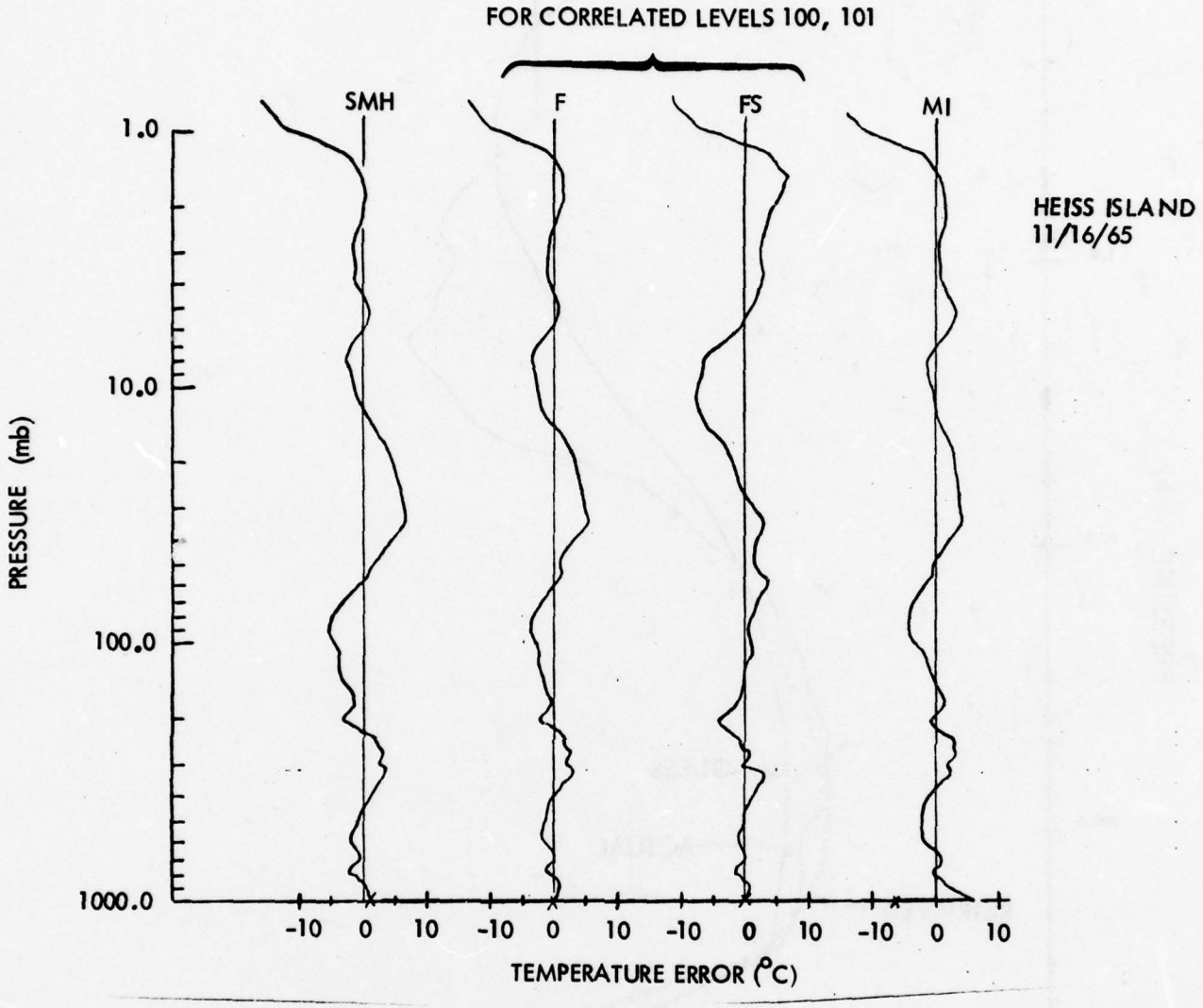

Figure 35 Comparison of Retrieval Errors when Levels 100, 101 are Assumed Correlated in the F and FS methods. Heiss Island 11/16/65.

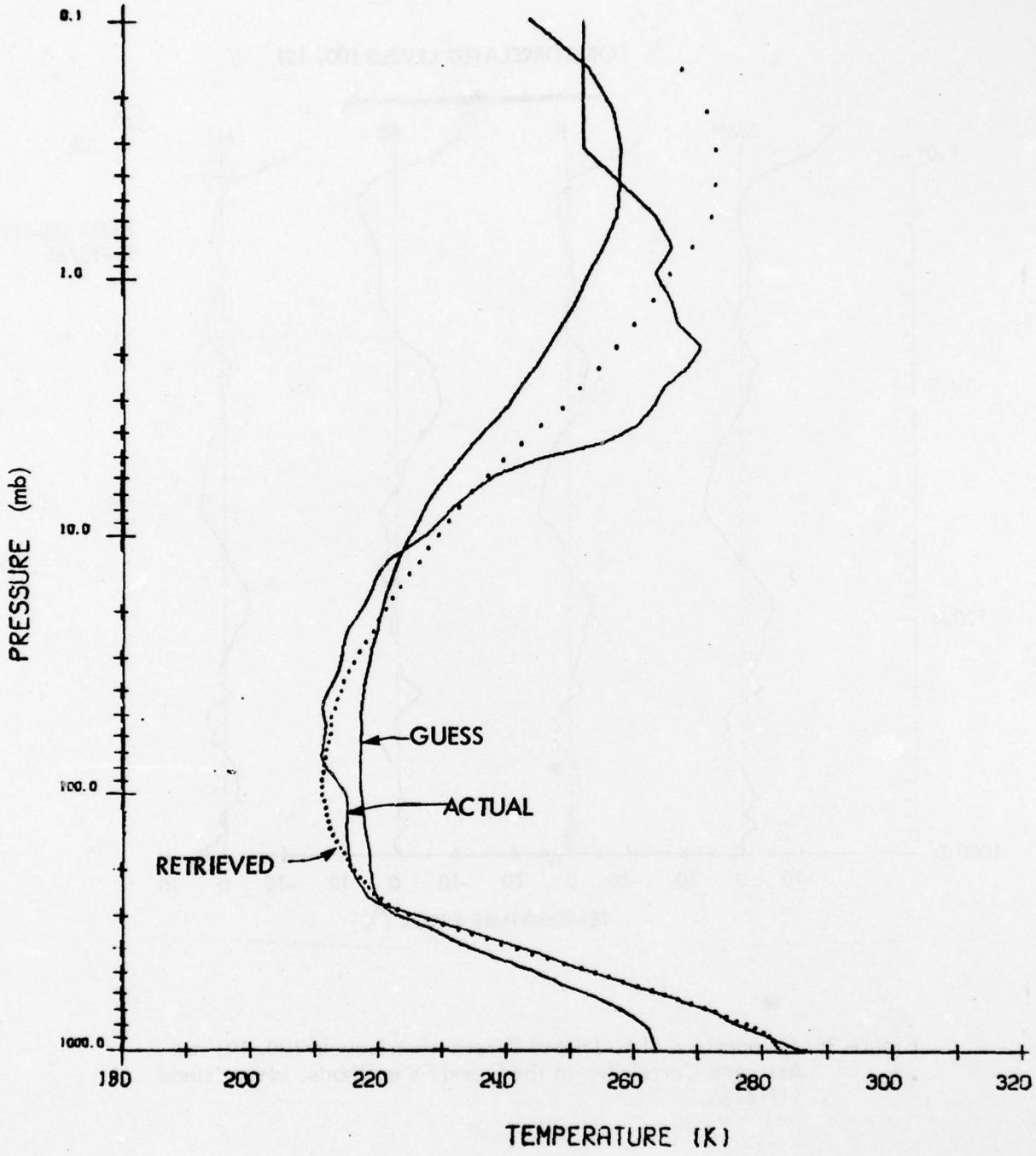

Figure 36 Simulated Retrievals by the Smith Method. Actual Profile is Point Mugu 2/17/75 Radiosonde.

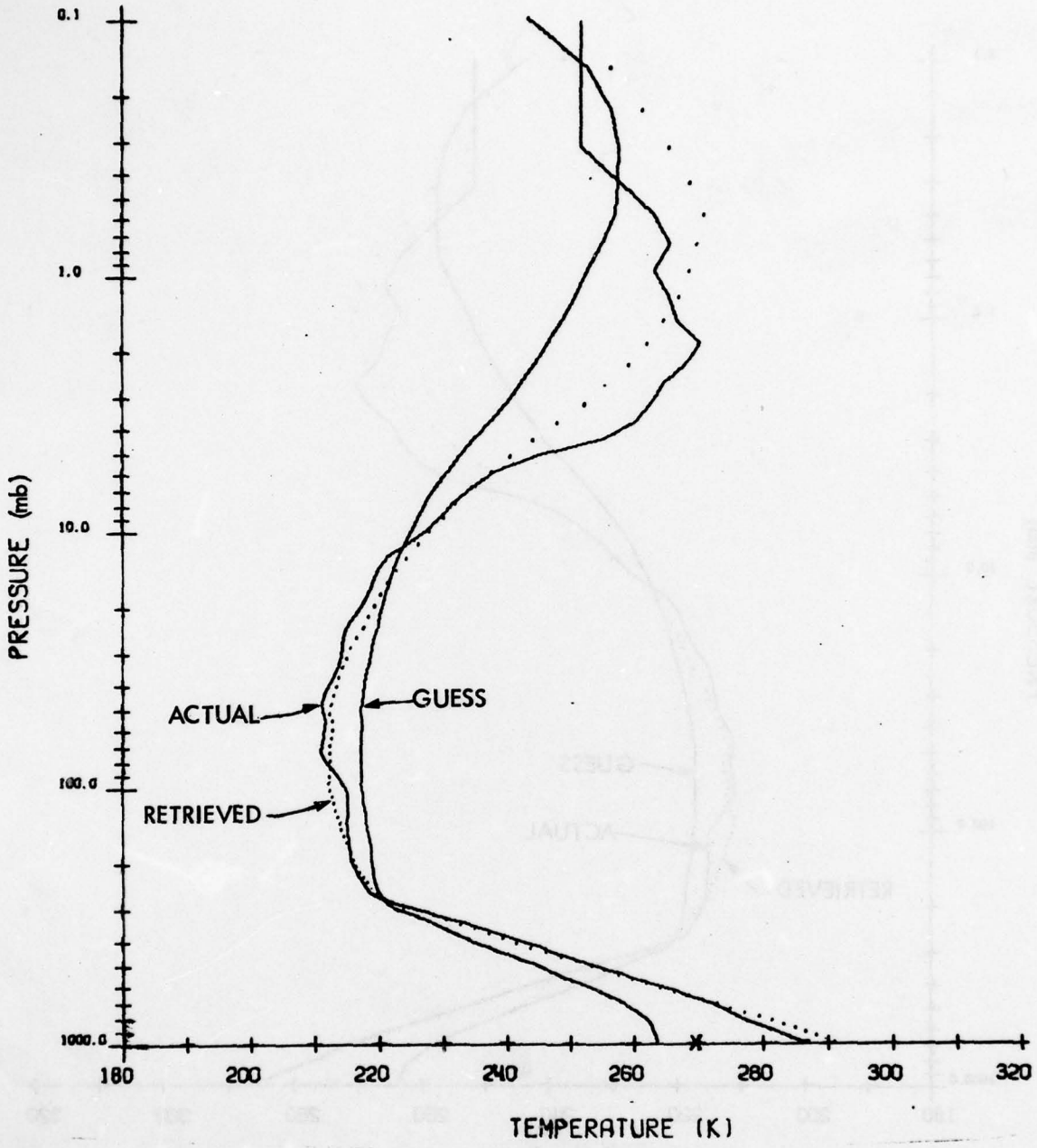

Figure 37 Simulated Retrievals by the Fleming Method. Actual Profile is Point Mugu 2/17/75 Radiosonde.

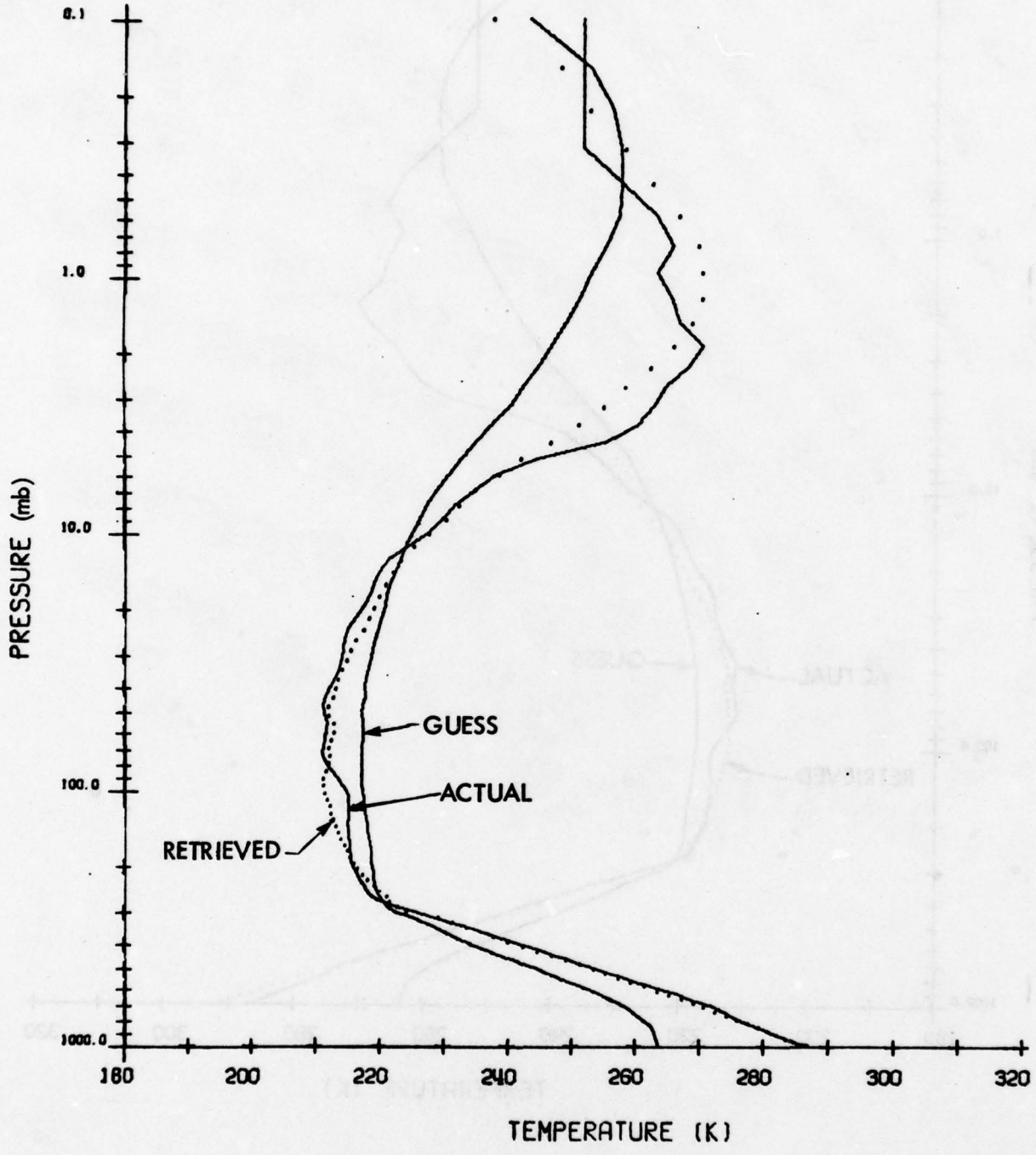

Figure 38 Simulated Retrievals by the Full-Statistics Method. Actual Profile is Point Mugu 2/17/75 Radiosonde.

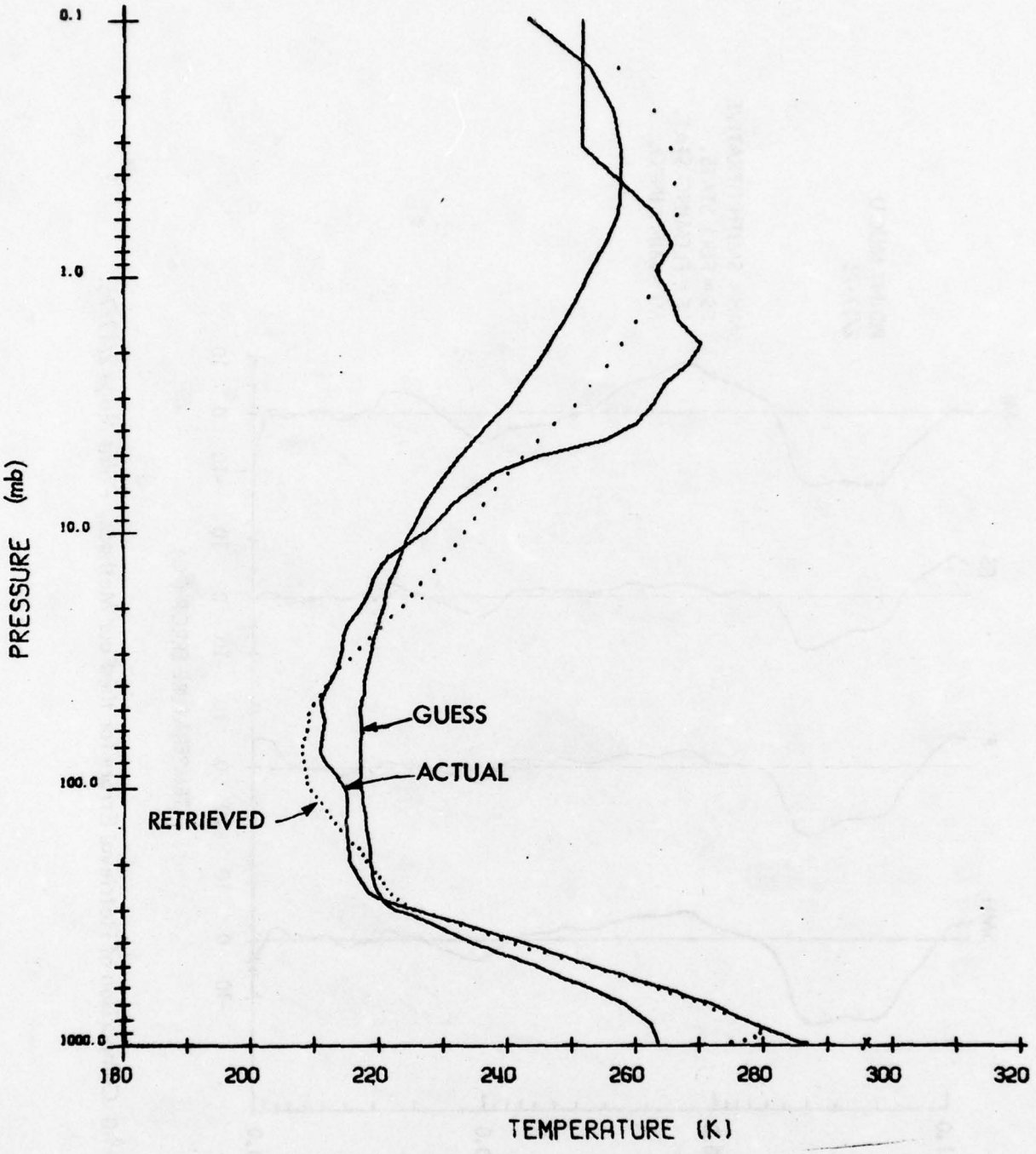

Figure 39 Simulated Retrievals by the Minimum-Information Method. Actual Profile is Point Mugu 2/17/75 Radiosonde.

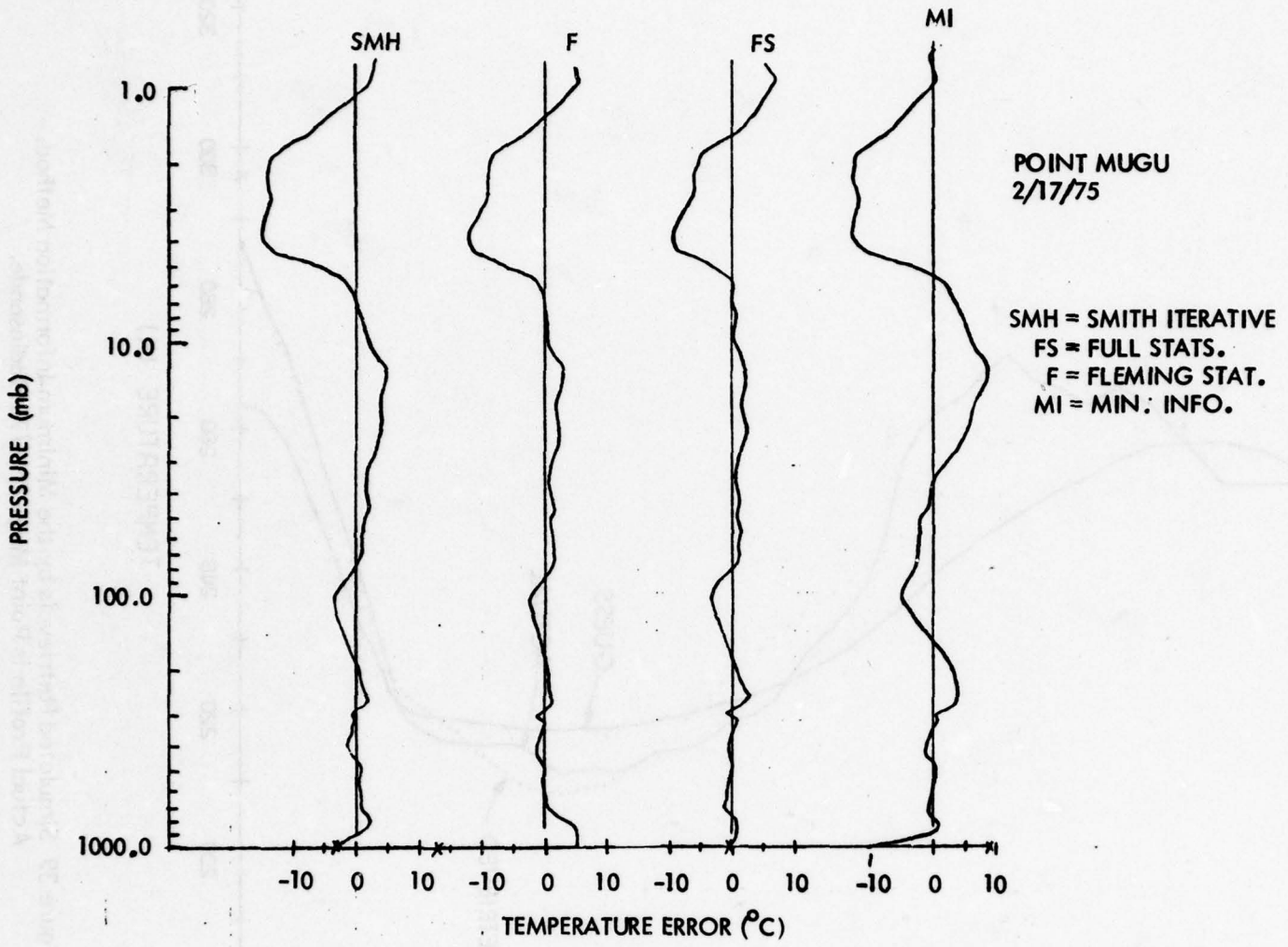

Figure 40 Comparison of Retrieval Errors for the Four Methods. Point Mugu 2/17/75.

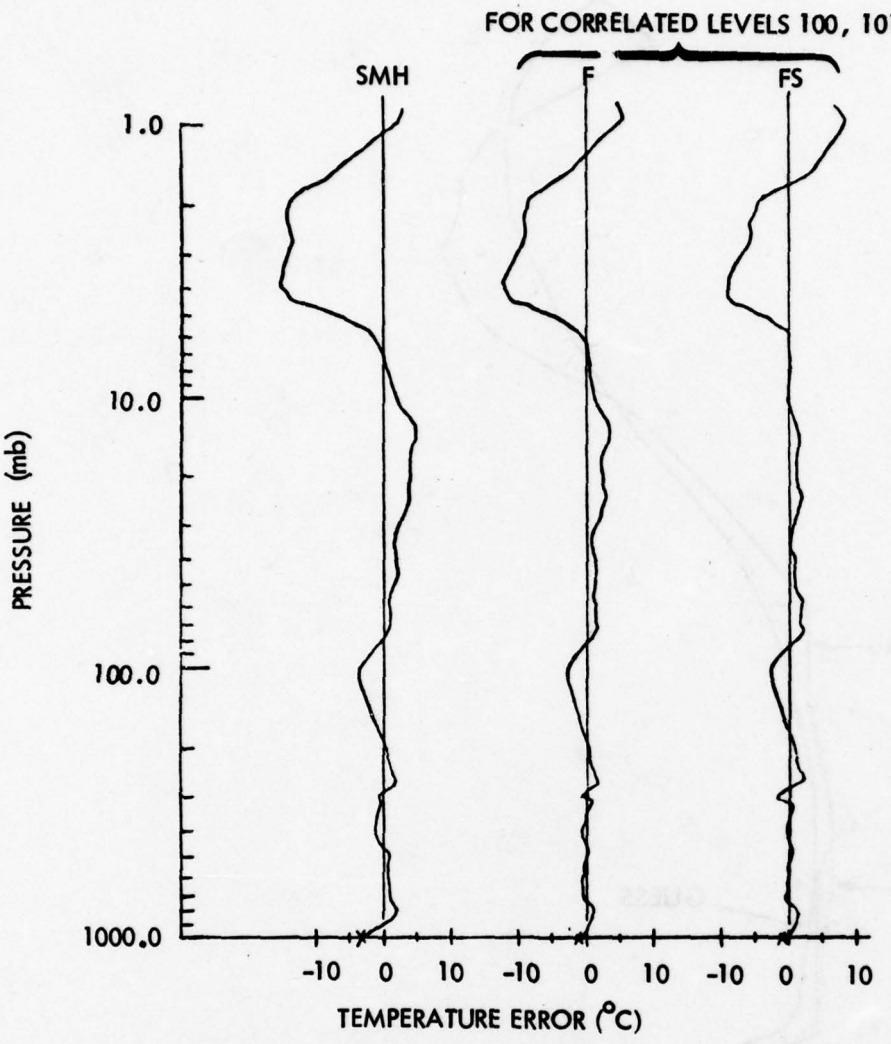

Figure 41 Comparison of Retrieval Errors when Levels 100, 101 are Assumed Correlated in the F and FS Methods. Point Mugu 2/17/75.

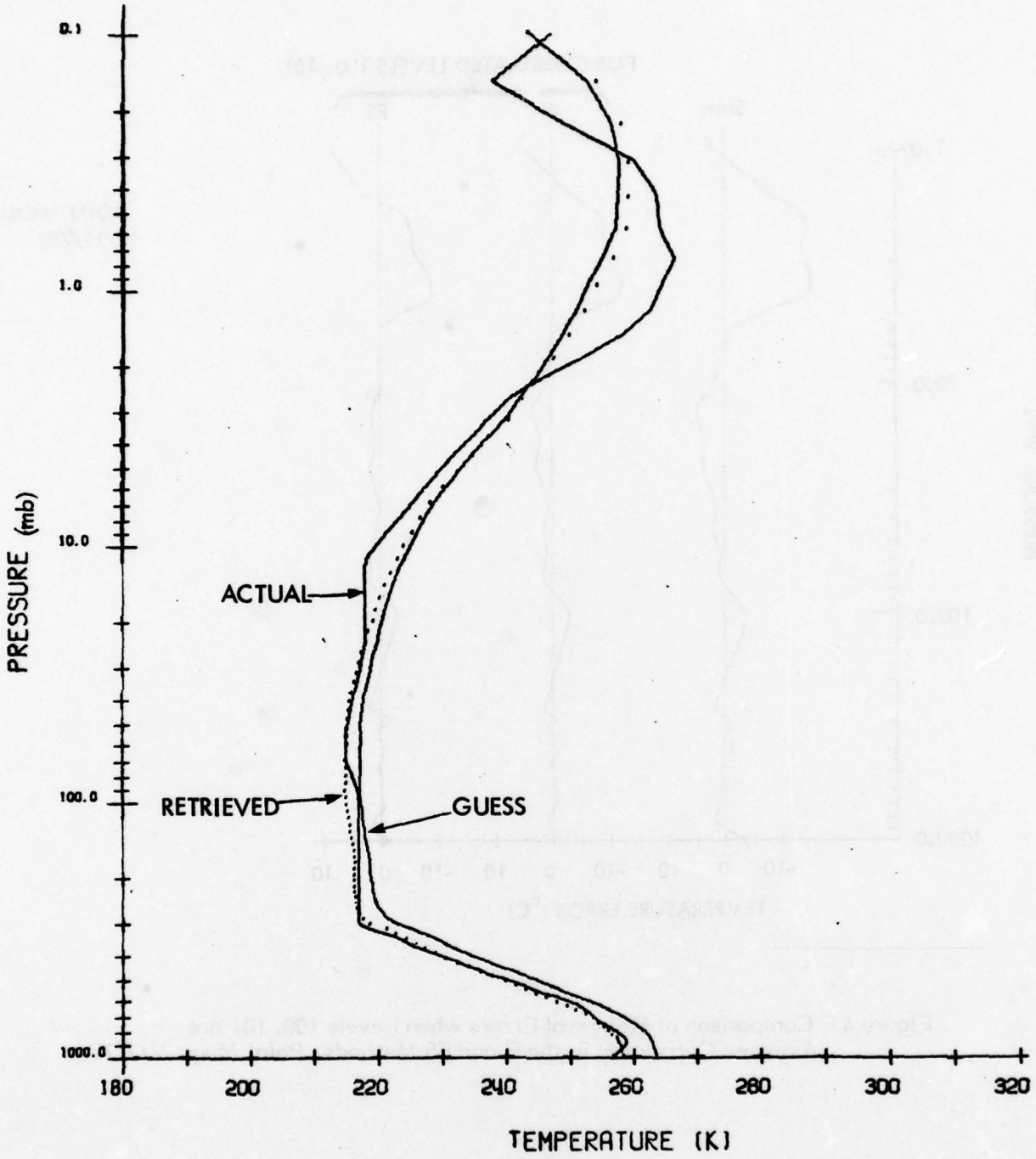

Figure 42 Simulated Retrieval by the Smith Method. Actual Profile is West Geirinish 10/22/66 Radiosonde.

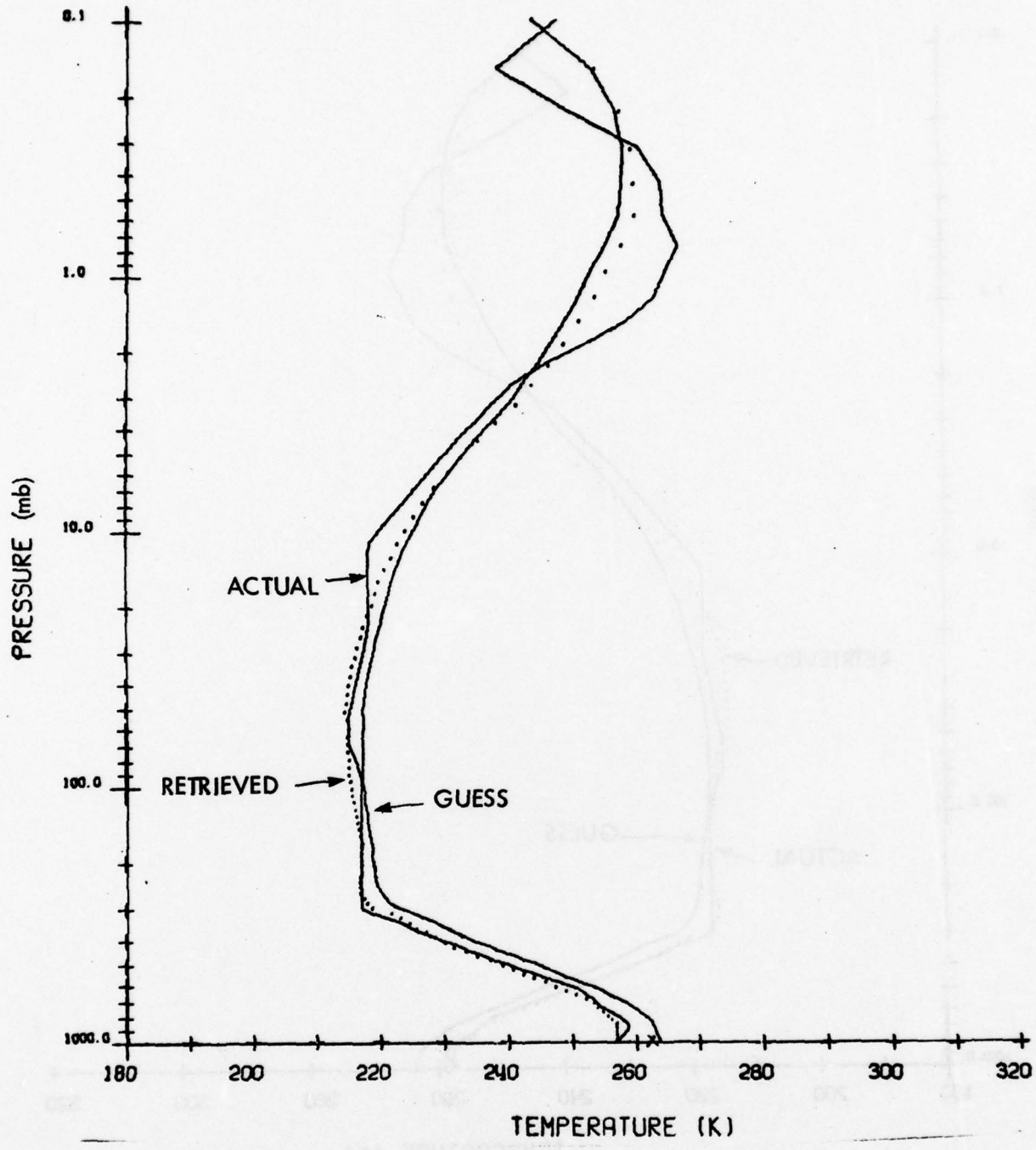

Figure 43 SimulatedRetrieval by the Fleming Method. Actual Profile is West Geirinish 10/22/66 Radiosonde.

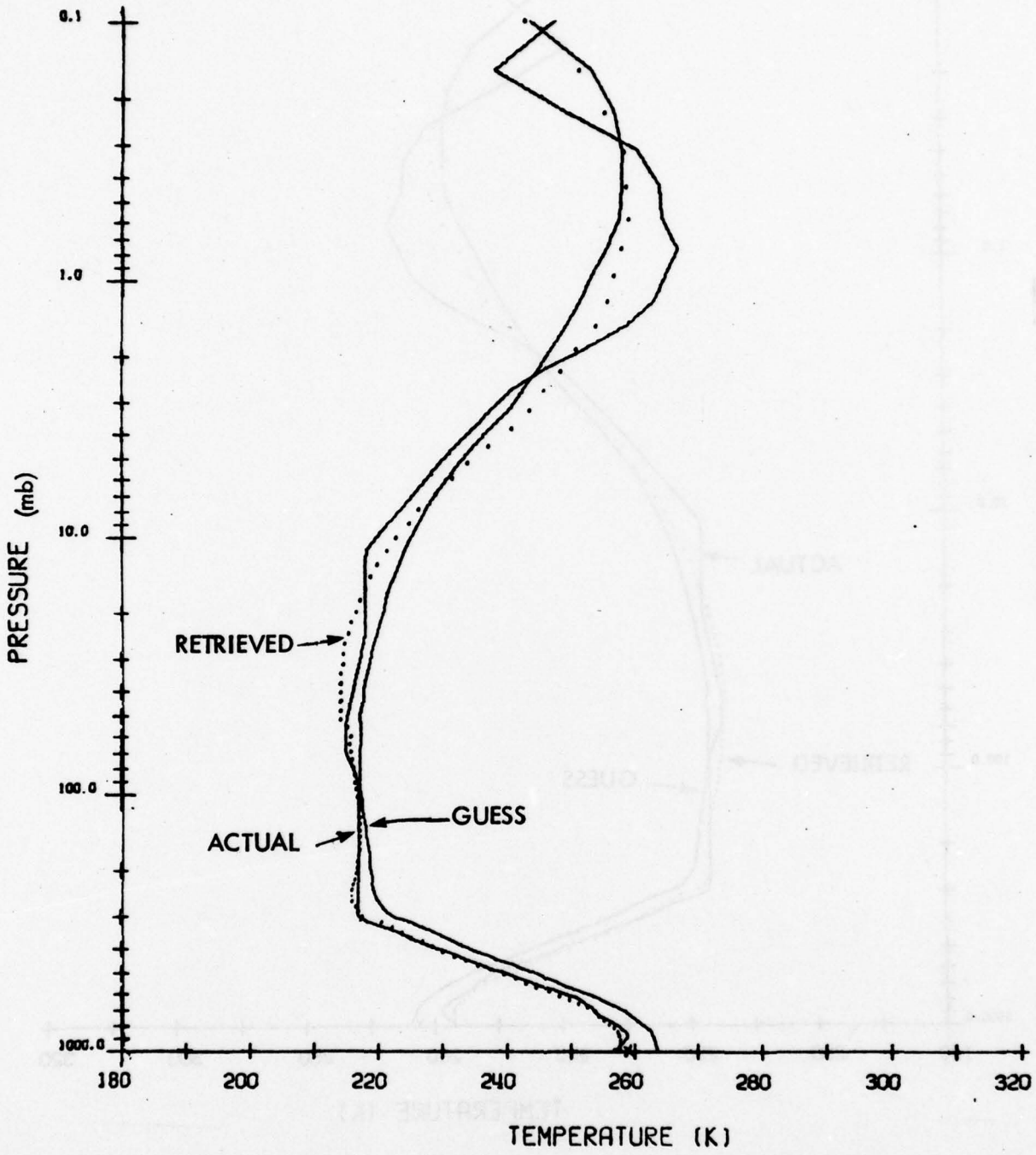

Figure 44 Simulated Retrieval by the Full-Statistics Method. Actual Profile is West Geirinish 10/22/66 Radiosonde.

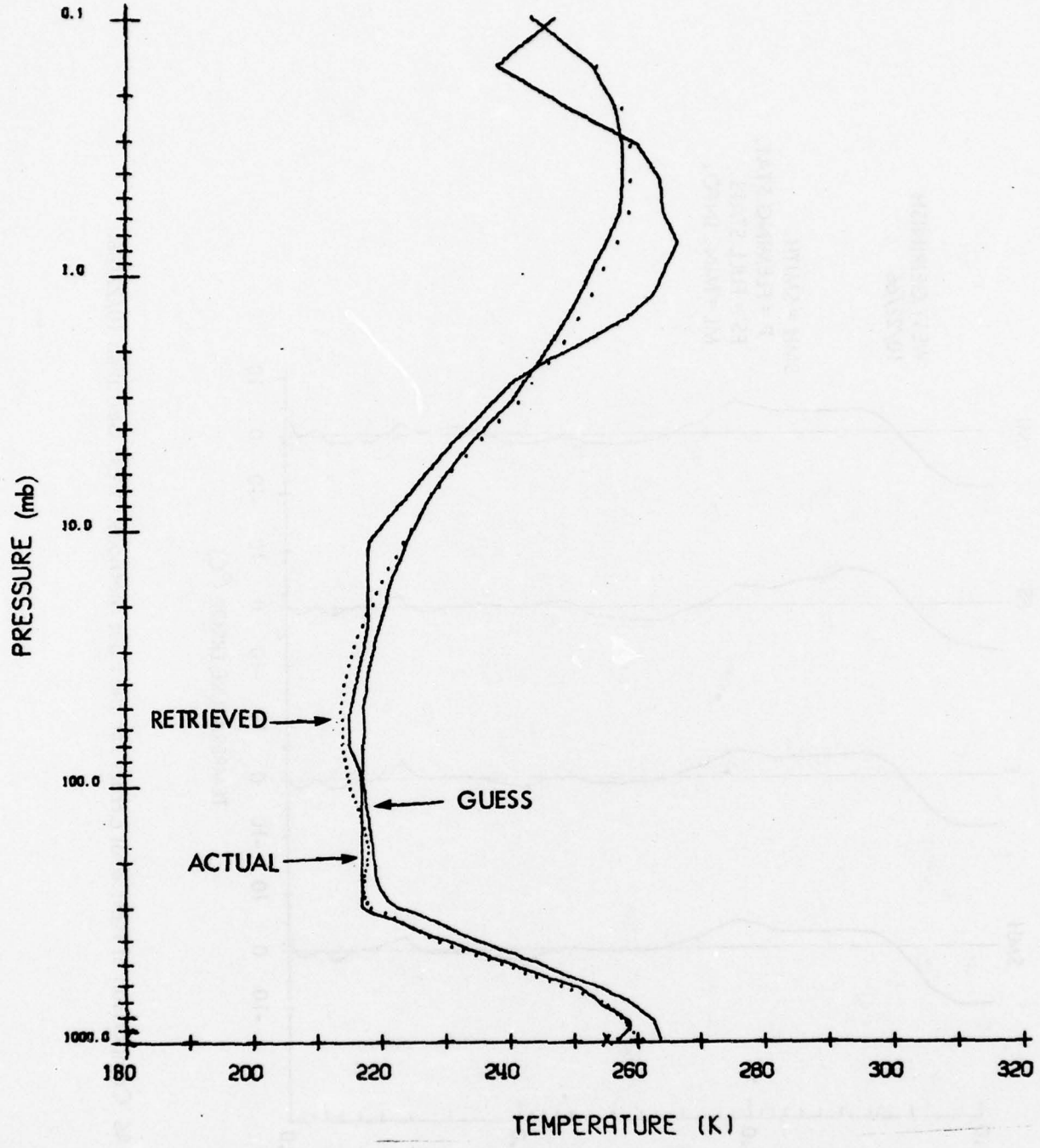

Figure 45 Simulated Retrieval by the Minimum-Information Method.
Actual Profile is West Geirinish 10/22/66 Radiosonde.

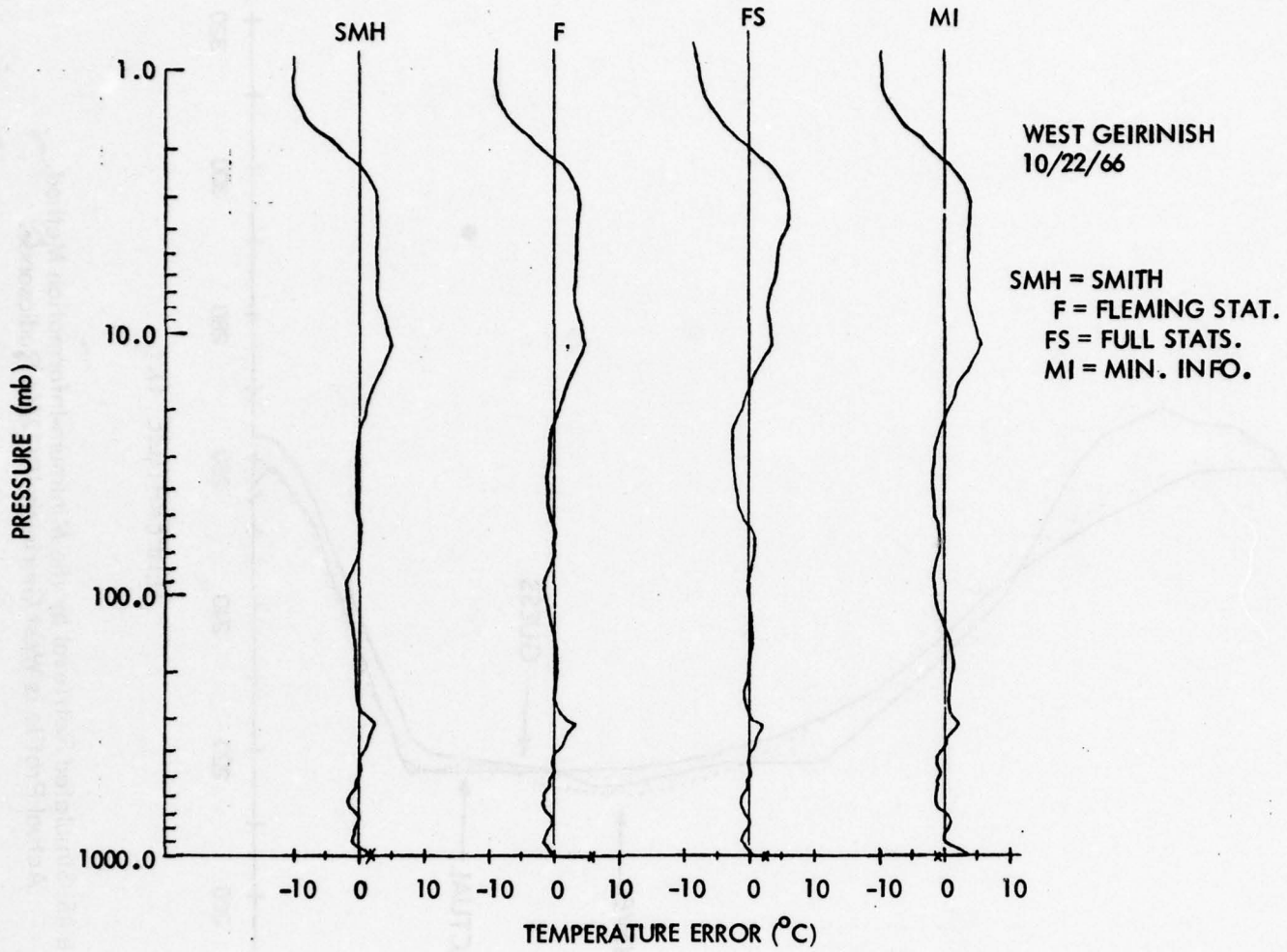

Figure 46 Comparison of Retrieval Errors for the Four Methods. West Geirinish 10/22/66.

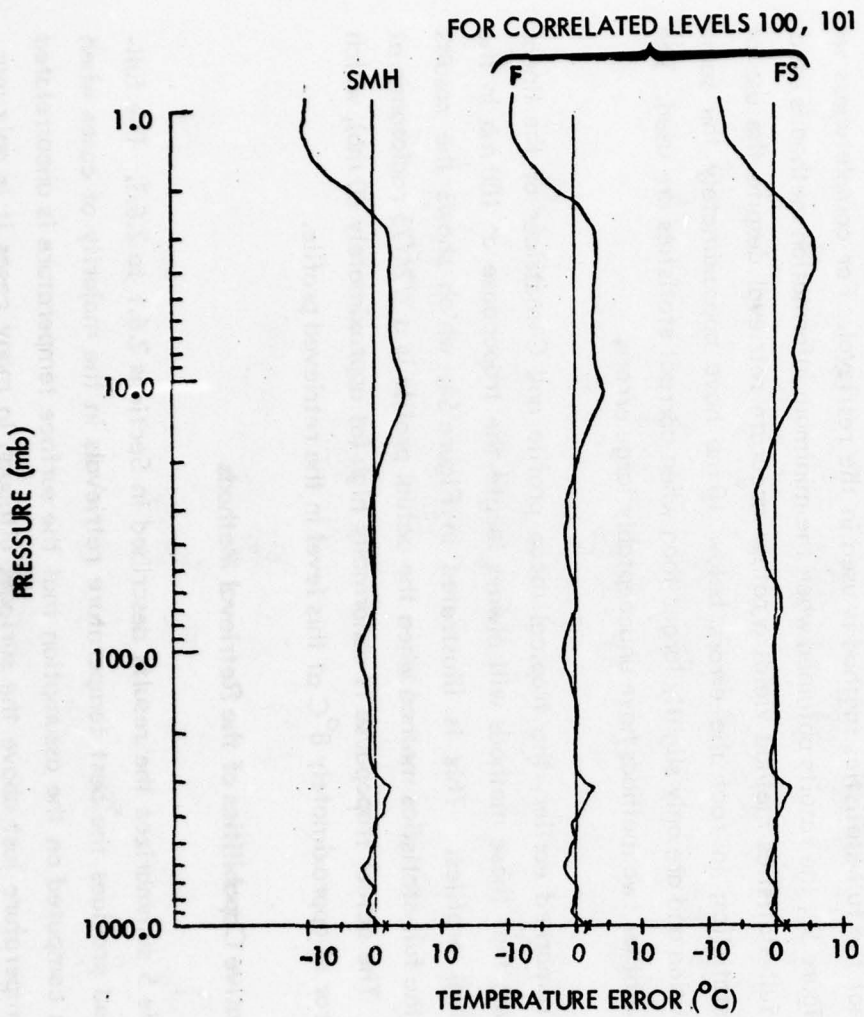

Figure 47 Comparison of Retrieval Errors When Levels 100, 101 are Assumed Correlated in the F and FS Methods. West Geirinish 10/22/66.

when the alternate S–matrix (assumption of no surface discontinuity) is used. Therefore, we show only one retrieval (the one obtained by the Fleming method) for each of the tropical cases; Figure 48 shows the Kwajalein retrieval and Figure 49 the Fort Sherman retrieval. The corresponding temperature errors are shown in Figure 50.

The very different character of the plots of the K–matrix columns of the Fleming method (Figure 19 or 20) and the C–matrix columns of the full-statistics method (Figure 15 or 17) suggests that retrievals obtained by these two methods may be affected quite differently by the use of inappropriate statistics. Figure 51 shows a retrieval obtained by the Fleming method for a tropical case when the mean (guess) profile and C–matrix are those defined for extratropical latitudes. Figure 52 represents the same case, except that the full-statistics method is used in the retrieval. For completeness we also show, in Figure 53, the results obtained when the minimum information method is used. Note that the full-statistics method yields a rather accurate retrieval despite the use of inappropriate statistics; in fact the errors below 10 mb have approximately the same vertical distribution and are only slightly larger than when correct statistics are used. The retrievals of the other two methods have unacceptably large errors.

As remarked earlier, the tropical mean profile and C–matrices of the linear methods are such that these methods will always locate the tropopause at 100 mb in the retrieved tropical profiles. This is illustrated in Figure 54, which shows the results obtained using the full-statistics method when the actual profile is a 2/24/75 radiosonde at Barking Sands. The actual tropopause is abnormally high (at approximately 80 mb), which results in an error of approximately 8°C at this level in the retrieved profile.

2.6.4 Relative Capabilities of the Retrieval Methods

Table 5 summarizes the results described in Sections 2.6.1 to 2.6.3. The full-statistics method provides the best temperature retrievals in the majority of cases when the S–matrix is computed on the assumption that the surface temperature is uncorrelated with the air temperature just above the surface, although in many cases it is only marginally better than the Smith method. When perfect correlation is assumed, the Fleming statistical method gives the best results overall, although in two-thirds of the cases it is equal to or only marginally better than the full-statistics method. These results show that the full-statistics method is less sensitive than the Fleming method to the assumed air-surface temperature correlation. Moreover, it is much more tolerant of the use of

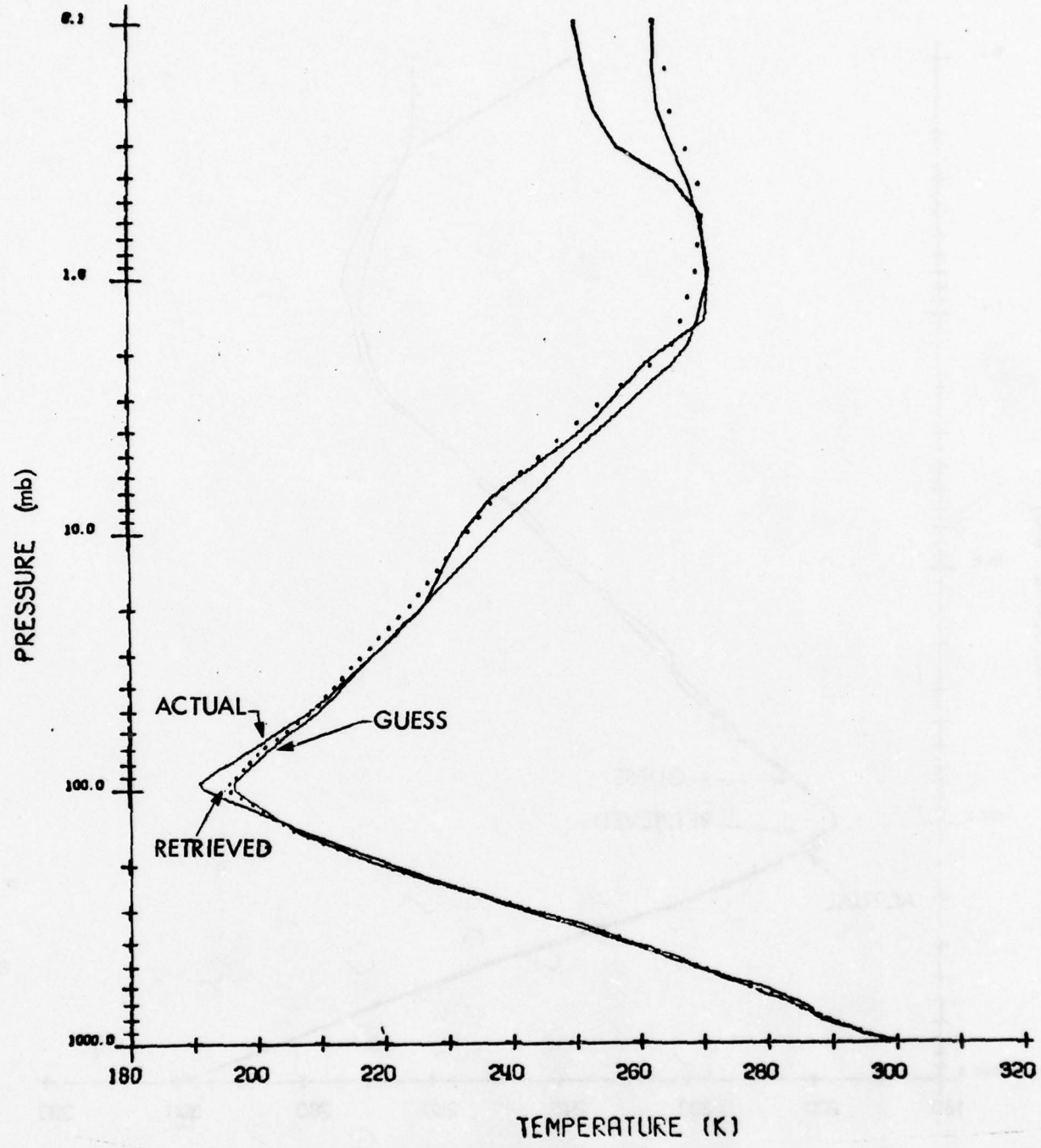

Figure 48 Simulated Retrieval by the Fleming Method. Actual Profile is Kwajelein 2/27/75 Radiosonde.

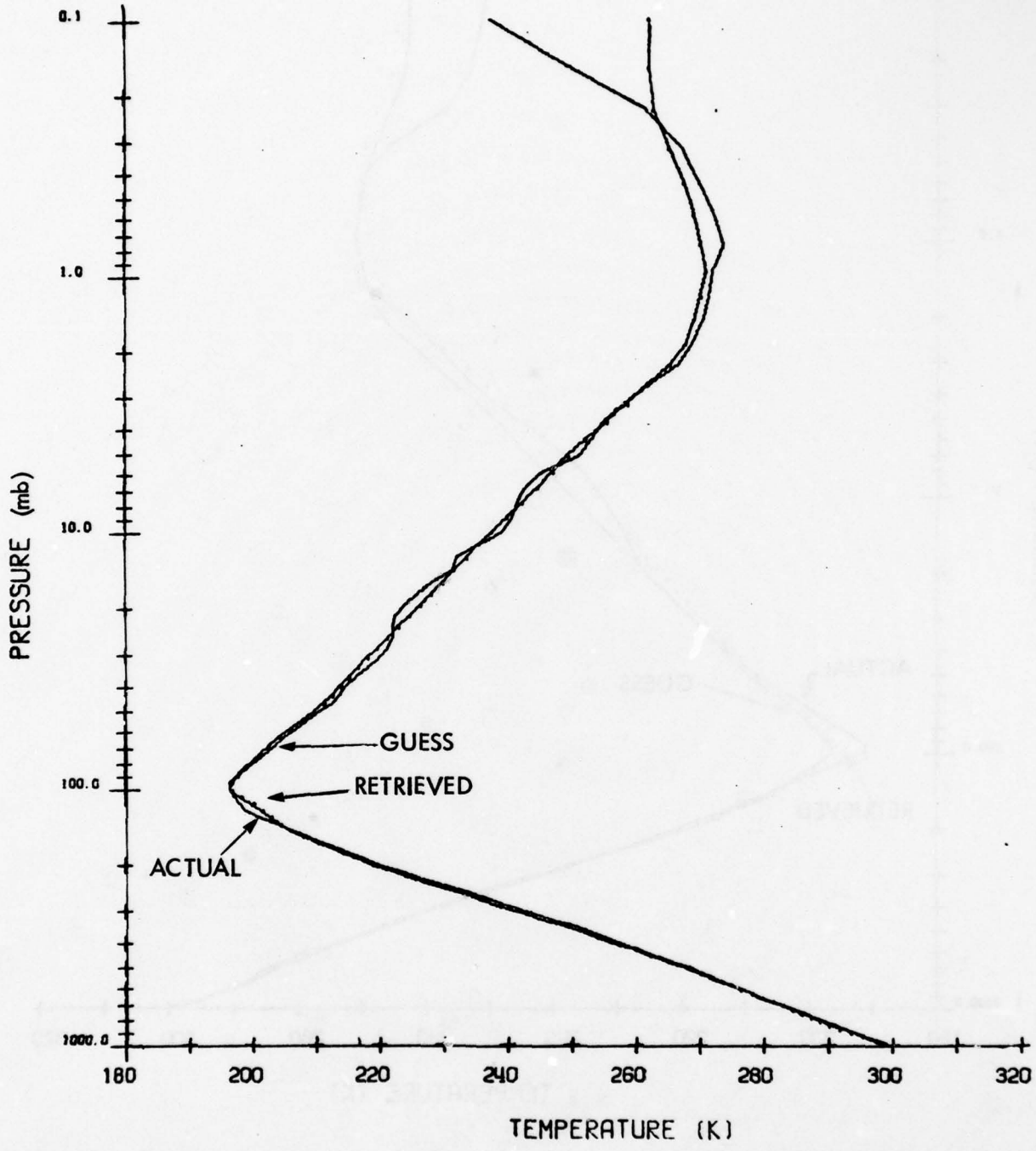

Figure 49 Simulated Retrieval by the Fleming Method. Actual Profile is Fort Sherman 5/8/67 Radiosonde.

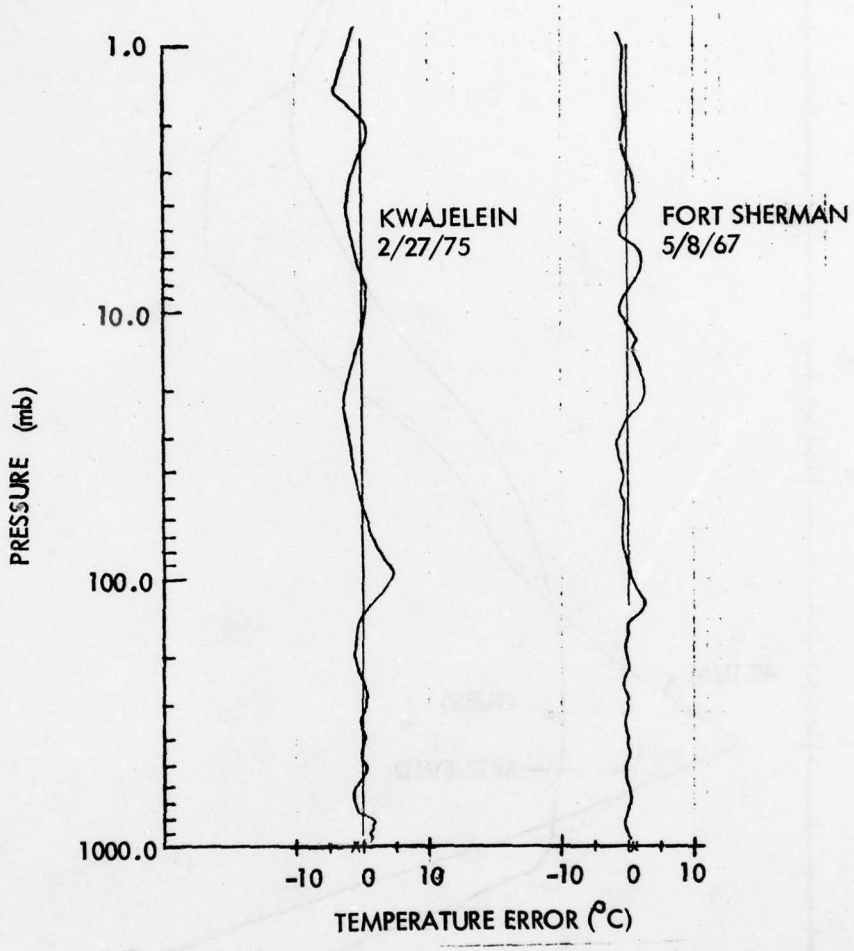

Figure 50 Approximate Retrieval Errors (All Methods) For The Tropical Cases, Kwajelein 2/27/75 and Fort Sherman 5/8/67.

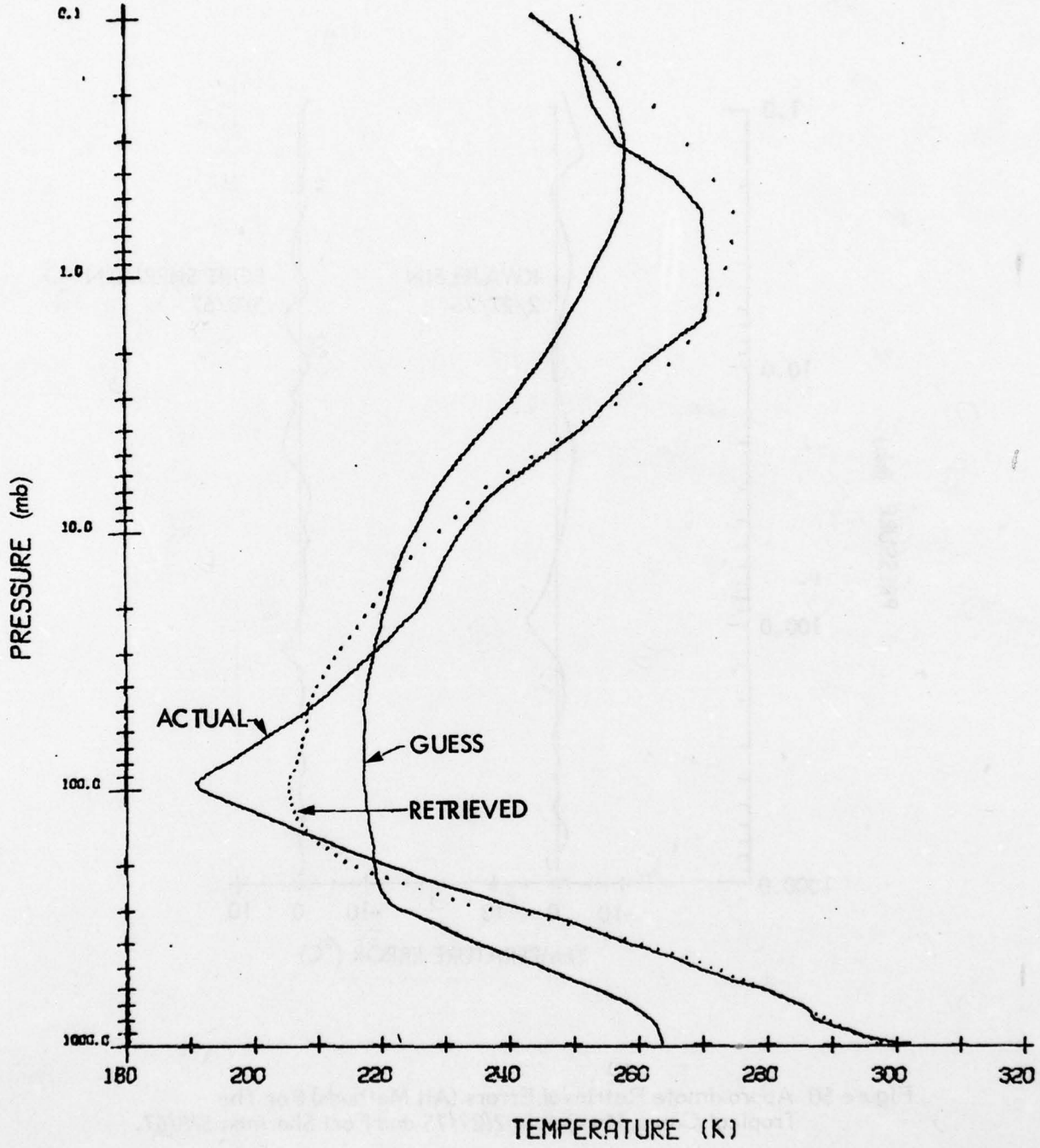

Figure 51 Simulated Retrieval by the Fleming Method Using Inappropriate Statistics. Actual Profile is Kwajelein 2/27/75 Radiosonde.

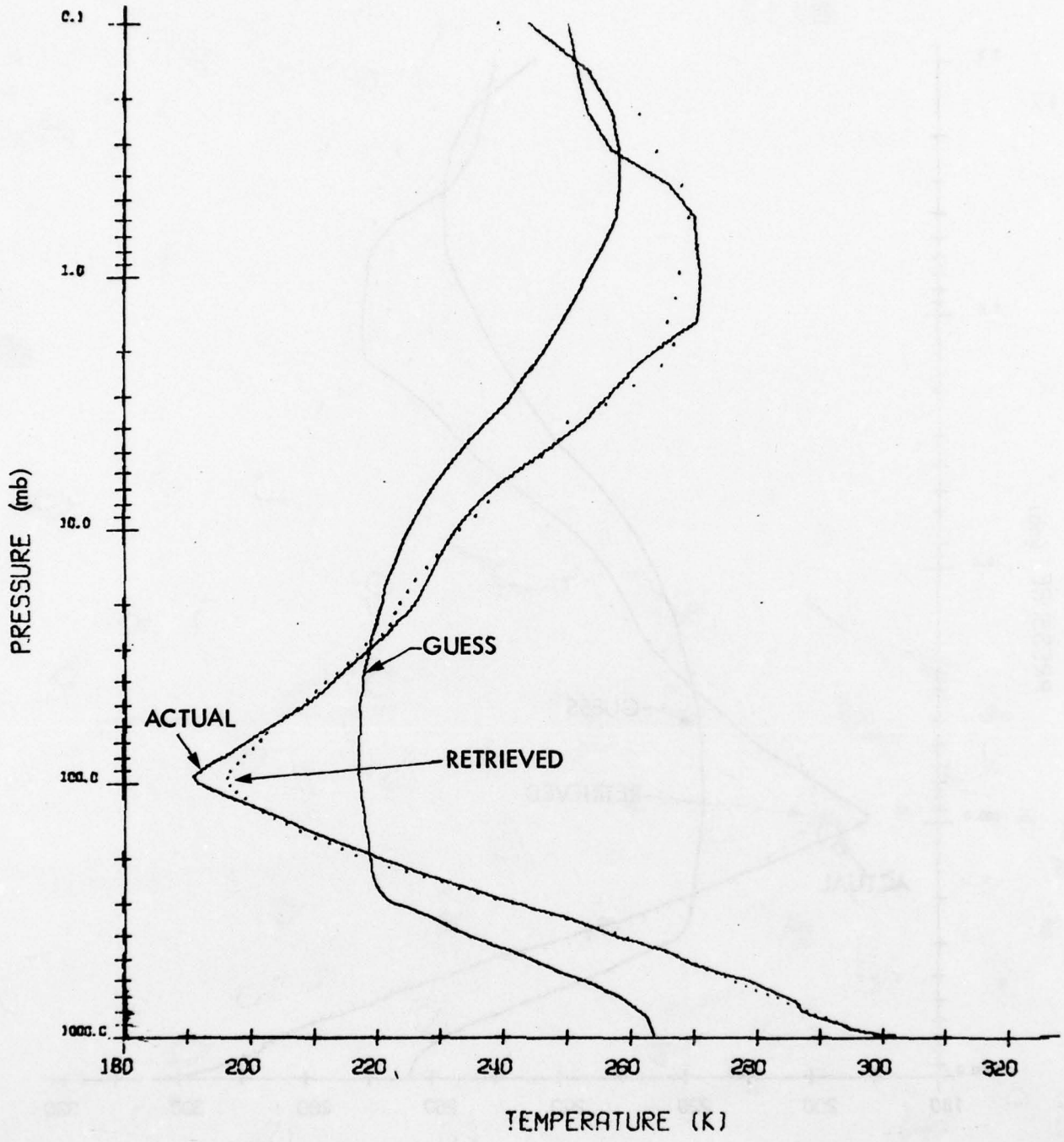

Figure 52 Simulated Retrieval by the Full-Statistics Method Using Inappropriate Statistics. Actual Profile is Kwajelein 2/27/75 Radiosonde.

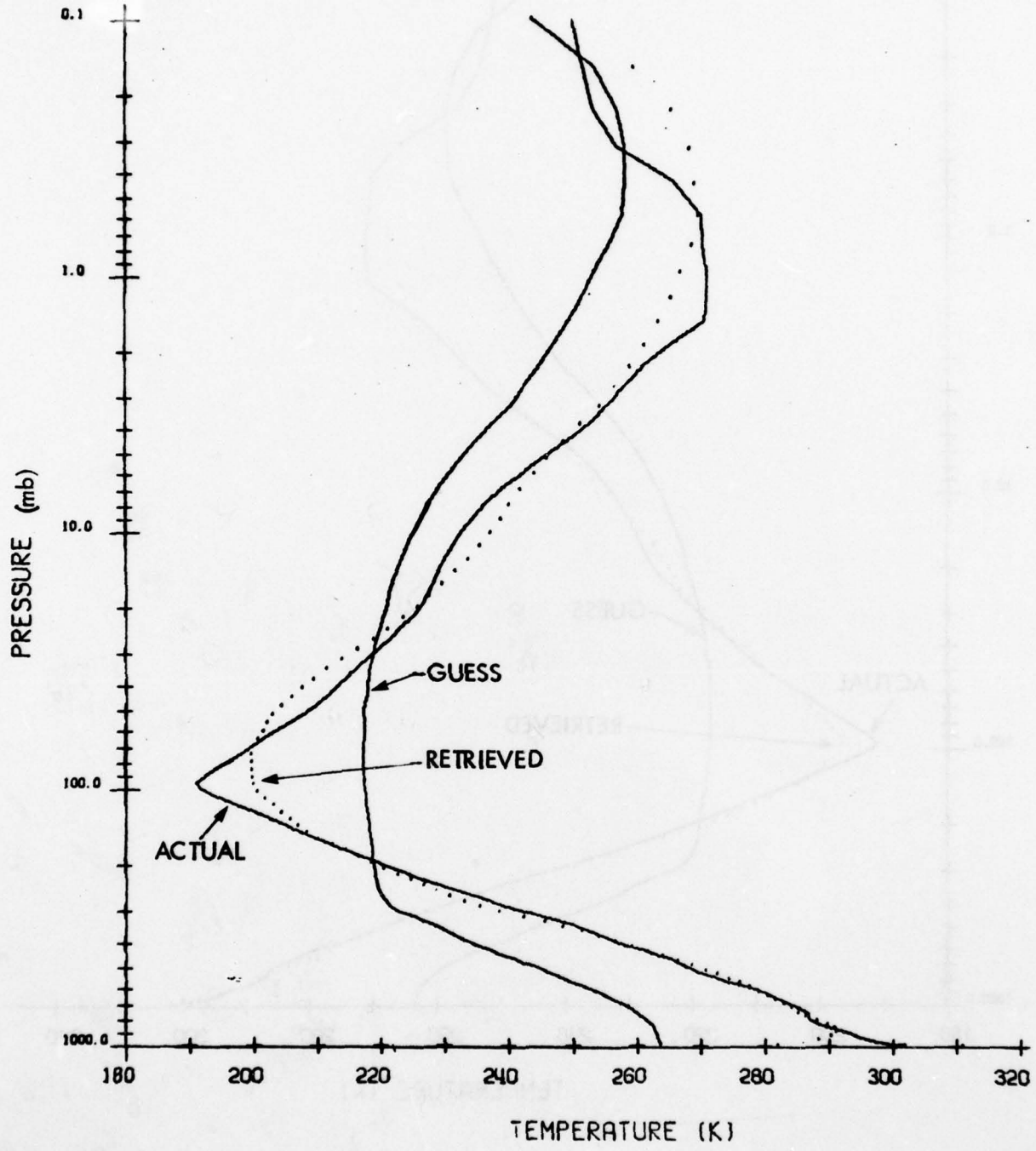

Figure 53 Simulated Retrieval by the Minimum-Information Method Using Inappropriate Statistics. Actual Profile is Kwajelein 2/27/75 Radiosonde.

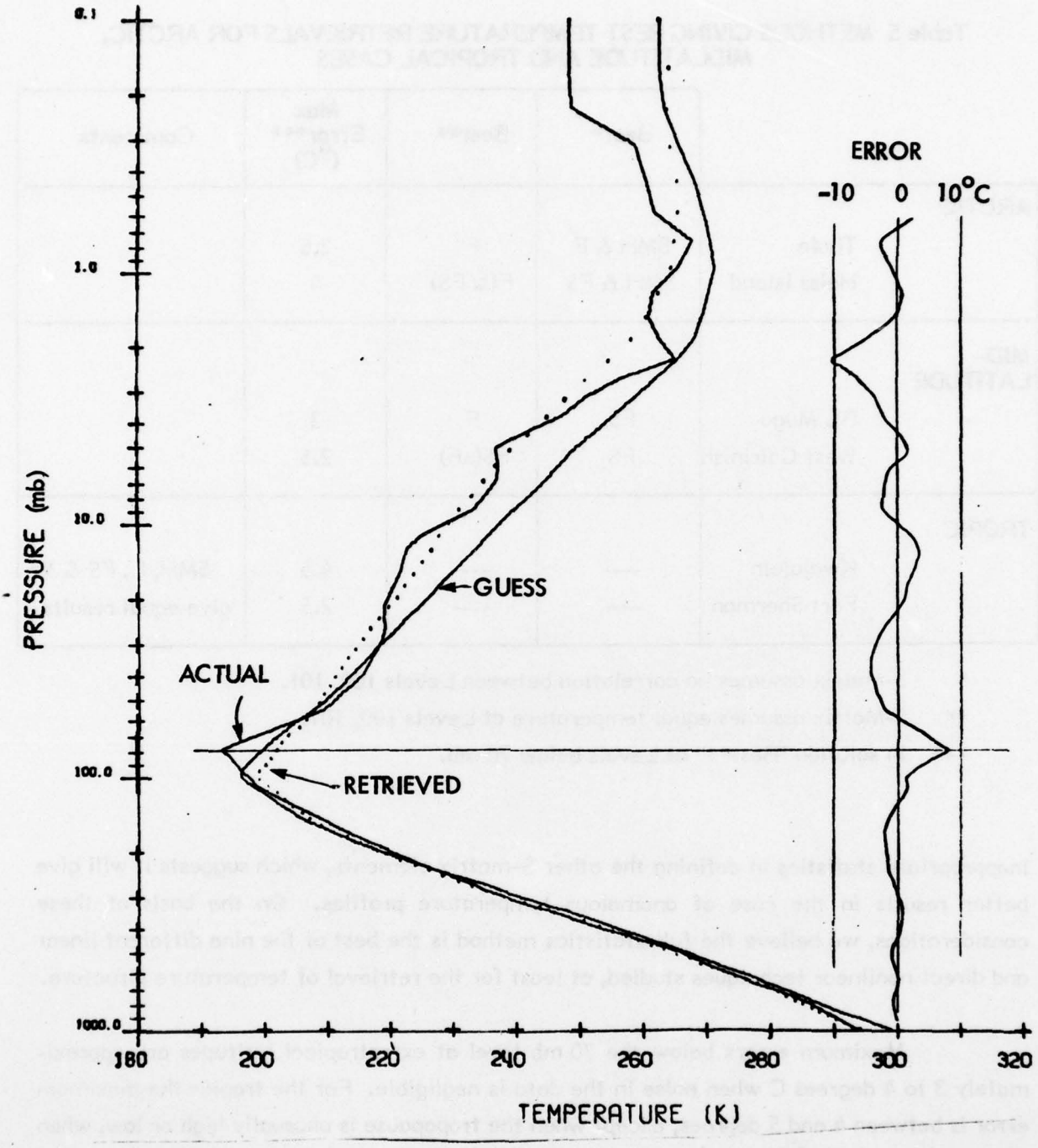

Figure 54 Simulated Retrieval by the Full-Statistics Method. Actual Profile is Barking Sands 2/24/75 Radiosonde.

Table 5 METHODS GIVING BEST TEMPERATURE RETRIEVALS FOR ARCTIC, MIDLATITUDE AND TROPICAL CASES

		Best*	Best**	Max Error*** (°C)	Comments
ARCTIC					
	Thule	SMH & F	F	2.5	
	Heiss Island	SMH & FS	F(≃FS)	4	
MID-LATITUDE					
	Pt. Mugu	FS	F	3	
	West Geirinish	FS	FS(=F)	2.5	
TROPIC					
	Kwajalein	----	----	4.5	SMH, F, FS & MI
	Fort Sherman	----	----	2.5	give equal results

* S-Matrix assumes no correlation between Levels 100, 101.

** S-Matrix assumes equal temperature at Levels 100, 101.

*** In solution "Best**" at Levels below 70 mb.

inappropriate statistics in defining the other S–matrix elements, which suggests it will give better results in the case of anomalous temperature profiles. On the basis of these considerations, we believe the full-statistics method is the best of the nine different linear and direct nonlinear techniques studied, at least for the retrieval of temperature structure.

Maximum errors below the 70 mb level at extratropical latitudes are approximately 3 to 4 degrees C when noise in the data is negligible. For the tropics the maximum error is between 4 and 5 degrees, except when the tropopause is unusually high or low, when much larger errors will occur.

SECTION 3
STUDY OF WATER VAPOR RETRIEVAL

3.1 SELECTION AND DEFINITION OF ALGORITHMS

The radiative transfer equation, usually written in the form

$$I(\nu) = B(\nu, T_s)\ \tau(\nu, p_s) - \int_{1}^{\tau(\nu, p_s)} B(\nu, p)\, d\tau(\nu, p), \tag{39}$$

can be integrated by parts, which gives

$$I(\nu) = \left[B(\nu, T_s) - B(\nu, p_s)\right]\ \tau(\nu, p_s) + B(\nu, p_t) + \int_{B(\nu, p_t)}^{B(\nu, p_s)} \tau(\nu, p)\, dB(\nu, p), \tag{40}$$

where $I(\nu)$ is the upwelling spectral radiance, $\tau(\nu, p)$ is the transmittance of the atmosphere above level p, and $B(\nu, p)$ is Planck's function evaluated at temperature $T(p)$. Subscripts s and t refer to the bottom and top of the atmosphere, respectively; however, in the first term of Equation 40, $B(\nu, T_s)$ denotes the emission of the surface at temperature T_s, whereas $B(\nu, p_s)$ is Planck's function evaluated at the air temperature $T(p_s)$ just above the surface. It is often assumed that $T_s = T(p_s)$, which would eliminate the first term.

Replace $I(\nu)$ in Equation 40 by $\Delta I(\nu)$ and $\tau(\nu, p)$ by $\Delta(\ln u^*)\, d\tau/d\ln u^*$, where $\Delta I(\nu)$ is the perturbation in radiance caused by a perturbation $\Delta \ln u^*(p)$, and $u^*(p)$ is defined as the reduced water vapor optical thickness above level p:

$$u^*(p) = \int_0^{u(p)} \frac{p}{p_o} \sqrt{\frac{T_o}{T}}\, du'(p) \qquad (41)$$

This quantity is proportional to $u(p)\bar{\gamma}(p)$, the actual water thickness times the Curtis-Godson mean line halfwidth. The choice of $u^*(p)$ or $\ln u^*(p)$ as the variable defining the atmospheric water distribution is based on the fact that the DMSP water vapor transmittances are in the strong-line absorption region at nearly all pressure levels (see Section 3.2).

Writing Equation 40 in a quadrature form and in terms of the perturbations $\Delta I(\nu)$ and $\Delta \ln u^*$, we obtain

$$\Delta I_i = \sum_{j=1}^{J} P_{ij}\, \Delta \ln u_j^*; \quad i = 1, 2, \ldots 6 \qquad (42)$$

where

$$P_{i,1} = \frac{1}{2} \frac{d\tau_{i,1}}{d\ln u^*} \left[B_{i,2} - B_{i,1}\right],$$

$$P_{i,j} = \frac{1}{2} \frac{d\tau_{i,j}}{d\ln u^*} \left[B_{i,j+1} - B_{i,j-1}\right], \quad j = 2, 3, \ldots, J-1 \quad , \qquad (43)$$

$$P_{i,J} = \frac{1}{2} \frac{d\tau_{i,J}}{d\ln u^*} \left[2B_{i,J+1} - B_{i,J} - B_{i,J-1}\right]$$

where J is the number of quadrature points in the atmosphere, and $B_{i, J+1}$ is the surface radiance. As in the analysis of temperature retrieval techniques, we chose quadrature points corresponding to equal increments of $p^{2/7}$. The mesh extends from the 100 mb level to the surface, and over this region matches the mesh used for temperature retrievals. This results in a total of J = 53 quadrature points. From Equations 42 and 43, we see that the vertical weighting function on $\Delta \ln u^*$ ($p^{2/7}$) is $(d\tau/d\ln u^*)(dB/dp^{2/7})$.

The different water vapor retrieval techniques to be examined will solve for the profile $\Delta \ln u_j^*$, representing the difference between the actual $\ln u_j^*$ profile and an initial guess profile; ΔI_i are differences between the measured radiances and those computed for the guess profile. In subsequent iterations the solution profile replaces the initial guess or previous solution. The solution has converged when (and if) the ΔI_i's become less than the rms noise level. The profile of integrated water, u(p), can be obtained from u*(p) using the inverse of Equation 41:

$$u(p) = \int_0^{u^*(p)} \frac{p_o}{p(x)} \sqrt{\frac{T(x)}{T_o}}\, dx\,(p). \qquad (44)$$

The water vapor algorithms selected for study are the same four that were studied with respect to temperature retrieval in Section 2.6. However, only the two linear methods were actually evaluated (see Section 1.1).

3.1.1 Linear Inverse Methods

In matrix notation Equation 42 is

$$\Delta \underset{\sim}{I} = P \cdot (\Delta \ln \underset{\sim}{u^*}) \qquad (45)$$

and its regularized inverse is

$$\Delta \ln \underset{\sim}{u^*} = C \Delta \underset{\sim}{I} \qquad (46)$$

If the Foster-Twomey regularization is used,

$$C \equiv C^{(MI)} = P^T \left[PP^T + \alpha I \right]^{-1}, \tag{47}$$

$$\alpha = \sigma_E^2 / \sigma_{\ln u^*}^2, \tag{48}$$

and Equation 46 is the minimum information solution. Here I is the 6-by-6 identity matrix, σ_E is noise equivalent radiance and $\sigma_{\ln u^*}^2$ is the expected variance of $u^*/\langle u^* \rangle$ averaged over all pressure levels.

If statistical regularization is used

$$C \equiv C^{(FS)} = SP^T \left[PSP^T + S_E \right]^{-1} \tag{49}$$

where S is the covariance matrix of $u^*/\langle u^* \rangle$ and S_E is the 6-by-6 matrix of noise covariances. We will assume that $S_E = \sigma_E^2 I$, with $\sigma_E = 2 \times 10^{-8}$ W/cm^2-sr-cm^{-1}. These solutions are analogous to those used in the linear methods for temperature retrieval: $\Delta \ln \underset{\sim}{u^*}$ plays the role of $\underset{\sim}{\Delta B}_r$ and P the role of W.

3.1.2 Smith Iterative Technique

The iterative method described by Smith[1] and also by Smith and Howell[11], starts with the assumption that the altitude variation of $\Delta \ln u^*$ in Equation 42 will be relatively weak compared to that of the weighting functions (rows of P). If $\Delta \ln u_j^*$ is assumed constant within the layers sensed by a particular channel, we can write (from Equation 42),

$$\Delta \ln u_j^* \simeq \Delta I_i / \sum_{j=1}^{J} P_{ij} . \tag{50}$$

This is a relaxation formula for revising $\ln u_j^*$, which yields six independent new estimates of the profile u_j^*. Smith calculates a single profile as a weighted sum of the six estimates, where the weighting function is P_{ij}:

$$\Delta \ln u_j^* = \frac{1}{\sum_{i=1}^{6} P_{ij}} \sum_{i=1}^{6} \left[\frac{P_{ij} \, \Delta I_i}{\sum_{j=1}^{J} P_{ij}} \right] \tag{51}$$

Note that Equation 51 is a linear transformation; in matrix notation

$$\Delta \ln \underset{\sim}{u}^* = C \, \Delta \underset{\sim}{I} \tag{52}$$

with

$$C_{ji} \equiv C_{ji}^{(S)} = \frac{P_{ij}}{\left(\sum_{i=1}^{6} P_{ij} \right) \left(\sum_{j=1}^{J} P_{ij} \right)} \tag{53}$$

However, the Smith method (and the "linear" methods and the Fleming statistical methods) are linear only through the first solution of Equation 52. In subsequent iterations P and C must be recalculated, since P_{ij} depends on the current u* through $d\tau_i(u_j^*)/d \ln u^*$.

3.1.3 Fleming Statistical Method

As in the linear and Smith iterative methods the solution has the general form of Equation 52. The C–matrix can be obtained by analogy to the equations used for

temperature retrieval: substitute Equation 28 into 25 and then average over the channels, as in the Smith method. The result is

$$C_{ji} \equiv C_{ji}^{(F)} = \frac{P_{ij} \sum_{n=1}^{J} S_{jn} P_{in}}{\left[\sum_{i=1}^{6} P_{ij}\right]\left[\sum_{j=1}^{J}\left(P_{ij} \sum_{n=1}^{J} S_{jn} P_{in}\right) + \sigma_E^2\right]} \quad (54)$$

where S_{jn}, the covariance of $u^*/\langle u^* \rangle$, replaces S_{ijn} in Equation 28, and P_{ij} replaces W_{ij}.

3.2 TRANSMISSION FUNCTIONS FOR THE DMSP WATER VAPOR CHANNELS

Computed water vapor spectral transmittance profiles $\tau(\nu, p)$ were provided by Dr. McClatchey of AFGL for 218 selected radiosondes. Also provided were the spectral responses of the six DMSP channels listed in Table 6. From these data we computed 218 transmission profiles for each of the six channels. The results were plotted in various forms in order to obtain empirical transmittance functions for the six channels.

Table 6 DMSP H_2O CHANNELS

Channel Number (Used in this Study)	Nominal Center Frequency (cm^{-1})
1	353
2	347
3	397
4	408
5	420
6	441

Figure 55, from Zachor[12], shows the general behavior of absorptance versus optical thickness u and pressure p for a homogeneous path. This behavior is typical of laboratory data and the predictions of all band models. Figure 56 shows computed absorptances for Channel 4 plotted in the form of Figure 55. Note that six distinct values of u are represented, and that the plotted points tend to fall on a single curve. The plot shows that most of the data is in the strong-line region to within a few percent in absorptance. If most of the Channel 4 transmittances are in the strong-line region, then so will be the transmittances of the other channels, since Channel 4 is the most transparent.

Figure 57 shows all of the computed transmittances for Channel 4 plotted as log $(1-\tau)$ versus log u^*. Again, the departure of the plotted values from a single curve is quite small. Some of the scatter is due undoubtedly to the effect of temperature in the transmittance. The scatter at very low u^* is due to truncation of the τ's and u's to four digits.

Figure 57 and similar plots for the other five channels were smoothed and used to obtain approximate empirical transmission functions $\tau(u^*)$ in table form. We then used the empirical functions to obtain plots of $d\tau/d \ln u^*$ versus u^*, which is a factor in the weighting function referred to in Section 3.1. These plots, however, exhibited ragged fine structure (Figure 58) which is not physically plausible and could tend to produce false structure in the retrieved humidity profiles. We then decided to fit empirical functions to the data in order to obtain a smooth representation of the weighting functions. For the empirical transmittance functions, we adopted the generalized strong-line form

$$-\ln \tau = K_1 x + K_2 x^2 + \ldots K_n x^n \qquad (55)$$

$$x = (u^*)^k$$

and determined the coefficients K_i and exponent k with the assistance of least-squares curve fitting codes.

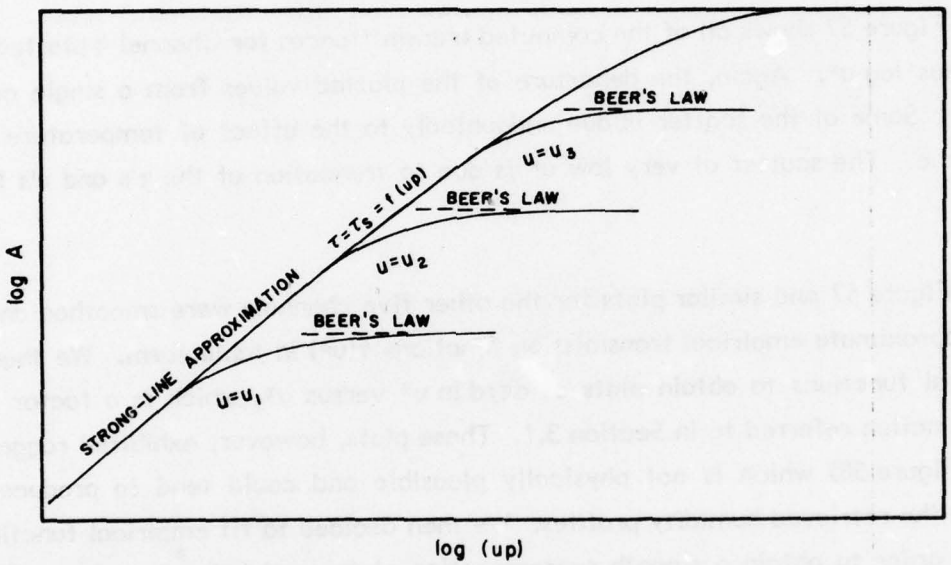

Figure 55 A Plot of the log of absorption vs log (up) for a typical laboratory run or absorption band model. The ordinate scale is greater than the scale of the abscissa to emphasize the strong-line and Beer's law regions. The straight portion of the strong-line envelope represents the "square-root" approximation, $A = \text{const.}(up)^{1/2}$

AD-A073 144 HONEYWELL ELECTRO-OPTICS CENTER LEXINGTON MA F/G 17/5
STUDY OF TEMPERATURE /MOISTURE RETRIEVAL CAPABILITIES OF DMSP /--ETC(U)
SEP 78 A S ZACHOR F19628-77-C-0184
UNCLASSIFIED 7809-4 AFGL-TR-78-0279 NL

2 OF 2
AD
A073144

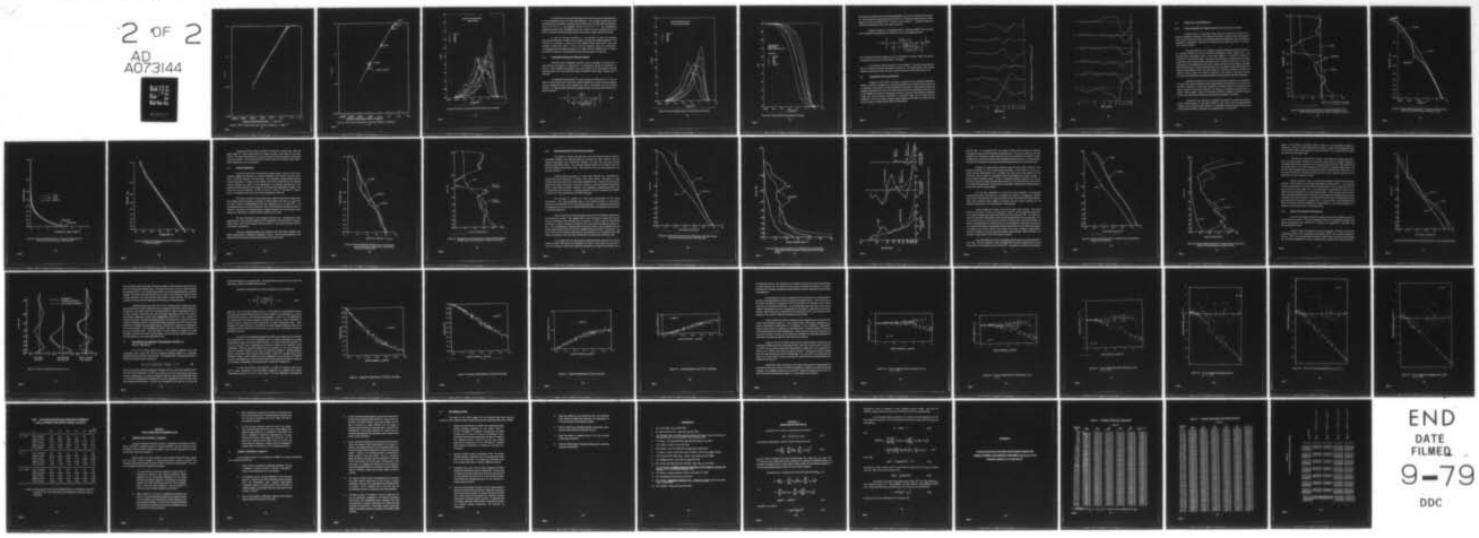

END
DATE
FILMED
9-79
DDC

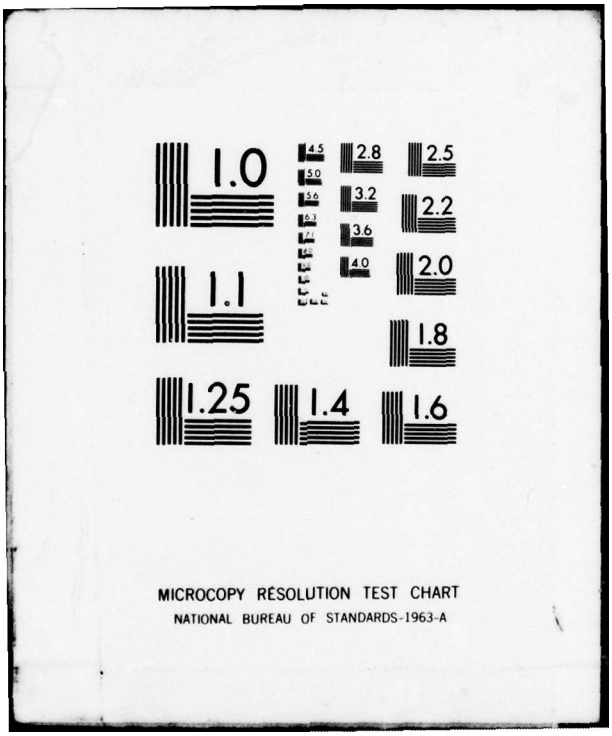
1.0
1.1
1.25
1.4
1.6
1.8
2.0
2.2
2.5
2.8
3.2
3.6
4.0
4.5
5.0
5.6
6.3
MICROCOPY RESOLUTION TEST CHART
NATIONAL BUREAU OF STANDARDS-1963-A

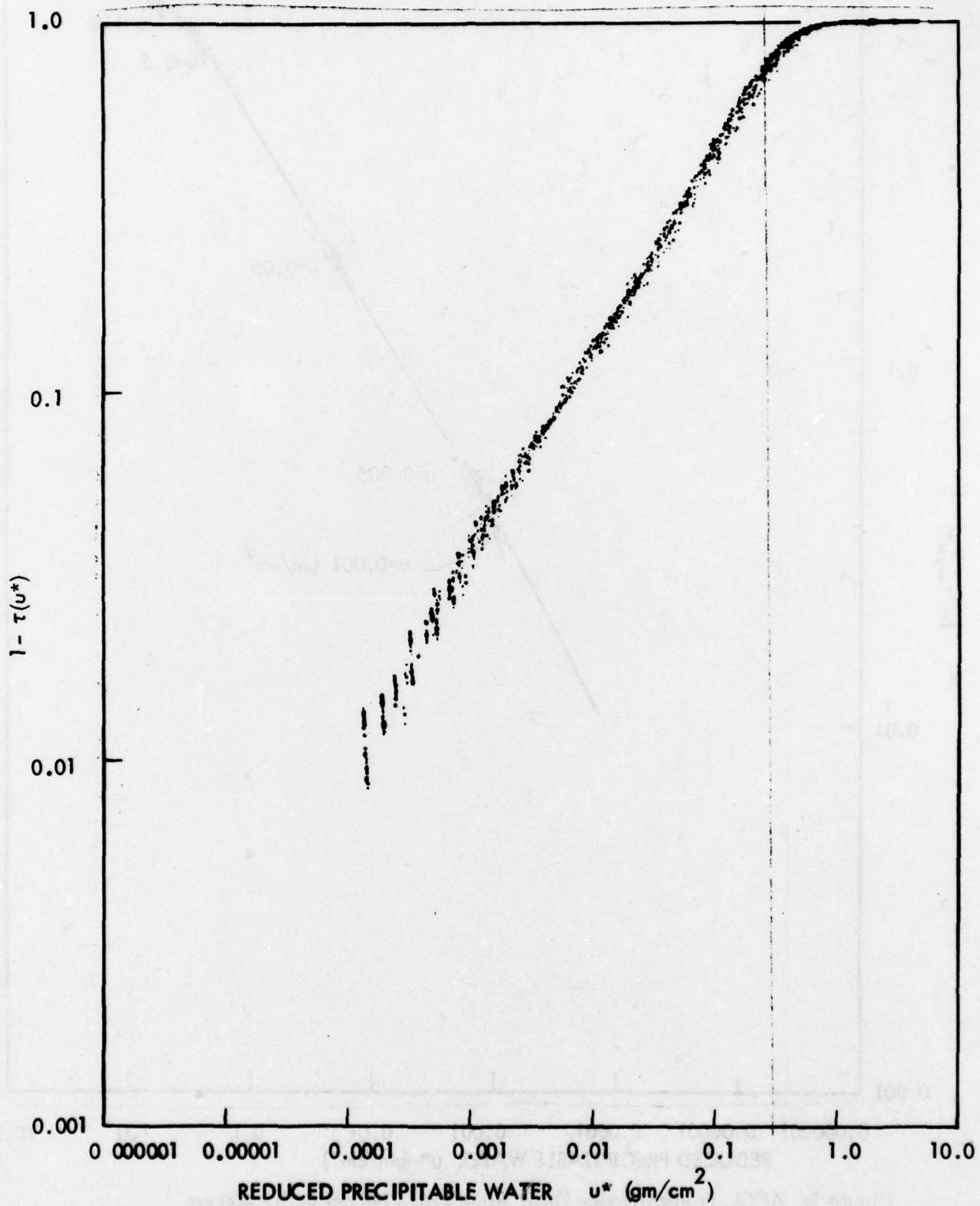

Figure 57 AFGL Transmittance Data $\tau(u^*)$ For Channel 4; $\nu = 408\ cm^{-1}$

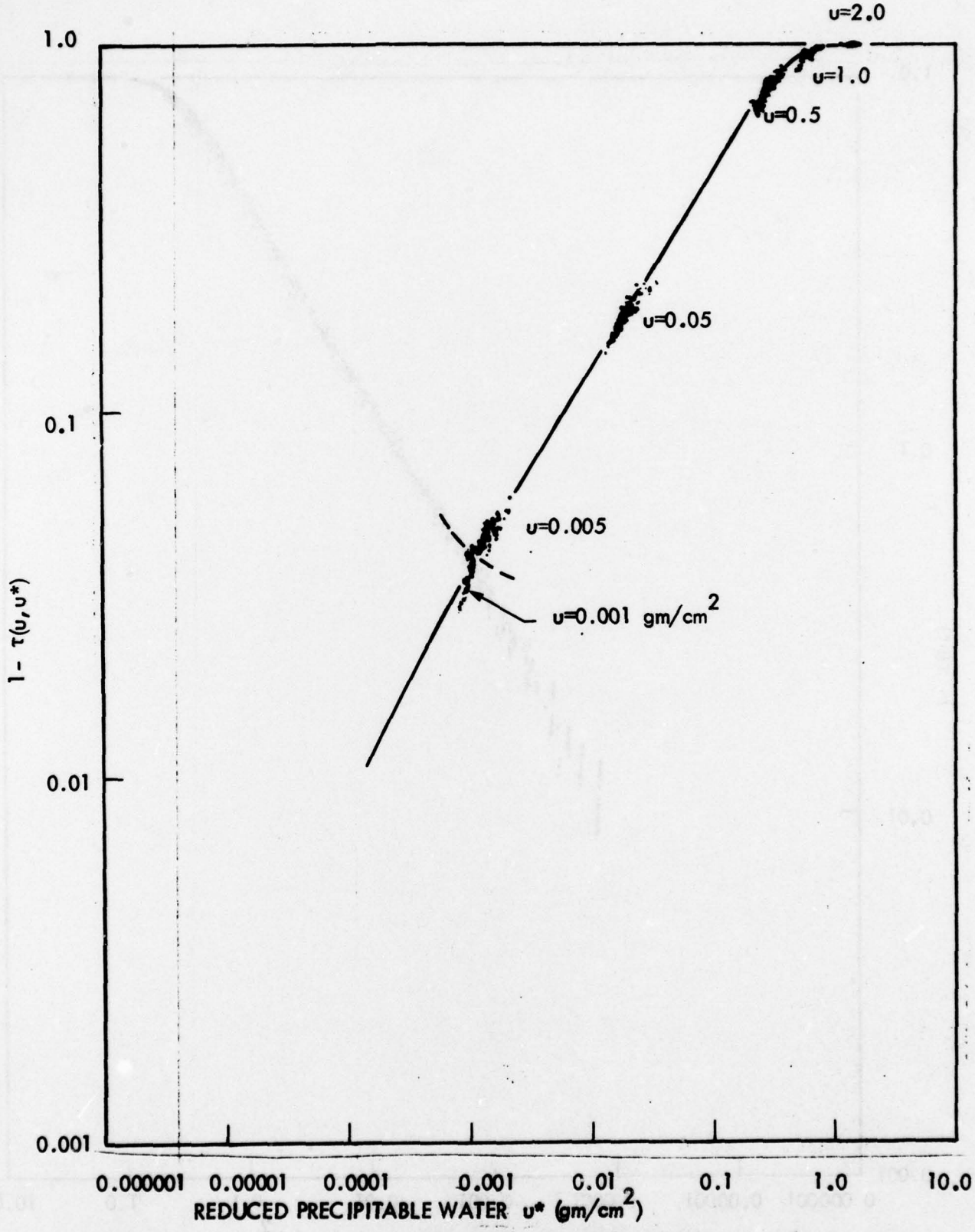

Figure 56 AFGL Transmittance Data $\tau(u,u^*)$ for Channel 4; $\nu = 408\ cm^{-1}$

7809-4

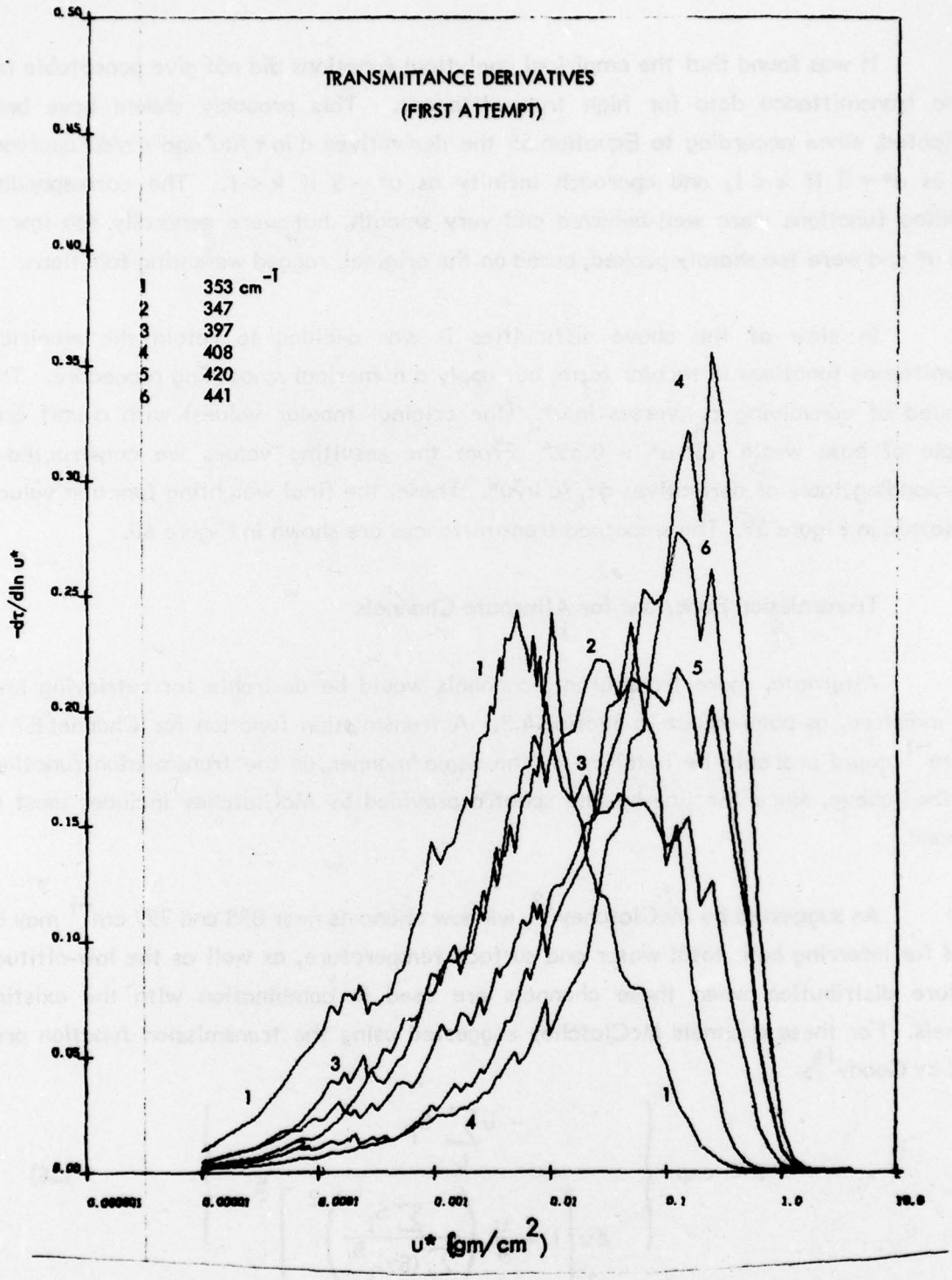

Figure 58 Numerical Transmittance Derivatives (First Attempt)

It was found that the empirical analytical functions did not give acceptable fits to the transmittance data for high transmittances. This probably should have been anticipated, since according to Equation 55 the derivatives $d \ln \tau / du^*$ and $d\tau/du^*$ approach zero as $u^* \to 0$ if $k < 1$, and approach infinity as $u^* \to 0$ if $k < 1$. The corresponding weighting functions were well-behaved and very smooth, but were generally too low at small u^* and were too sharply peaked, based on the original, ragged weighting functions.

In view of the above difficulties it was decided to retain the empirical transmittance functions in tabular form, but apply a numerical smoothing procedure. This consisted of convolving τ_k versus $\ln u^*_k$ (the original tabular values) with a unit area triangle of base width $\Delta \ln u^* = 0.35$. From the resulting values we constructed a corresponding table of derivatives $d\tau_k / d \ln u^*$. These, the final weighting function values, are plotted in Figure 59. The smoothed transmittances are shown in Figure 60.

3.2.1 Transmission Functions for Alternate Channels

Alternate, more transparent, channels would be desirable for retrieving low-level moisture, as pointed out in Section 4.2. A transmission function for Channel E7 at 535 cm^{-1} could probably be obtained in the same manner as the transmission functions described above, since the line-by-line spectra provided by McClatchey includes most of this band.

As suggested by McClatchey[13], window channels near 898 and 797 cm^{-1} may be useful for inferring both total water and surface temperature, as well as the low-altitude moisture distribution when these channels are used in combination with the existing channels. For these channels McClatchey suggested using the transmission function proposed by Goody[14]:

$$\tau = \exp \left\{ \frac{- u \sum_i S_i}{\Delta \nu \left[1 + \frac{u}{4} \left(\frac{\sum S_i}{\sum (S\gamma)_i^{1/2}} \right)^2 \right]^{1/2}} \right\} \qquad (56)$$

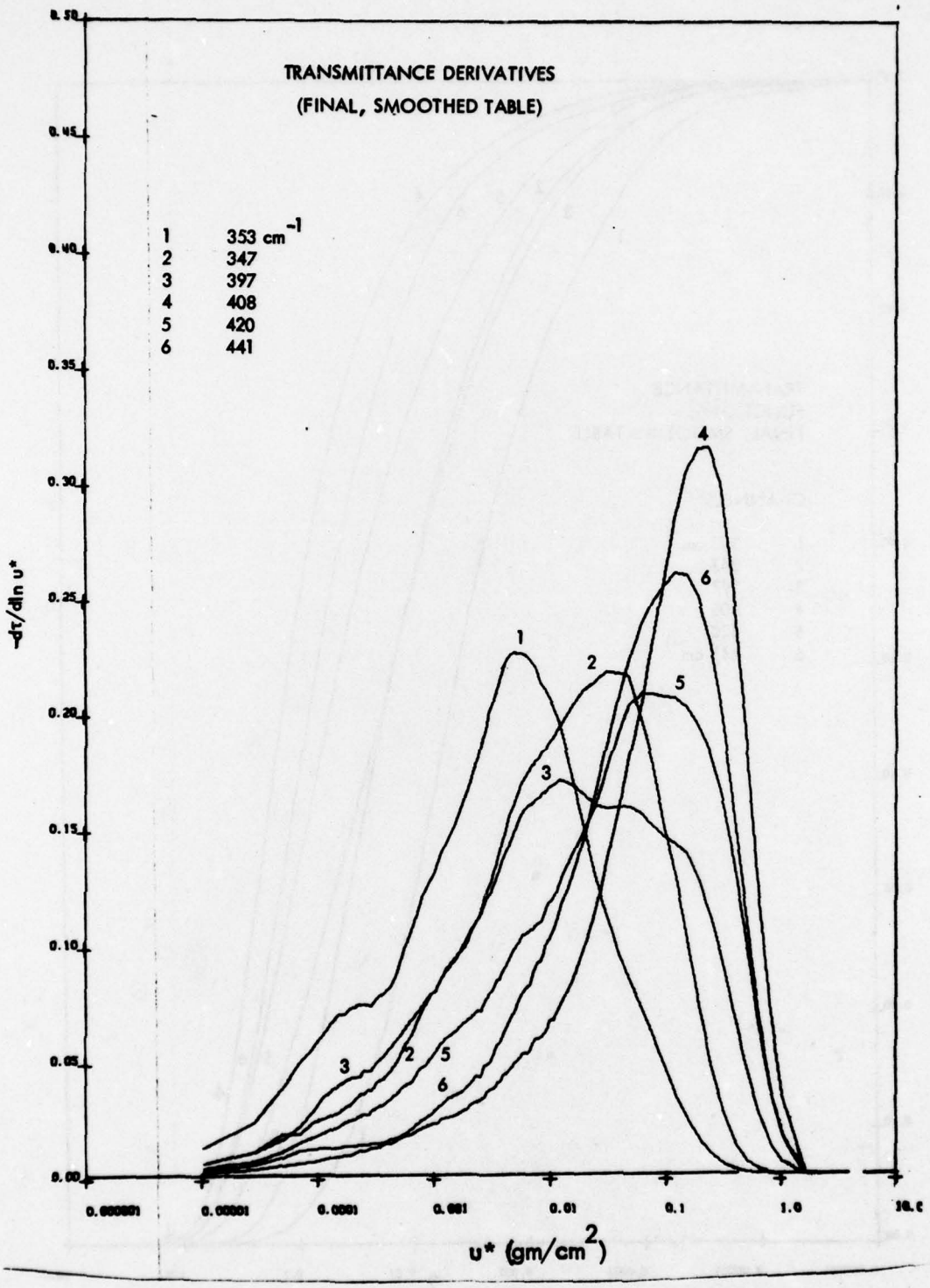

Figure 59 Final Smoothed Values of Transmittance Derivatives

7809-4

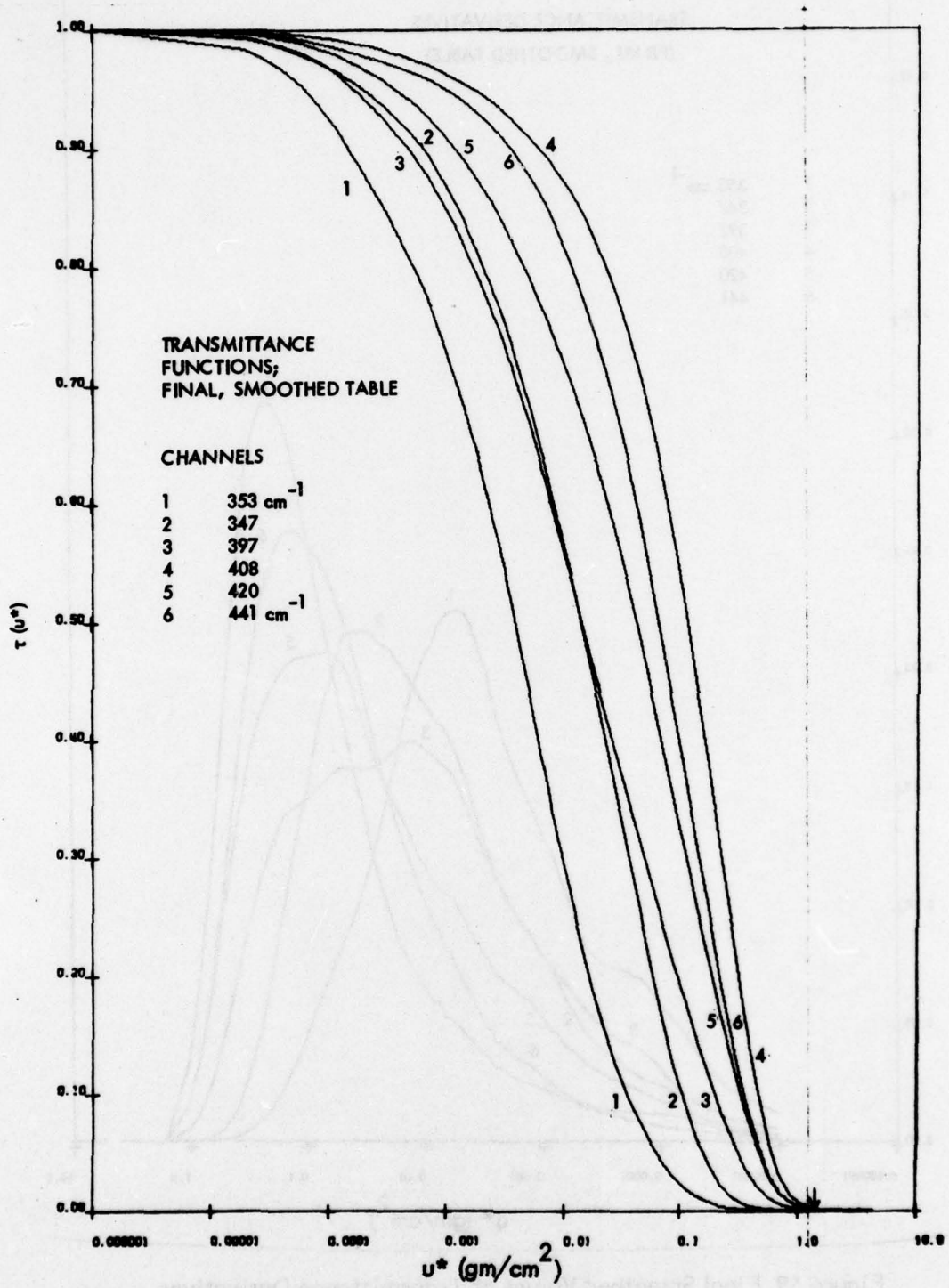

Figure 60 Final, Smoothed Transmittance Functions

7809-4

where the line intensity and root-intensity-halfwidth sums are over the lines in the interval $\Delta\nu$. McClatchey has computed $\sum S_i$ and $\sum (S\gamma)_i^{1/2}$ as a function of temperature for various spectral intervals, including 20 cm^{-1} bands at 795 and 900 cm^{-1}. Equation 56 does not include the contribution of the water vapor continuum.

Equation 56 applies to homogeneous paths. Following Godson[15] one can show that an appropriate generalization of Equation 56 for an inhomogeneous path is

$$\tau = \exp \left\{ \frac{-\int \sum S_i \, du}{\Delta\nu \left[1 + \frac{1}{4} \frac{\left[\int \left(\sum S_i \right) du \right]^2}{\int \left[\sum (S\gamma)_i^{1/2} \right]^2 du} \right]^{1/2}} \right\} \quad (57)$$

This transmission function together with the LOWTRAN 4 continuum model was used for computations involving the 795 and 900 cm^{-1} channels.

The alternate window channels at 795 and 900 cm^{-1} and the E7 band were not used in the formal retrievals described in Section 3.4. The effectiveness of the window channels in determining total water and surface temperature is discussed in Section 3.5.

3.3 C-MATRICES FOR H_2O RETRIEVAL

Figures 61 and 62 show C-matrices computed for the minimum information method. The first corresponds to a wet tropical profile with 4.4 gm/cm^2 total water, and the second to a dry arctic case with 0.06 gm/cm^2 total water. These matrices, which are typically iterated several times, do not characterize the retrieval solutions in the same way as the constant C-matrices for temperature retrieval. However, they indicate the pressure ranges over which humidity information is retrievable under very wet and very dry conditions. For the wet tropical case the range is approximately 200 mb to 700 mb; for the dry arctic case it is approximately 300 mb to the surface.

Figure 61 C-Matrix; Tropical Case, $\alpha = 2 \times 10^{-15}$ $(W/cm^2\text{-sr-}cm^{-1})^2$

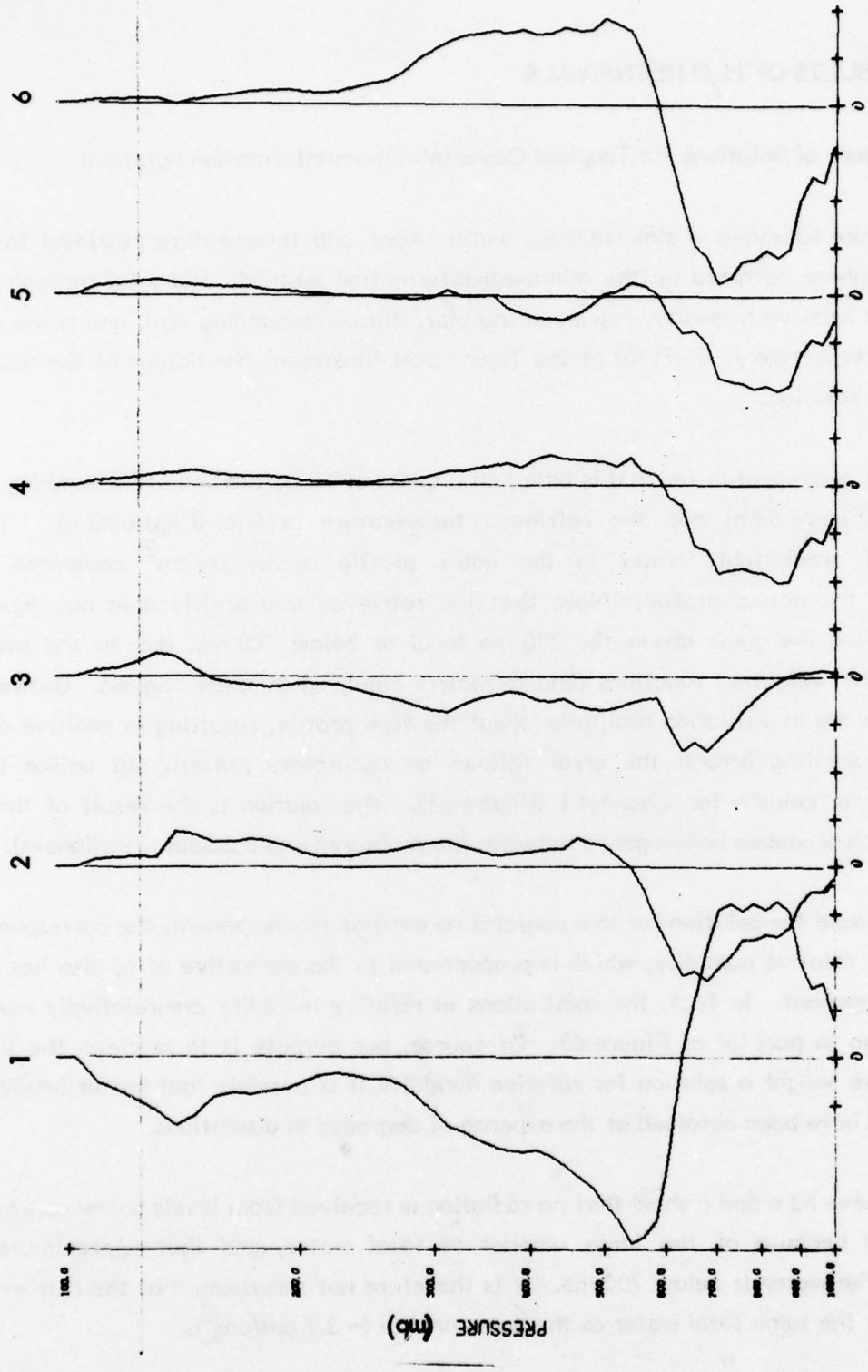

Figure 62 C-Matrix; Arctic Case, $\alpha = 4.4 \times 10^{-6}$ $(W/cm^2 \cdot sr\text{-}cm^{-1})^2$

7809-4

3.4 RESULTS OF H_2O RETRIEVALS

3.4.1 Nature of Solutions for Tropical Cases (Minimum-Information Solution)

Figure 63 shows a simultaneous water vapor and temperature retrieval for a tropical atmosphere obtained by the minimum-information method. Parts (a) through (d) show retrieved relative humidity, retrieved log u(p), the corresponding u(p), and retrieved temperature, respectively. Part (b) of the figure best illustrates the nature of the water vapor retrieval solution.

The guess profile for ln u is based on a guess of 60 percent relative humidity at all altitudes (Figure 63 a) and the retrieved temperature profile (Figure 63 d). The resulting total precipitable water in the guess profile is 3.7 gm/cm^2 compared to 4.4 gm/cm^2 in the actual profile. Note that the retrieved ln u profile does not depart significantly from the guess above the 200 mb level or below 700 mb, due to the small amplitude of the weighting functions (and C-matrix columns) in these regions. Between 200 and 700 mb the ln u solution oscillates about the true profile, resulting in positive and negative compensating errors; the error follows an oscillatory pattern not unlike the original C-matrix column for Channel 1 (Figure 61). The solution is the result of three iterations (which produced convergence between the measured and calculated radiances).

Because the solution for ln u contains an oscillatory component, the corresponding solution for relative humidity, which is proportional to the derivative of u, also has an oscillatory component. In fact, the oscillations in relative humidity are relatively much larger, as shown in part (a) of Figure 63. Of course, our purpose is to retrieve the ln u profile. Had we sought a solution for relative humidity it is possible that better behaved solutions would have been obtained at the expense of degraded ln u solutions.

Figures 63 a and c show that no radiation is received from levels below approximately 700 mb because of the large amount of total water, and that approximately 75 percent of the water is below 700 mb. It is therefore not surprising that the retrieved profile contains the same total water as the guess profile (~ 3.7 gm/cm^2).

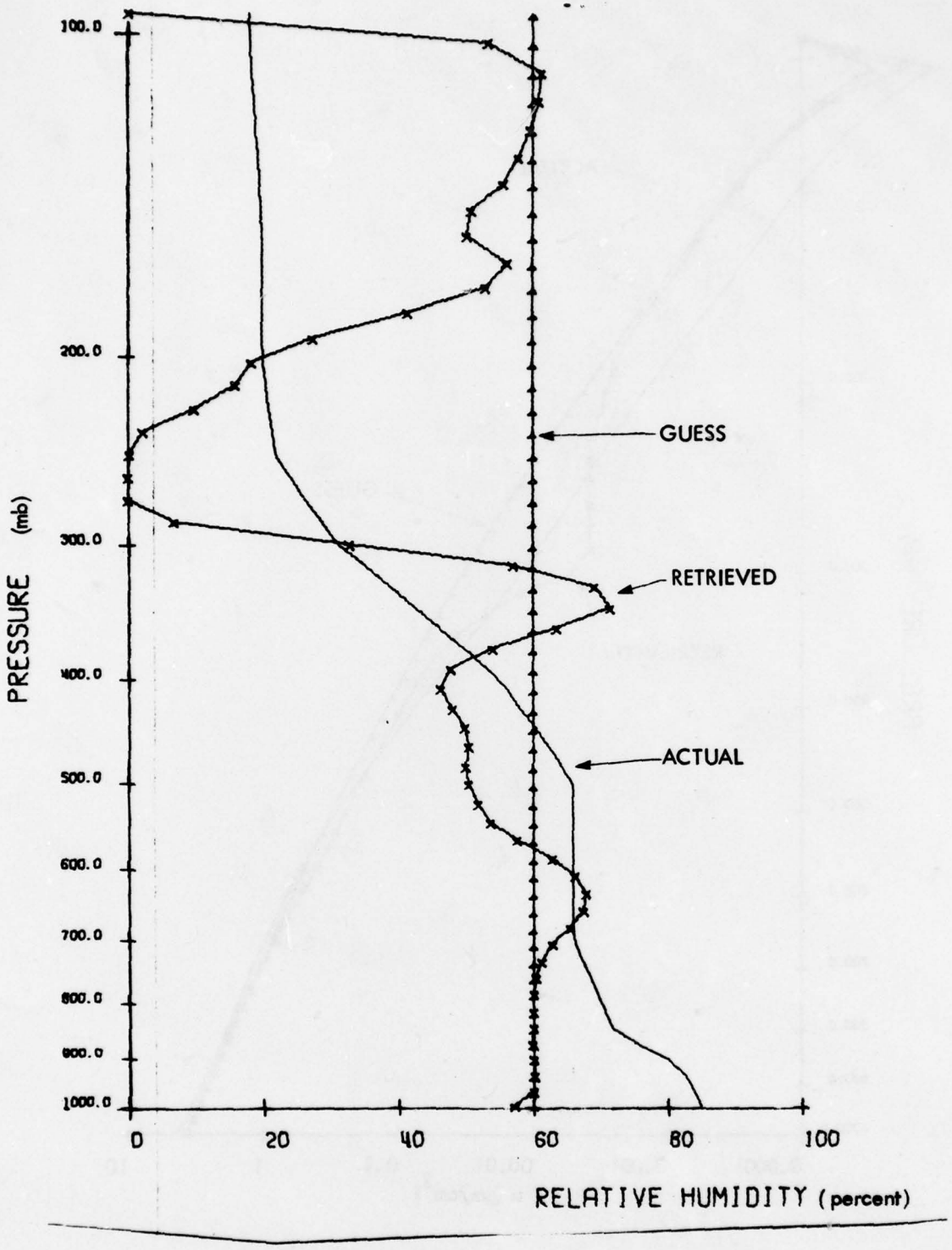

Figure 63a Water Vapor Retrieval For A Tropical Atmosphere By The Minimum-Information Method. (Retrieved Relative Humidity).

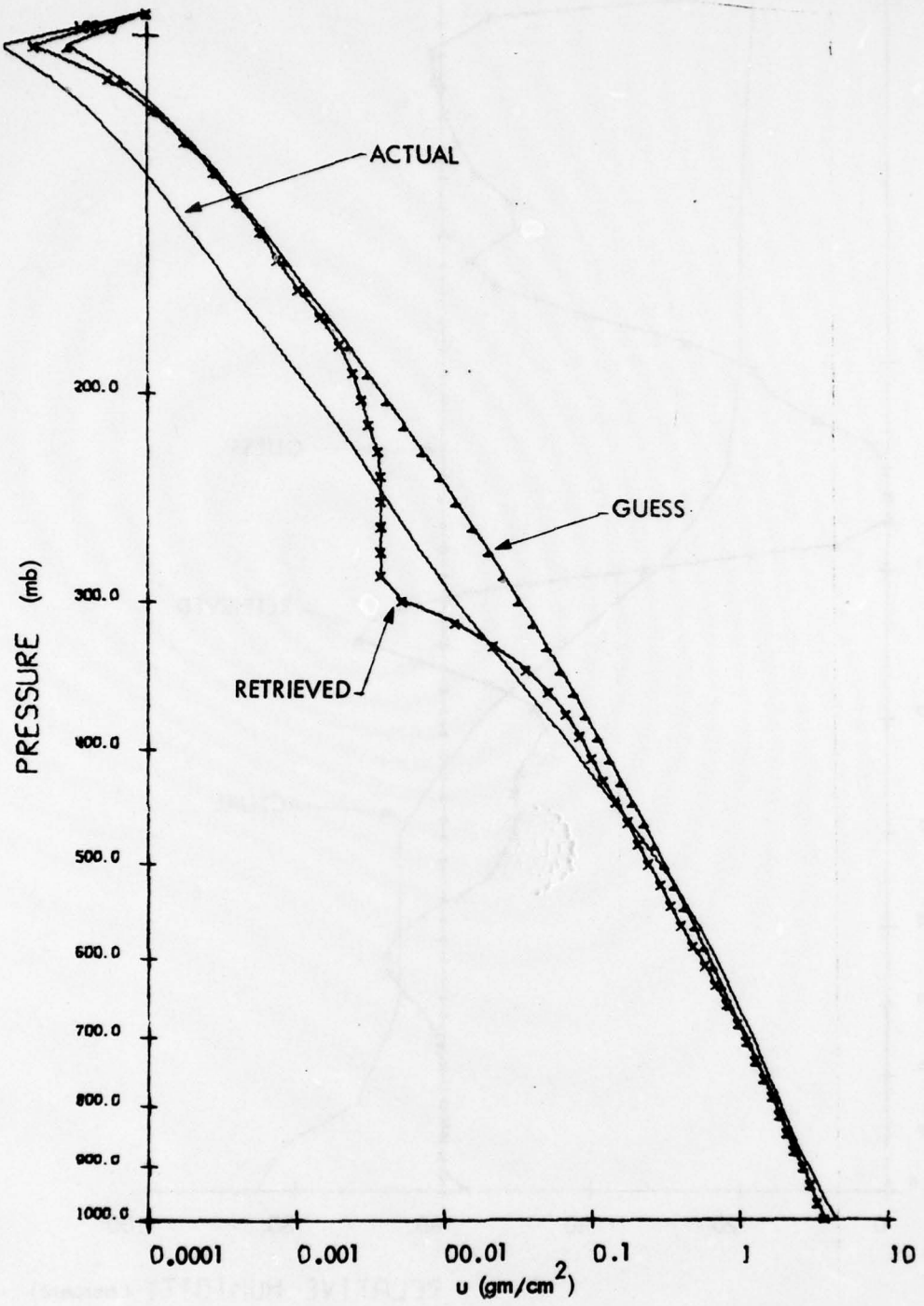

Figure 63b Water Vapor Retrieval For A Tropical Atmosphere By The Minimum-Information Method. Retrieved In u(p).

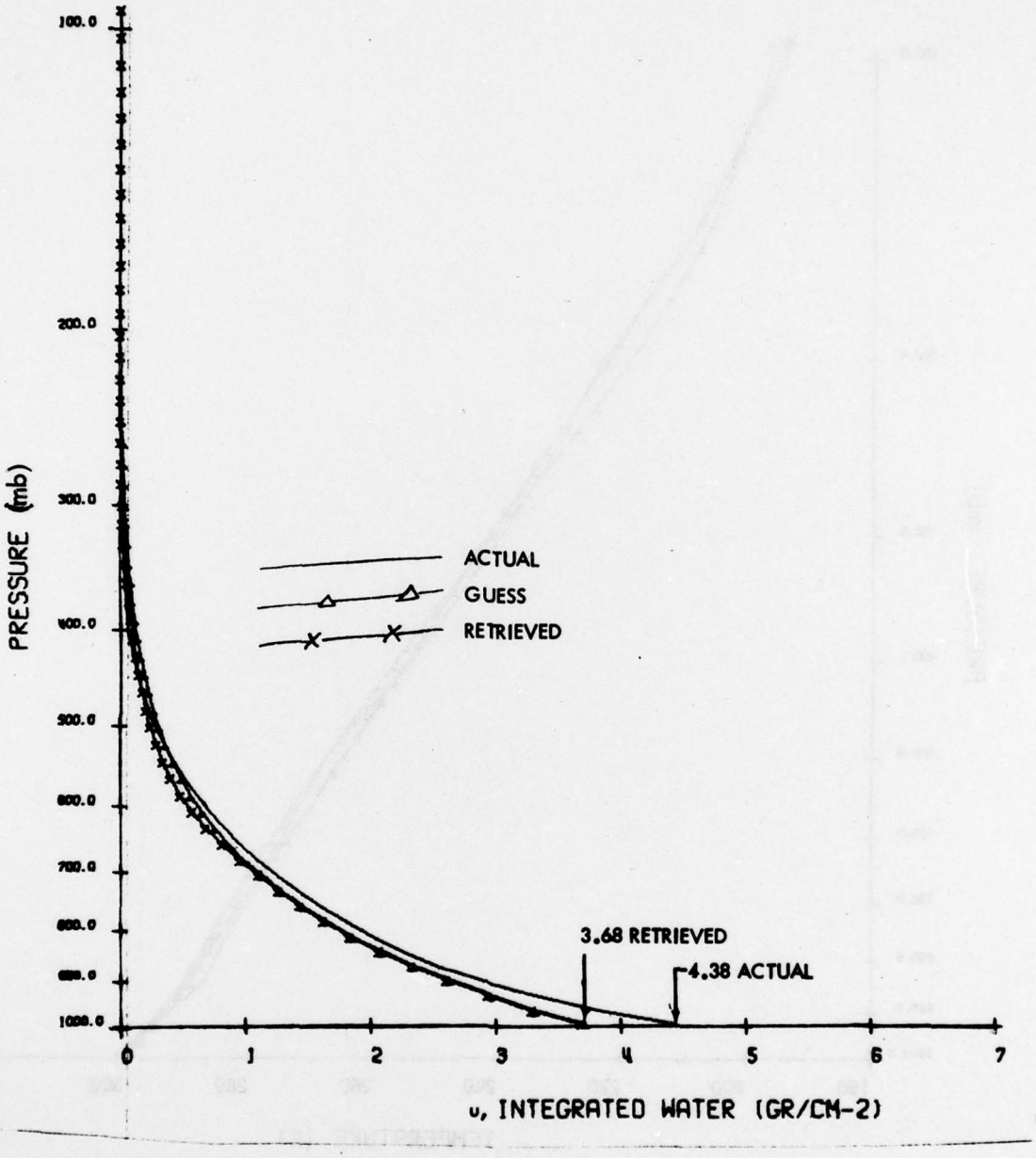

Figure 63c Water Vapor Retrieval For A Tropical Atmosphere By The Minimum-Information Method. Retrieved u(p).

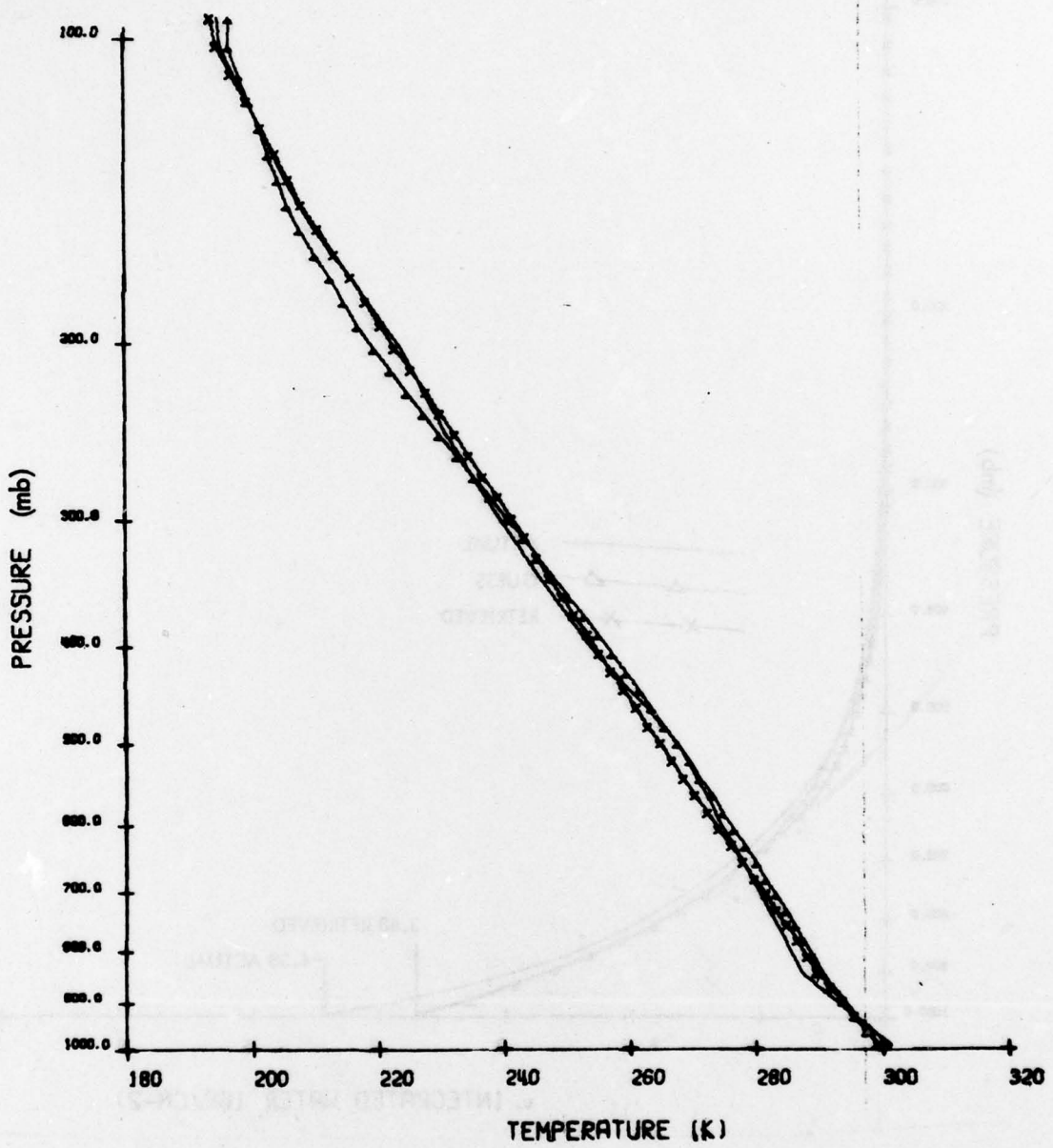

Figure 63d Retrieved Temperature Profile For Case Shown In Parts (a) Through (c).

Figure 64 shows the relative humidity retrieved for a similar case. Here the guess profile is a linear approximation (in relative humidity versus log p) to the actual profile. The total retrieved water is 4.5 gm/cm^2, approximately the same as for the guess and actual profiles. The retrieved humidity profile, while much smoother, bears only a slight resemblance to the actual profile.

3.4.2 Channel Redundancies

Figure 59, which shows the weighting function factor $-d\tau/d \ln u^*$ for the six channels, suggests that Channel 2 is somewhat redundant with Channel 3, and that Channels 4, 5 and 6 are redundant with each other. Since redundancy among channels tends to promote instability, it is logical to ask whether some of the oscillations in the retrieved moisture profiles are a result of the redundancies. We therefore repeated one of the tropical retrievals described above using only the three most independent channels: from Figure 59 these are Channels 1, 2 and 4, at 353 cm^{-1}, 347 cm^{-1} and 408 cm^{-1}, respectively. The conditions were the same as those represented in Figure 63.

The moisture profile retrieved using three channels differed only slightly from that obtained using the original six channels. In fact plotted in the form ln u versus ln p, the result would be indistinguishable from the "retrieved" curve in Figure 63 b. The corresponding relative humidity profiles for the 3- and 6-channel retrievals are shown in Figure 65. Note that the 3-channel result is slightly smoother than the 6-channel result; however, the differences in relative humidity values are very small.

We also performed 3- and 6-channel retrievals for a moderately dry case, represented by a Fort Churchill (latitude 59° N) radiosonde with 0.78 gm/cm^2 total precipitable water. The 3- and 6-channel results for both ln u and relative humidity were the same within a few percent.

The above comparisons show that virtually all the information available in the DMSP measurements is contained in Channels 1, 2 and 4. The retrievals presented in the following sections used only these three channels, except where noted.

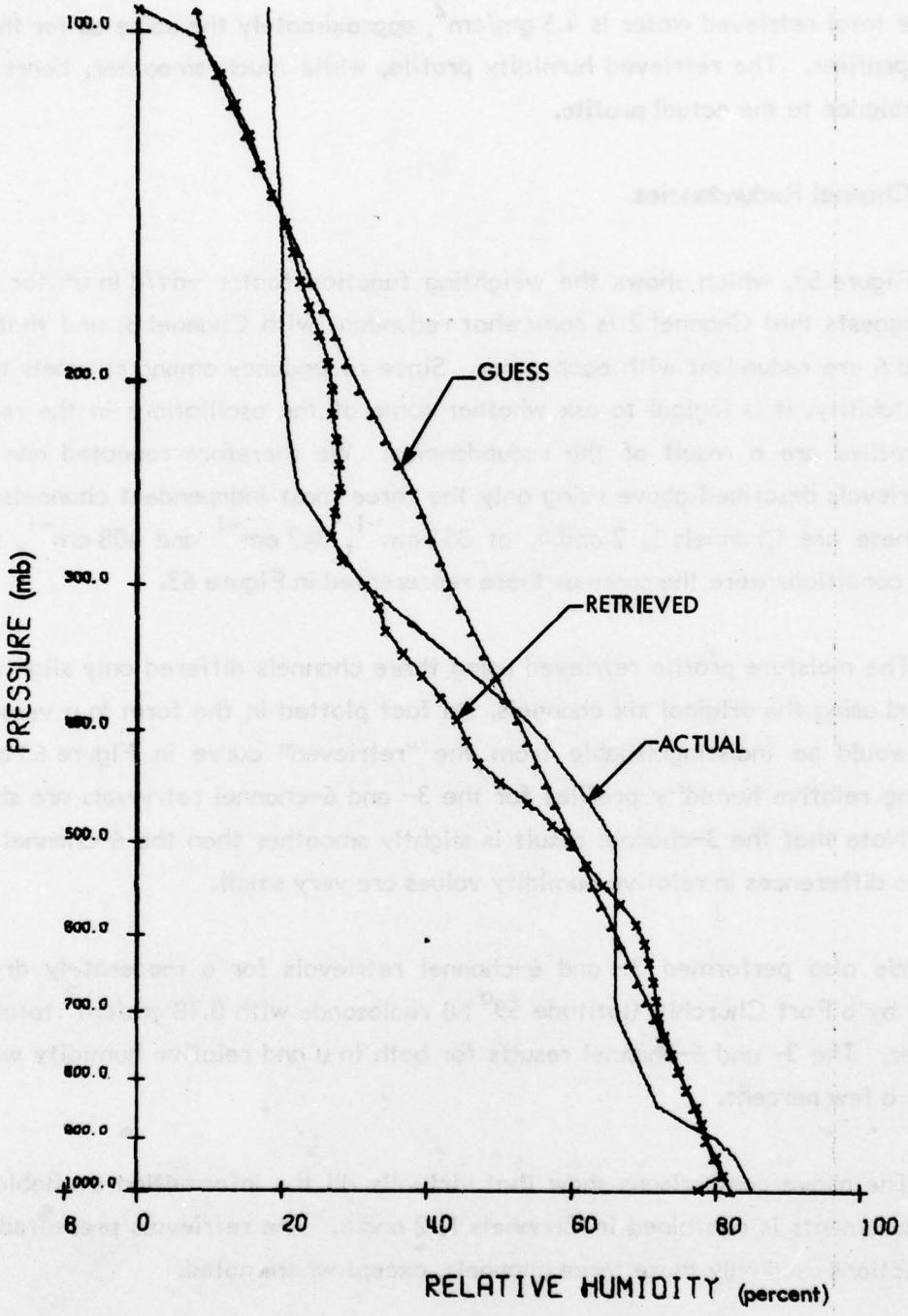

Figure 64 Retrieved Relative Humidity For A Tropical Case. Same Case As Figure 63(a) Except Guess Relative Humidity Profile is Linear.

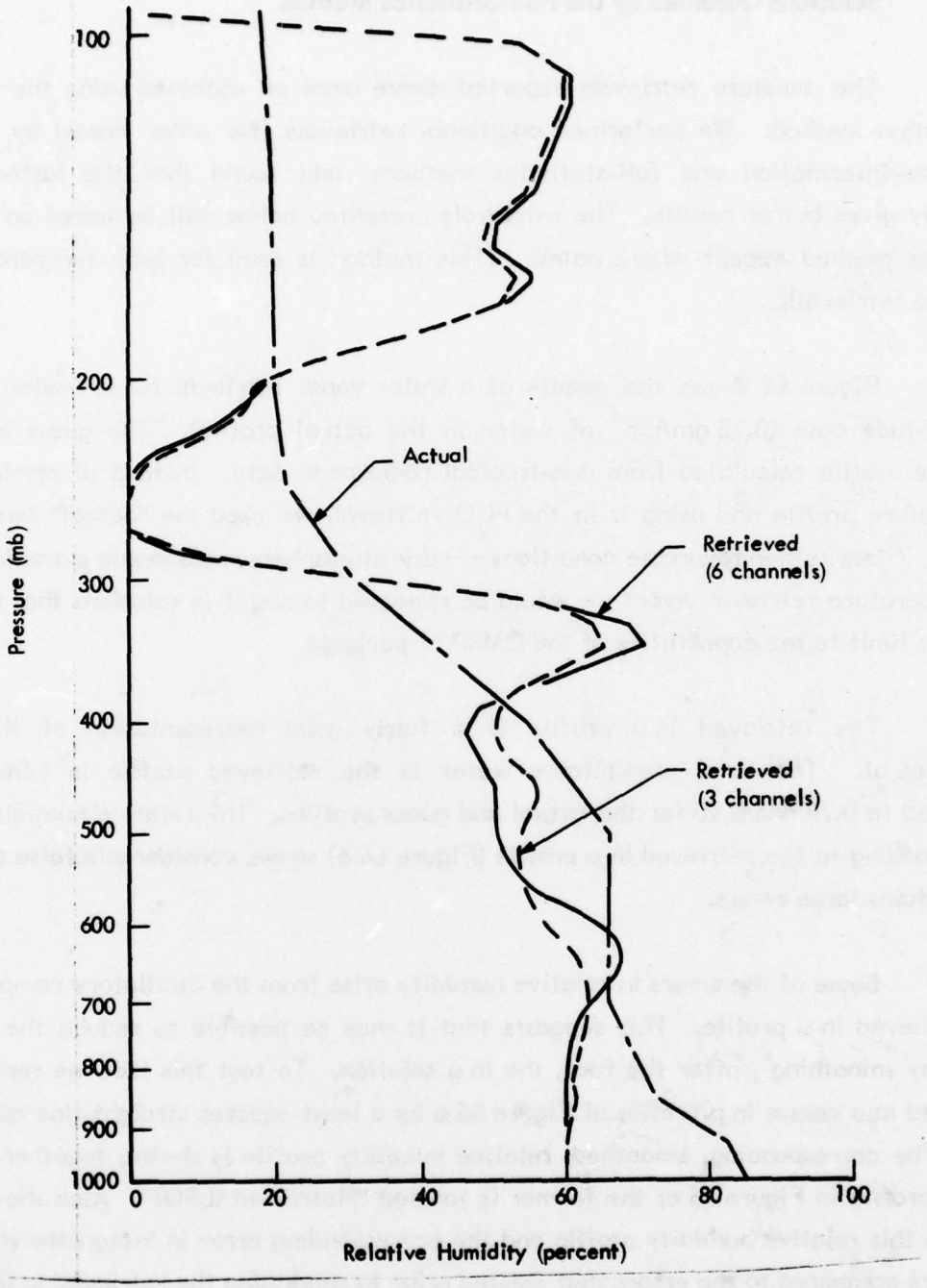

Figure 65 Retrieval of a Tropical Relative Humidity Profile Using The 6 DMSP Channels, and Using Only 3 Channels (1,2, and 4).

3.4.3 Solutions Obtained by the Full-Statistics Method

The moisture retrievals reported above were all obtained using the minimum information method. We performed additional retrievals (for other cases) by both the minimum-information and full-statistics methods, and found that the latter method generally gives better results. The retrievals presented below will be based on the full-statistics method except where noted. (This method is used for both temperature and moisture retrieval).

Figure 66 shows the results of a water vapor retrieval for a moderately dry, high-latitude case (0.78 gm/cm^2 of water in the actual profile). The guess is a mean moisture profile calculated from non-tropical radiosonde data. Instead of retrieving the temperature profile and using it in the H_2O retrieval, we used the "actual" temperature profile. These rather favorable conditions -- dry atmosphere, reasonable guess for ln u(p), no temperature retrieval errors -- would be expected to result in solutions that represent an upper limit to the capabilities of the DMSP H-package.

The retrieved ln u profile is a fairly good representation of the actual (Figure 66 a). The total precipitable water in the retrieved profile is 1.04 gm/cm^2, compared to 0.78 and 0.40 for the actual and guess profiles. The relative humidity profile corresponding to the retrieved ln u profile (Figure 66 b) shows considerable false structure, and contains large errors.

Some of the errors in relative humidity arise from the oscillatory components of the retrieved ln u profile. This suggests that it may be possible to reduce the humidity errors by smoothing , after the fact, the ln u solution. To test this idea we replaced the retrieved ln u versus ln p profile of Figure 66 a by a least-squares straight-line approximation. The corresponding, smoothed, relative humidity profile is shown, together with the actual profile in Figure 66 c; the former is labeled "Retrieved (LSQ)". Also shown is the error in this relative humidity profile and the corresponding error in integrated water u(p); these are compared to the errors that existed prior to smoothing the retrieved ln u(p).

It is evident that the least-squares smoothing process improved the inferred relative humidity distribution, but degraded the ln u(p) or u(p) profile; the third set of curves of Figure 66 c shows that smoothing substantially increased the average error in

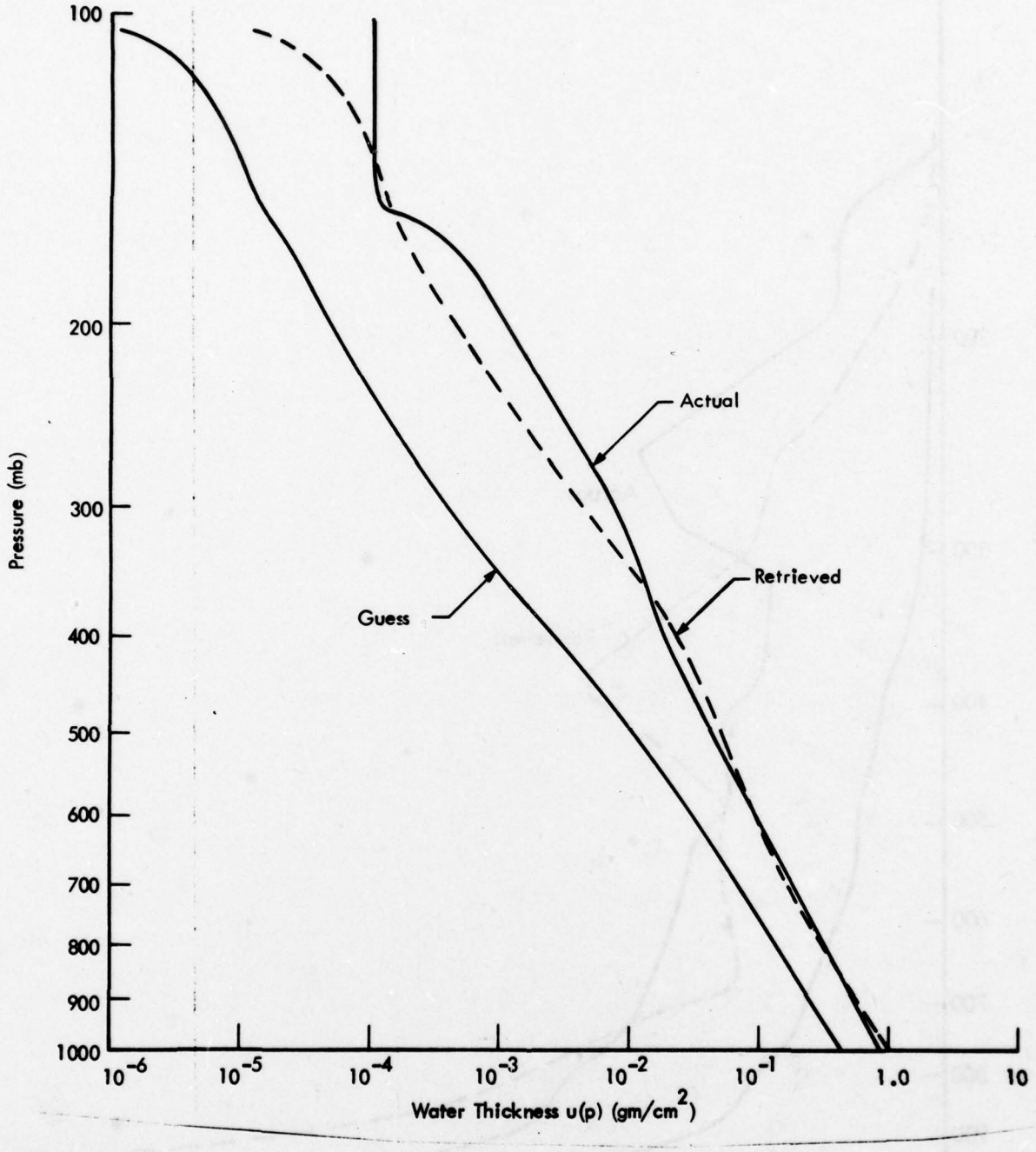

Figure 66a Water Vapor Retrieval For A Moderately Dry High-Latitude Case, (Full-Statistics Method). Retrieved u(p).

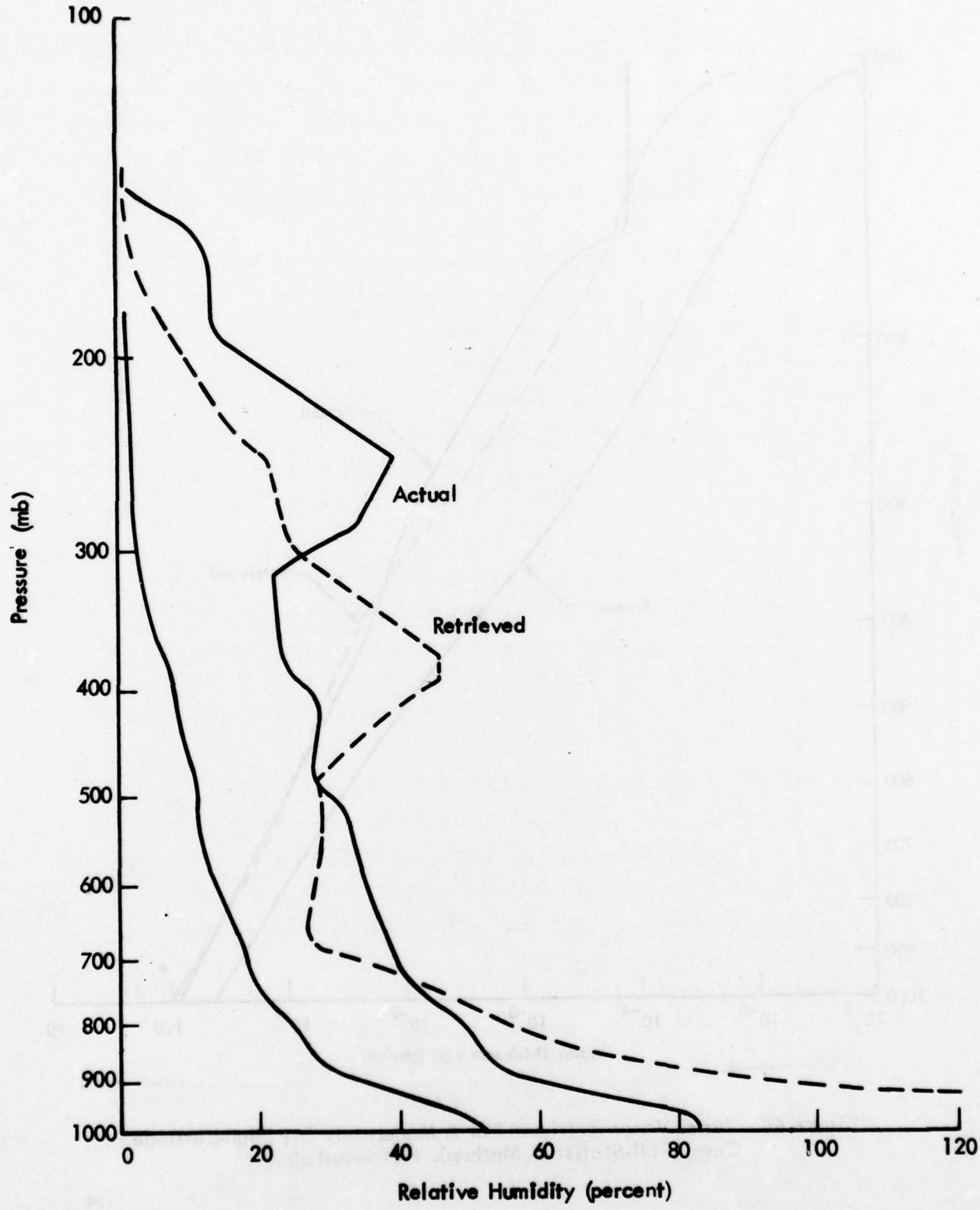

Figure 66b Water Vapor Retrieval For A Moderately Dry High-Latitude Case, (Full-Statistics Method). Retrieved Relative Humidity Profile.

7809-4

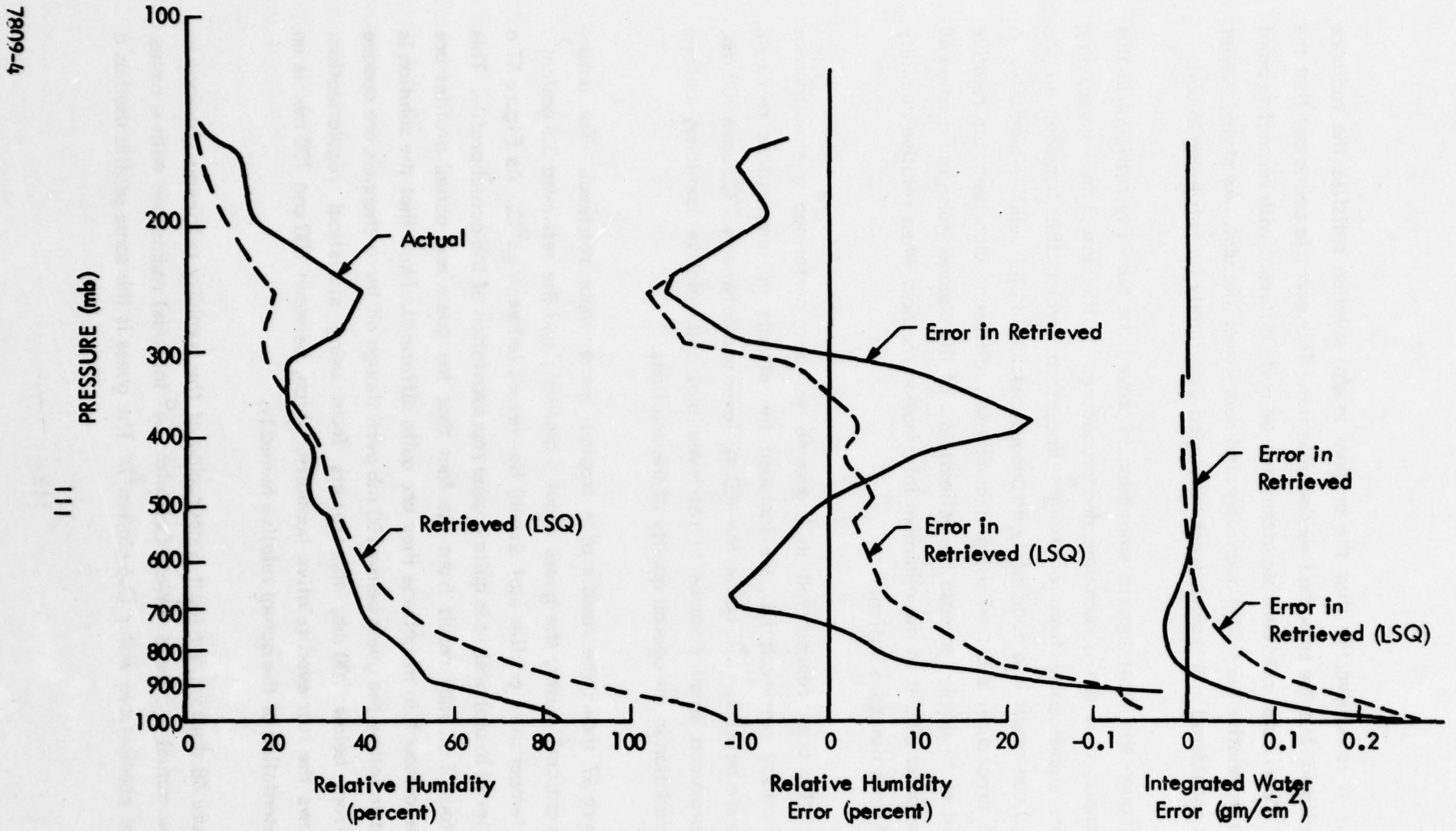

Figure 66c Retrieved Relative Humidity After Smoothing In u(p) Solution of Figure 66a

retrieved u(p). It is noteworthy that the original ln u(p) solution satisfies the radiance convergence criterion but the smoothed version does not. This example points out that the capabilities of a particular retrieval algorithm may be quite different with respect to point variables (such as relative humidity) and integrated quantities, like u(p). As stated earlier the algorithms considered in this study were developed specifically for retrieving ln u(p).

Although the least-squares smoothing improved the humidity retrieval in this particular example, it is not a recommended procedure. If the actual ln u versus ln p profile deviates significantly from a straight line, then forcing this behavior on the retrieved ln u(p) can result in a completely erroneous distribution for relative humidity. A better general procedure, short of using a completely different algorithm for relative humidity, would be to simply increase the estimate σ_E of the channel noise in Equation 49 (or increase the parameter α in the minimum information method) when relative humidity will be derived from the u(p) solution.

For the case represented in Figure 66 we also performed a simultaneous temperature-humidity retrieval; i.e., we included the effects of temperature retrieval errors, which were between $\pm 1^{\circ}$C below the 400 mb level and between $\pm 3^{\circ}$C above 400 mb. These errors produced small changes in retrieved u(p) and relative humidity, but no significant degradation in the overall quality of the solutions.

Figure 67 shows the results of a tropical water vapor retrieval. The actual profile has 4.4 gm/cm^2 water, the guess about 1 gm/cm^2, and the retrieved 3.3 gm/cm^2. The retrieved temperature profile (not shown) has errors between $\pm 3^{\circ}$C. As Figure 67 a shows, the retrieved ln u(p) profile is quite a good representation of the actual profile. This may be fortuitous, i.e., may result from the fact that the guess and actual profiles are similar in shape (although in magnitude they are quite different). Note that the solution is not constrained to follow the guess below 700 mb even though all three channels are opaque to radiation from below 700 mb; this results from using statistical regularization. Figure 67 b shows the retrieved relative humidity, which, between 200 and 700 mb, is an excellent representation of the actual relative humidity.

Figure 68 displays the least encouraging of the humidity retrievals obtained in this study. The actual profile is a West Geirinish (64° latitude) radiosonde with a rather large amount of precipitable water (3.6 gm/cm^2). The guess is the same profile used as a

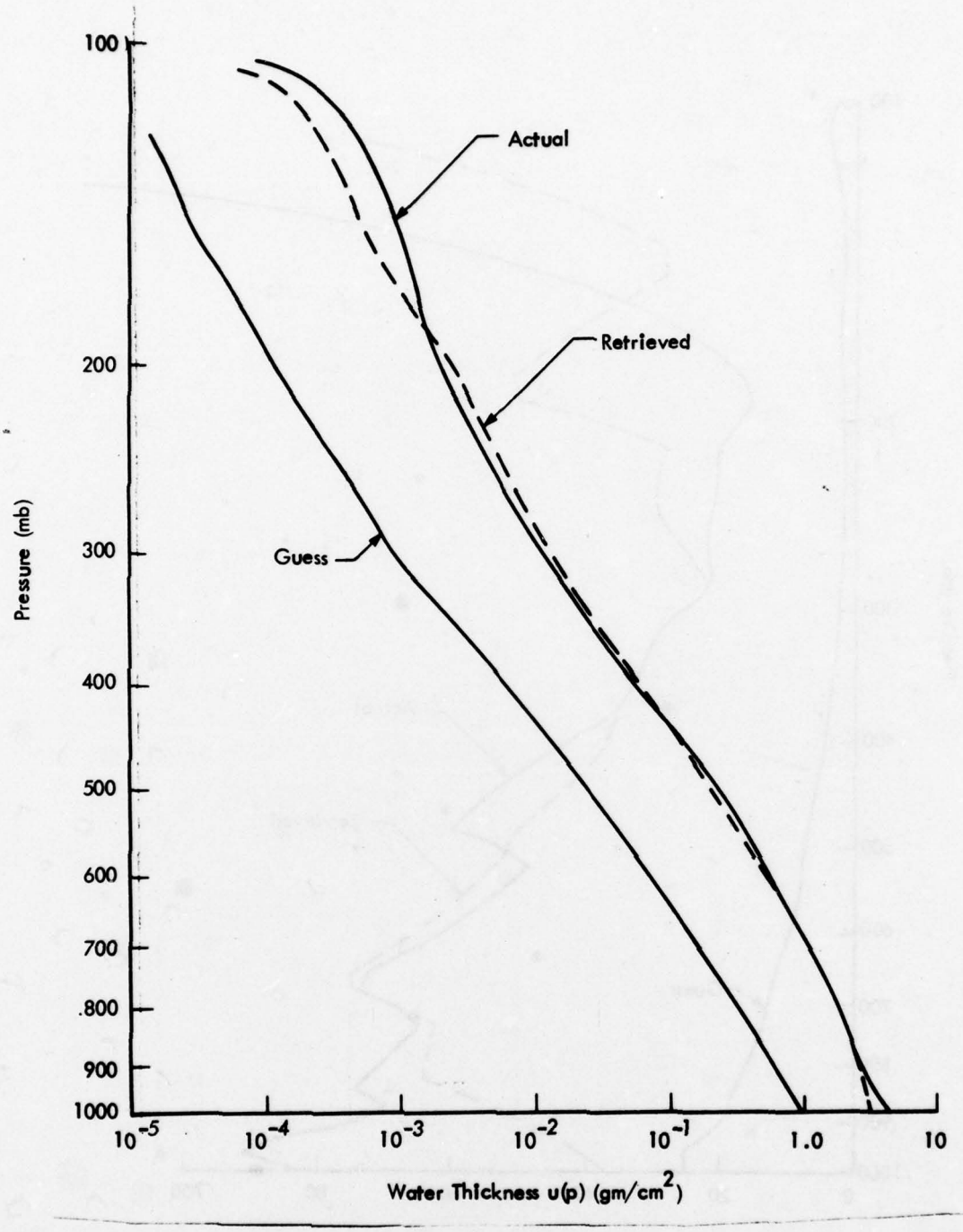

Figure 67a Water Vapor Retrieval For A Tropical Case, (Full-Statistics Method). Retrieved u(p).

7809-4

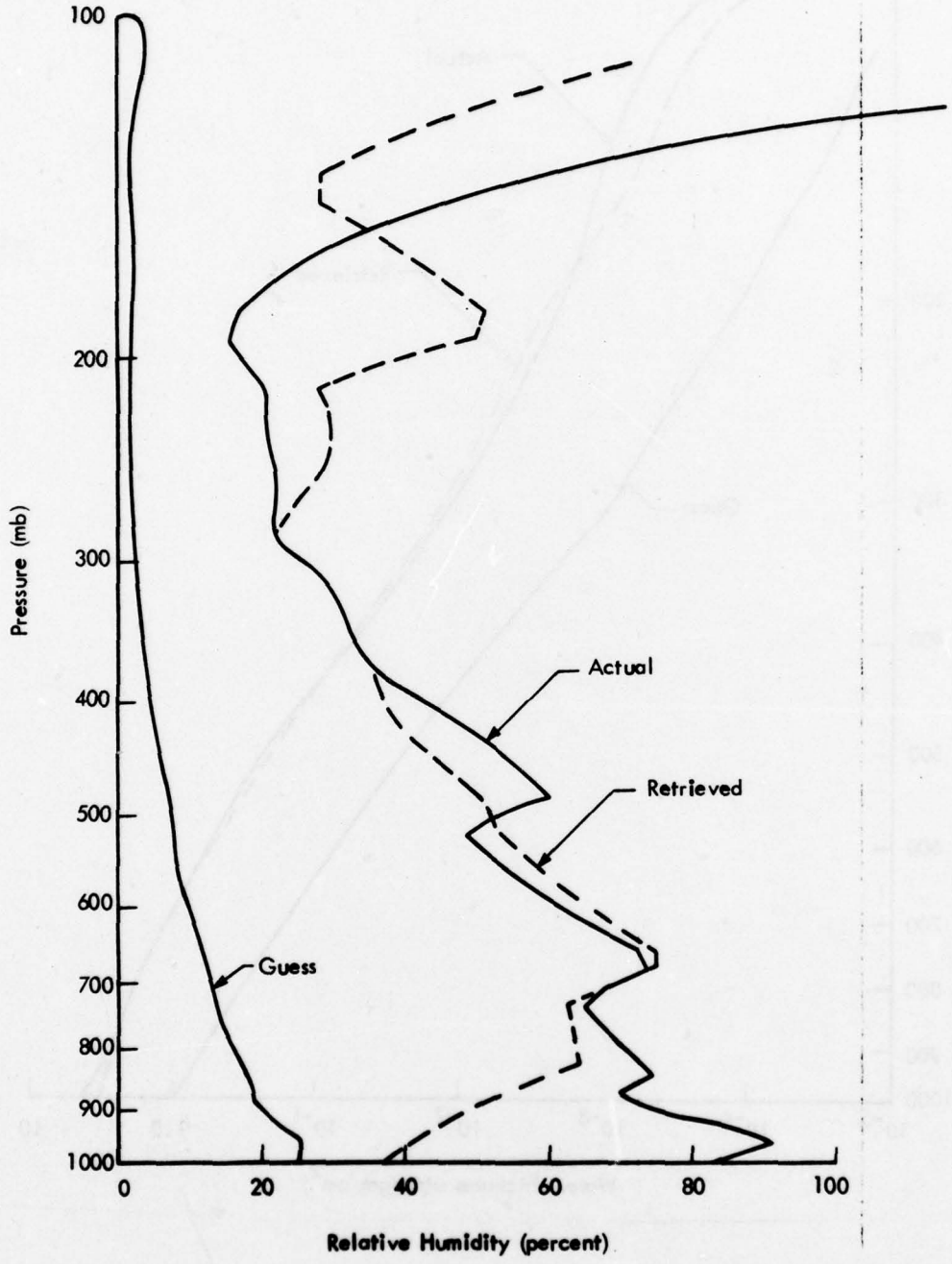

Figure 67b Water Vapor Retrieval For A Tropical Case, (Full-Statistics Method). Retrieved Relative Humidity Profile.

guess in the previously described retrievals based on the full-statistics method: it represents a mean for tropical latitudes but is scaled to 1 gm/cm^2 total precipitable H_2O. The covariance matrix S also represents tropical conditions. The retrieved profile contains 8.3 gm/cm^2 of precipitable water.

The retrieved ln u(p) profile is actually a reasonable low-resolution approximation to the guess profile. However, it is much too smooth, which is a property imposed by the guess profile and the covariances used in regularizing the solution. The smoothness of the solution results in the rather large error of 4.7 gm/cm^2 in total precipitable water. The errors in u(p) are equally large on a percentage basis at the 500 mb level. (Note that if we had used the minimum information method the total water would be determined by the guess, and the error would still be large.)

We also computed a mean ln u profile and covariance matrix S for extratropical latitudes. The data base is a set of 1200 radiosondes, provided by AFGL -- the same data used for the calculation of the tropical mean and covariance. The two means were found to have virtually the same shape; i.e., $\langle u \rangle$ for the tropics is approximately a factor of two higher than the extratropical $\langle u \rangle$ at all pressure levels. It was found also that the water vapor retrievals obtained by the full-statistics method depend only slightly on which mean-covariance set is used. Similarly, it was found that the solutions are unaffected when the guess u(p) profile is scaled by a constant factor. Thus, the errors in the retrieved profile shown in Figure 68 cannot be attributed to using statistics for the wrong latitudes, or to applying too small a scale factor to the guess profile.

3.4.4 Effects of Temperature Retrieval Errors

Errors in the retrieved temperature profile will naturally contribute to errors in the retrieved ln u profile. This error propagation effect was not studied in detail; a few sample computations were performed to estimate the magnitude of the effect and determine general trends.

Figure 69 shows the results of one such calculation. We first retrieved the temperature profile, which contained errors between $\pm 2.5^{\circ}$C, and a surface temperature error of -1.0°C. We then performed a humidity retrieval using in one case a correct guess for the vertical distribution of relative humidity, and in another case a correct guess for

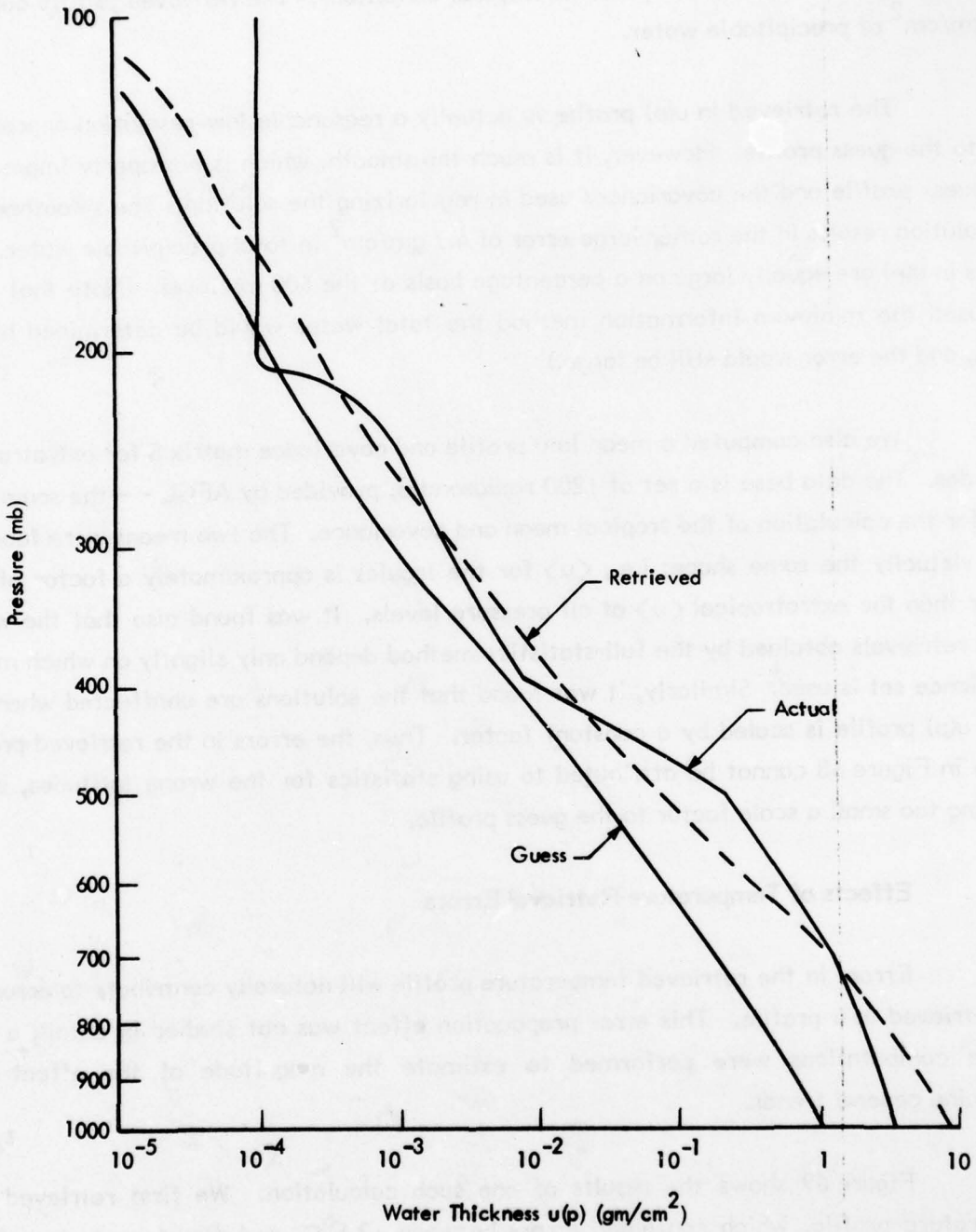

Figure 68 Retrieval Of A Wet Mid-latitude Profile. (Full-Statistics Method).

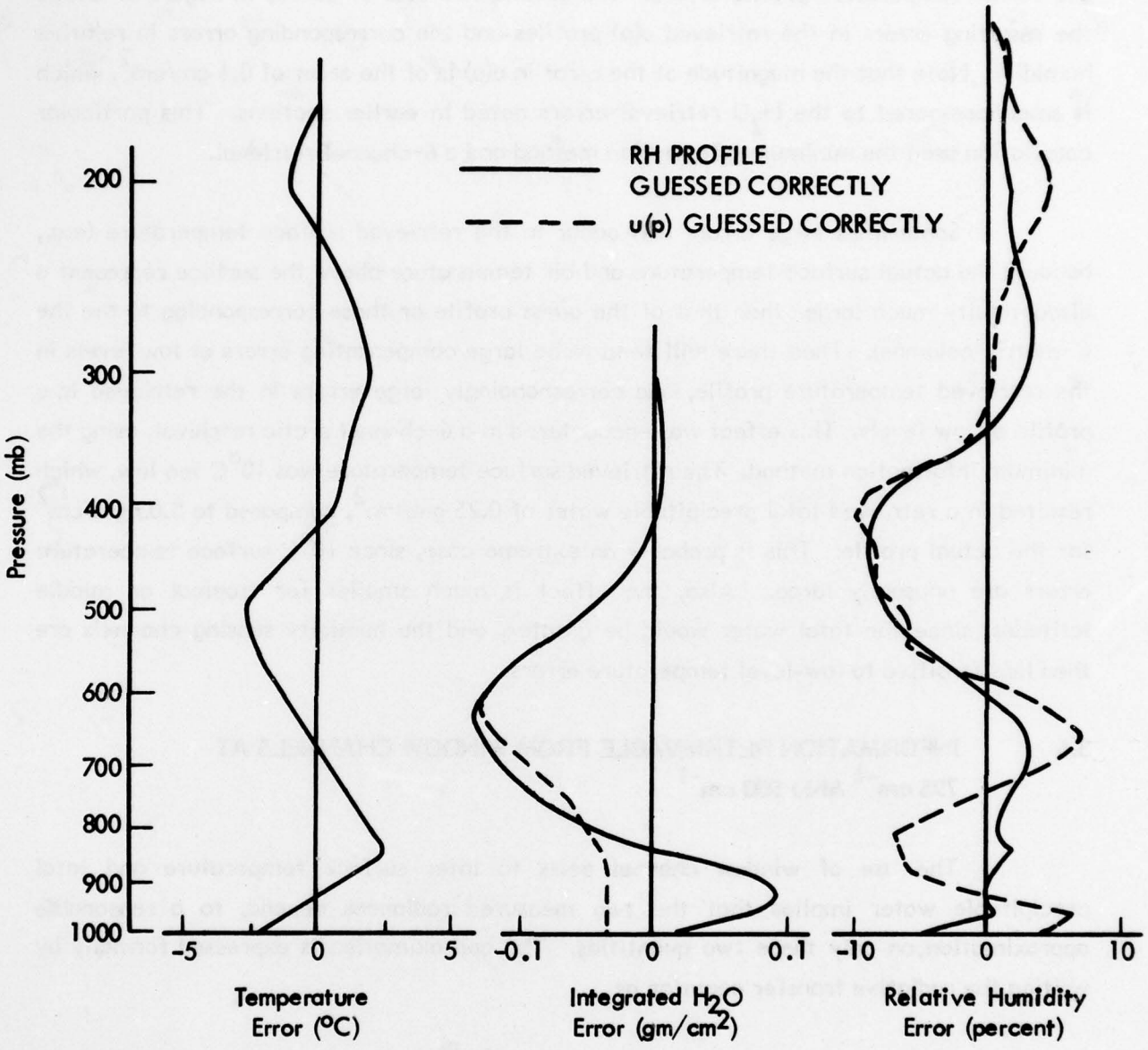

Figure 69 Effects of Temperature Retrieval Errors

the precipitable water profile u(p). When one of these is correct the other will be incorrect due to the temperature profile errors. The second two sets of curves in Figure 69 shows the resulting errors in the retrieved u(p) profiles and the corresponding errors in relative humidity. Note that the magnitude of the error in u(p) is of the order of 0.1 gm/cm^2, which is small compared to the H_2O retrieval errors noted in earlier sections. This particular calculation used the minimum information method and a 6-channel retrieval.

Sometimes large errors will occur in the retrieved surface temperature (e.g., because the actual surface temperature and air temperature above the surface represent a discontinuity much larger than that of the guess profile or those corresponding to the the C-matrix columns). Then there will tend to be large compensating errors at low levels in the retrieved temperature profile, and correspondingly large errors in the retrieved ln u profile at low levels. This effect was encountered in a 6-channel arctic retrieval, using the minimum information method. The retrieved surface temperature was 10°C too low, which resulted in a retrieved total precipitable water of 0.25 gm/cm^2, compared to 0.05 gm/cm^2 for the actual profile. This is probably an extreme case, since 10°C surface temperature errors are unusually large. Also, the effect is much smaller for tropical or middle latitudes, since the total water would be greater, and the humidity sensing channels are then less sensitive to low-level temperature errors.

3.5 INFORMATION RETRIEVABLE FROM WINDOW CHANNELS AT 795 cm^{-1} AND 900 cm^{-1}

The use of window channel pairs to infer surface temperature and total precipitable water implies that the two measured radiances depend, to a reasonable approximation, on only these two quantities. The approximation is expressed formally by writing the radiative transfer equation as

$$I_i (u_s, T_s) \simeq \tilde{\tau}_i (u_s) B_i (T_s) + \tilde{N}_i (u_s); \quad i = 1, 2 \qquad (58)$$

where I_i is the total upwelling radiance for channel i, $B_i (T_s)$ is the Planck blackbody emission for surface temperature T_s, and $\tilde{\tau}_i (u_s)$ and $\tilde{N}_i (u_s)$ are the transmittance and upward radiance, respectively, of the entire atmosphere when it contains total precipitable water u_s. The last two quantities are averages over a set of representative vertical water vapor and temperature distributions. The fact that averages must be used is, of course, the

reason the equation is an approximation. The approximation becomes more accurate with decreasing u_s and/or decreasing channel opacity.

According to Equation 58 the surface temperature may be expressed as

$$T_s = B_i^{-1}\left[\frac{I_i - \tilde{N}_i(u_s)}{\tilde{\tau}_i(u_s)}\right]; \quad i = 1, 2 \qquad (59)$$

where $B_i^{-1}(I_i)$ is the inverse Planck function. If the radiance I_i and empirical functions $\tilde{N}_i(u_s)$, $\tilde{\tau}_i(u_s)$ are given, Equation 59 can be used to obtain T_s as a function of u_s. In fact, two curves of T_s versus u_s can be obtained corresponding $i = 1$ and $i = 2$. The coordinates of the intersection of the curves represent solutions for T_s and u_s. This is essentially the algorithm used in inferring surface temperature and total precipitable water. When Equation 59 is used in this way, I_i represents the actual (measured) radiances, which do not necessarily satisfy Equation 58 for the actual u_s and T_s; that is, the solution values will generally be in error.

For each of 218 radiosonde profiles of humidity and temperature we calculated the transmittance of the entire atmosphere and its radiance (excluding the surface contribution) in each of the two window channels. Let these quantities be denoted τ_1^k, τ_2^k, N_1^k and N_2^k, with k indicating the particular member of the ensemble of 218 radiosondes. The four quantities plotted each as a function u_s^k, the total precipitable water for ensemble member k, are shown as Figures 70 through 73. Visually-estimated best-fit curves were drawn through these points to obtain the averages $\tilde{\tau}_i(u_s)$, $\tilde{N}_i(u_s)$ referred to above. These functions are each represented in the computer by a table of 65 values (see Appendix A). Note that the scatter in the plotted points becomes larger as u_s^k increases, corresponding to the deterioration in accuracy of Equation 58.

To test the accuracy of the algorithm, we used it to retrieve u_s and T_s for 218 x 3 cases, consisting of the 218-member radiosonde set combined with surface temperatures equal to T_1^k and $T_1^k \pm 5^\circ C$, where T_1^k are the radiosonde air temperatures

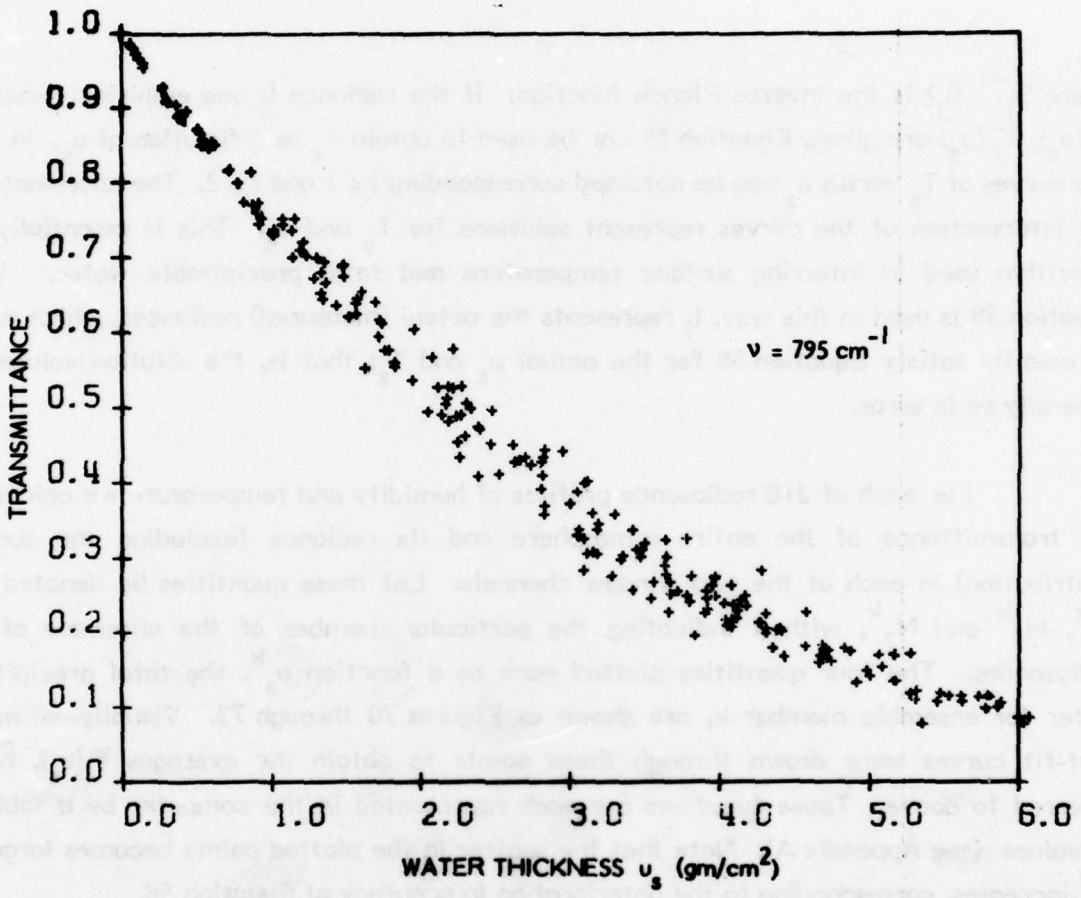

Figure 70 Computed Transmittances $\tau_l^k (u_s^k)$ for 218 Cases

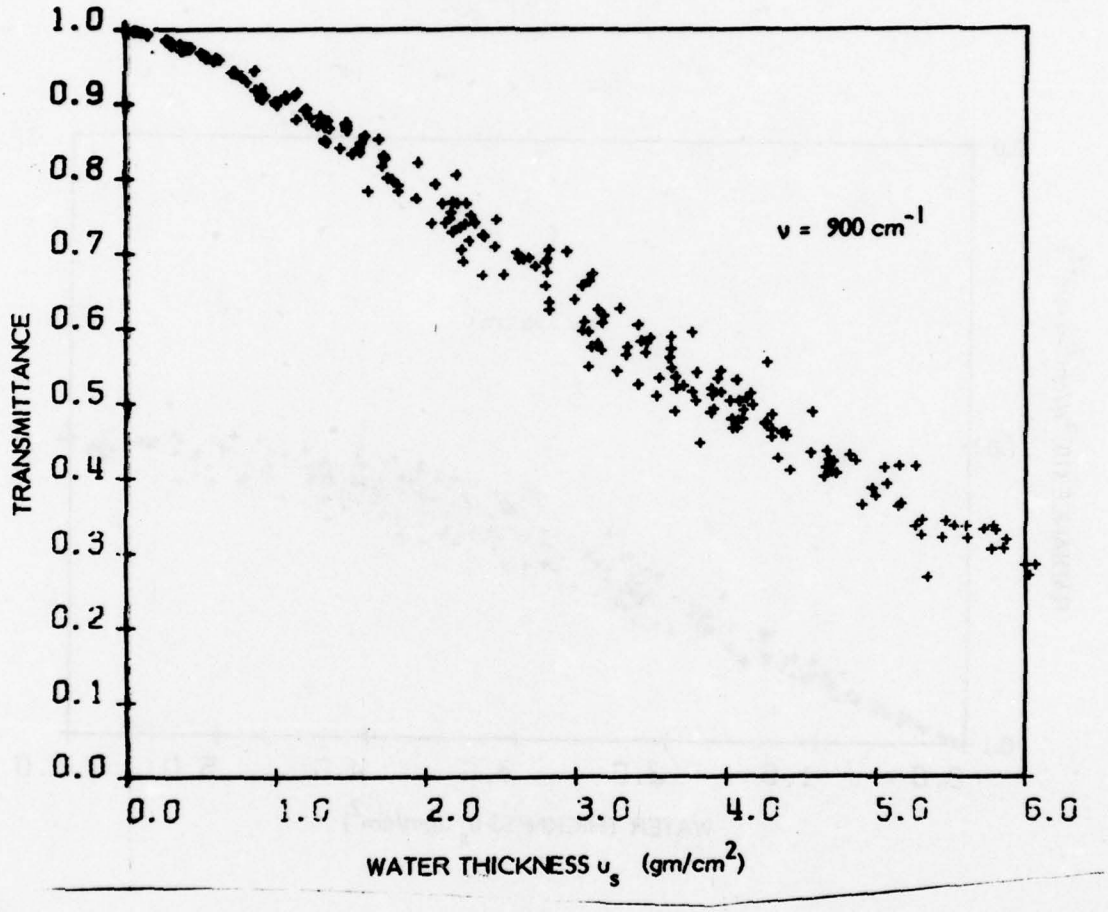

Figure 71 Computed Transmittances $\tau_2^k (u_s^k)$ for 218 Cases

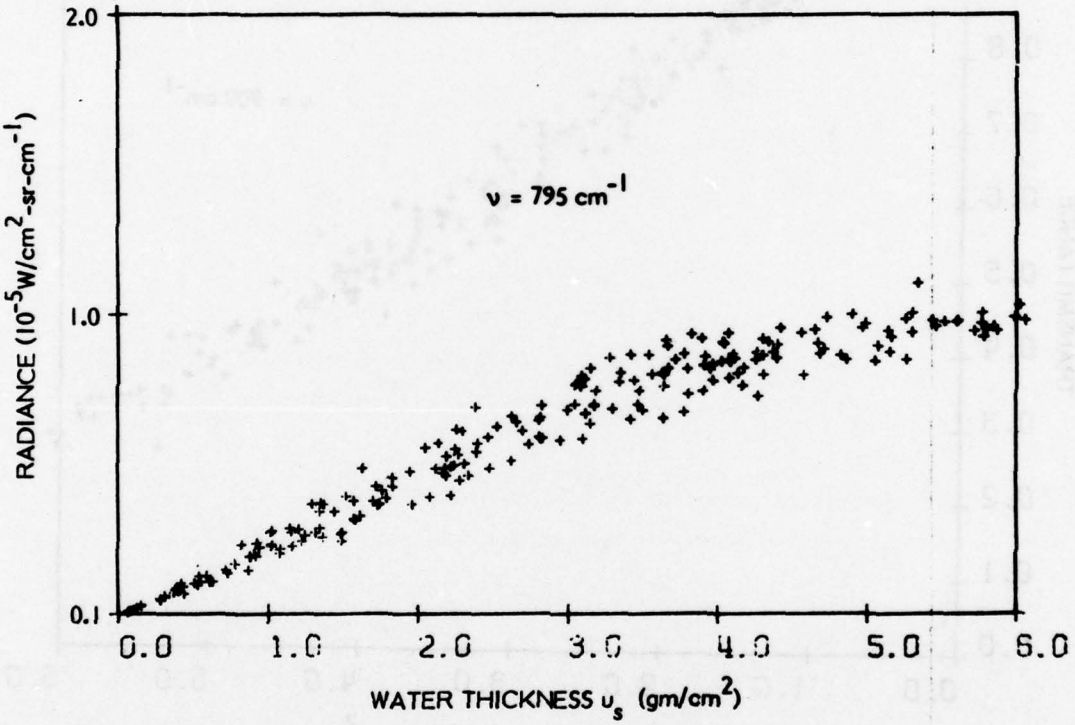

Figure 72 Computed Radiances $N_l^k (\upsilon_s^k)$ for 218 Cases

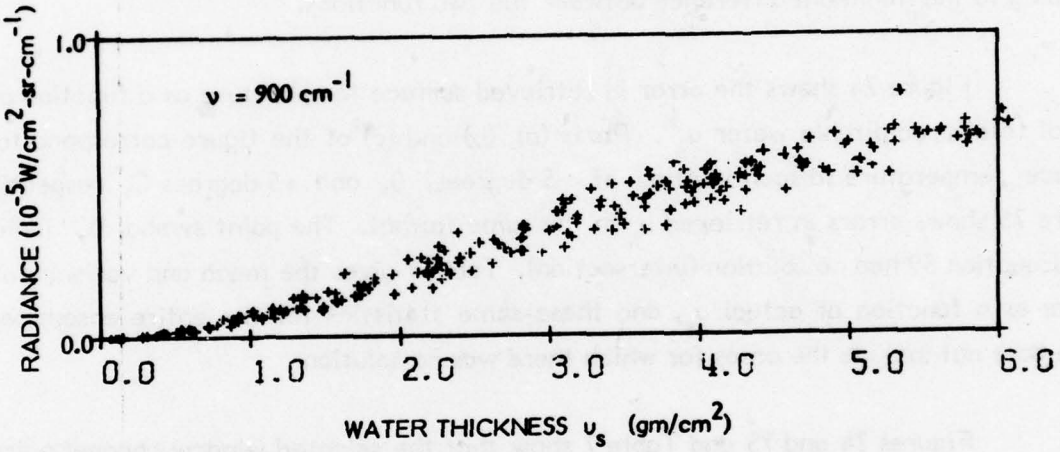

Figure 73 Computed Radiances N_2^k (u_s^k) for 218 Cases

just above the surface. We realize that this method of constructing surface temperatures is rather arbitrary, but we could not find any data describing the statistics of surface temperature, or possible correlations between effective surface temperature and low-level air temperature.

It was found that the pair of equations 59 do not always have a unique solution, because of the approximation inherent in using the averages $\tilde{N}_i$ and $\tilde{\tau}_i$. That is, for some of the values substituted into Equation 59 the two functions do not intersect, and in some cases there are multiple intersections. It was determined empirically that in the case of multiple intersections, the one corresponding to the largest u_s generally gave the best solution. When there were no intersections we determined u_s and T_s from the point corresponding to the minimum difference between the two functions.

Figure 74 shows the error in retrieved surface temperature as a function of the actual total precipitable water u_s^k. Parts (a), (b) and (c) of the figure correspond to air-surface temperature discontinuities of −5 degrees, 0, and +5 degrees C, respectively. Figure 75 shows errors in retrieved u_s in the same format. The point symbol "C" indicates that Equation 59 had no solution (intersection). Table 7 gives the mean and variance of the errors as a function of actual u_s, and these same statistics for the entire ensemble; the table does not include the cases for which there was no solution.

Figures 74 and 75 and Table 7 show that the selected window channel pairs are ineffectual in determining total precipitable water: even when the total water is less than 1 gm/cm^2 and the surface temperature discontinuity is within $\pm 5^\circ$C, the mean-plus-one-sigma error in inferred total water can equal 0.5 gm/cm^2. However, the window channels give fairly good estimates of surface temperature: for $u_s \leq 2$ gm/cm^2 the mean-plus-one-sigma error is less than 1°C, and it is less than 2°C for any of the unit thickness water bins between 0 and 5 gm/cm^2.

While these window channels are not useful by themselves for determining total precipitable water, they would be excellent candidates as additional sounding (inversion) channels. The weighting function for the 795 cm^{-1} channel was plotted in the format of Figure 59, and was found to have a peak at a u value greater than 4 gm/cm^2.

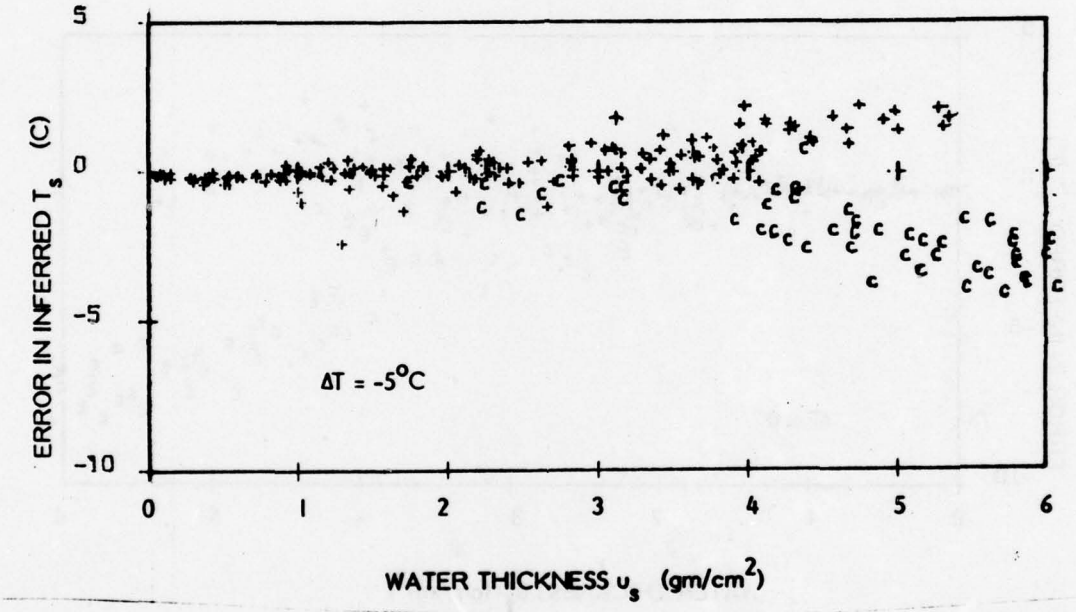

Figure 74 a Errors in Inferred Surface Temperature T_s for $T_s = T_1 - 5^{\circ}C$

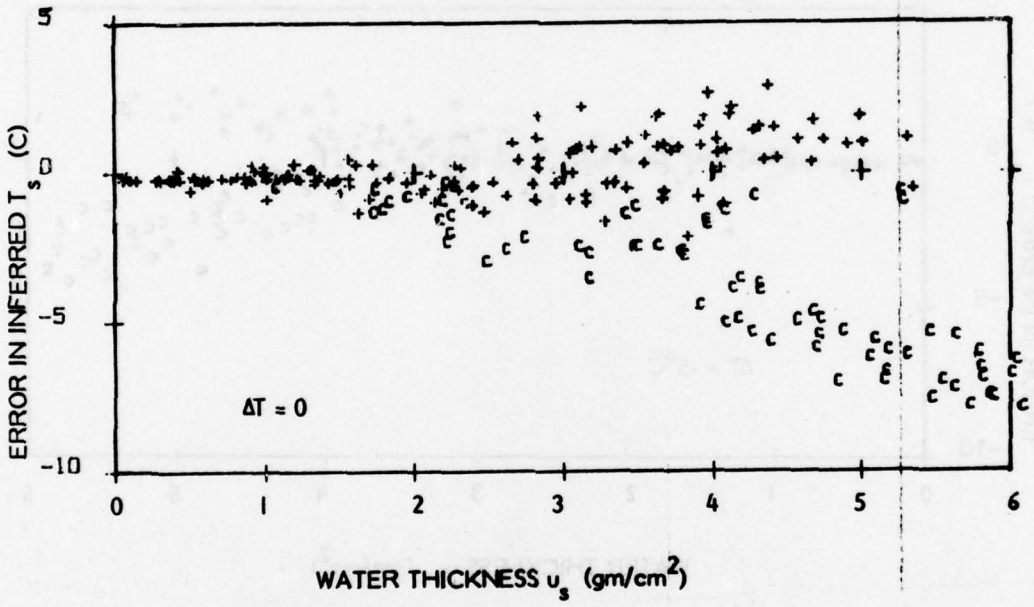

Figure 74 b Errors in Inferred Surface Temperature T_s for $T_s = T_1$

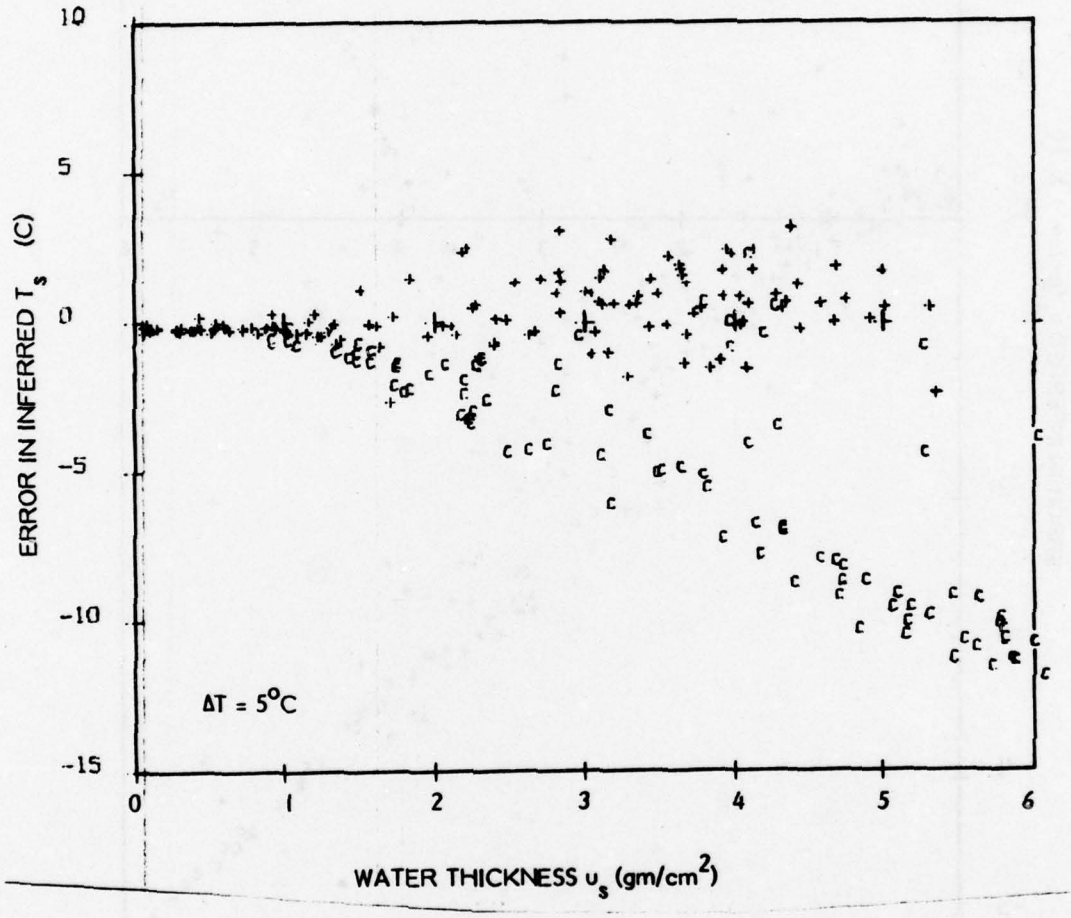

Figure 74 c Errors in Inferred Surface Temperature T_s for $T_s = T_1 + 5^{\circ}C$

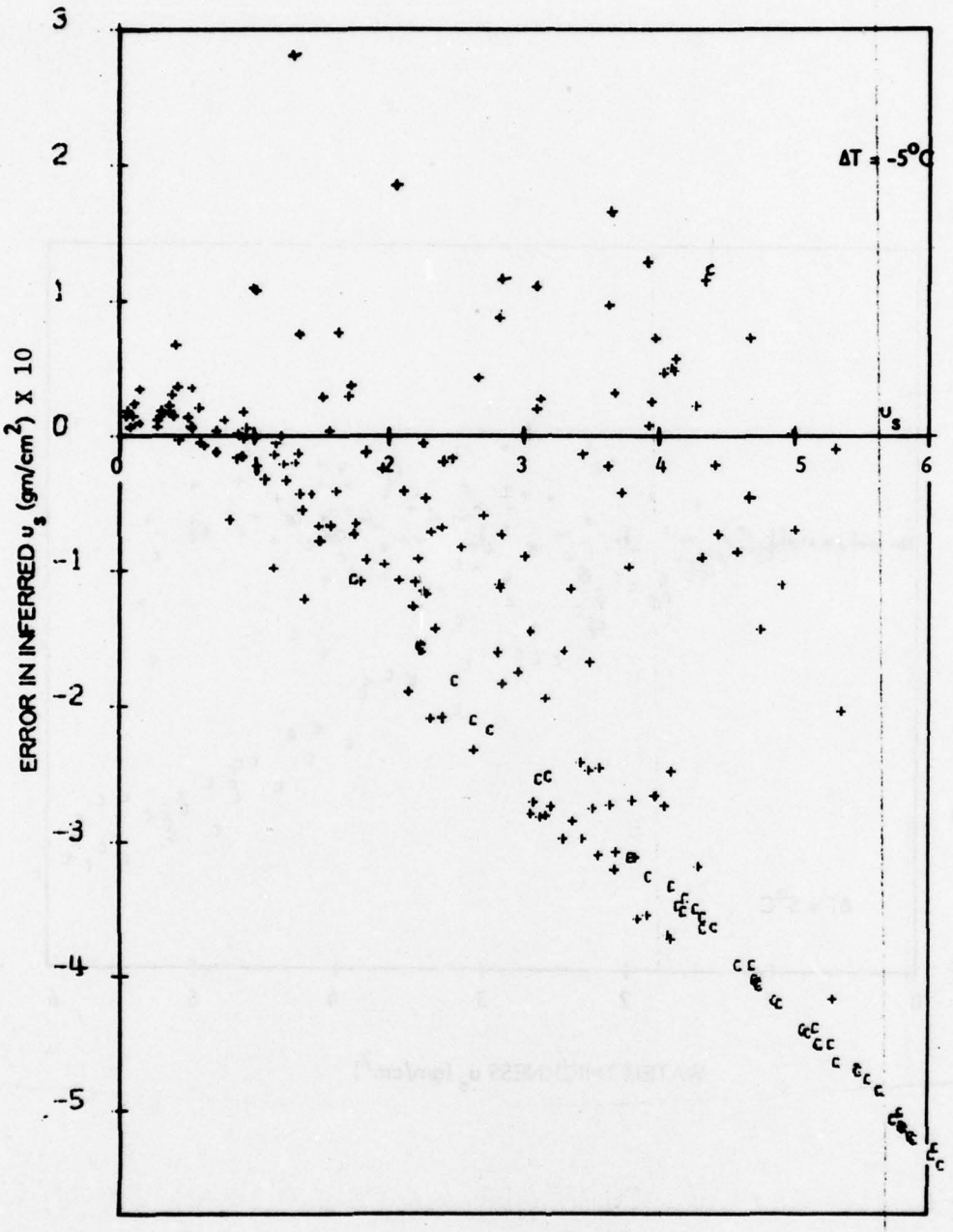

Figure 75a Error in Inferred Precipitable Water for $T_s = T_1 - 5^\circ C$

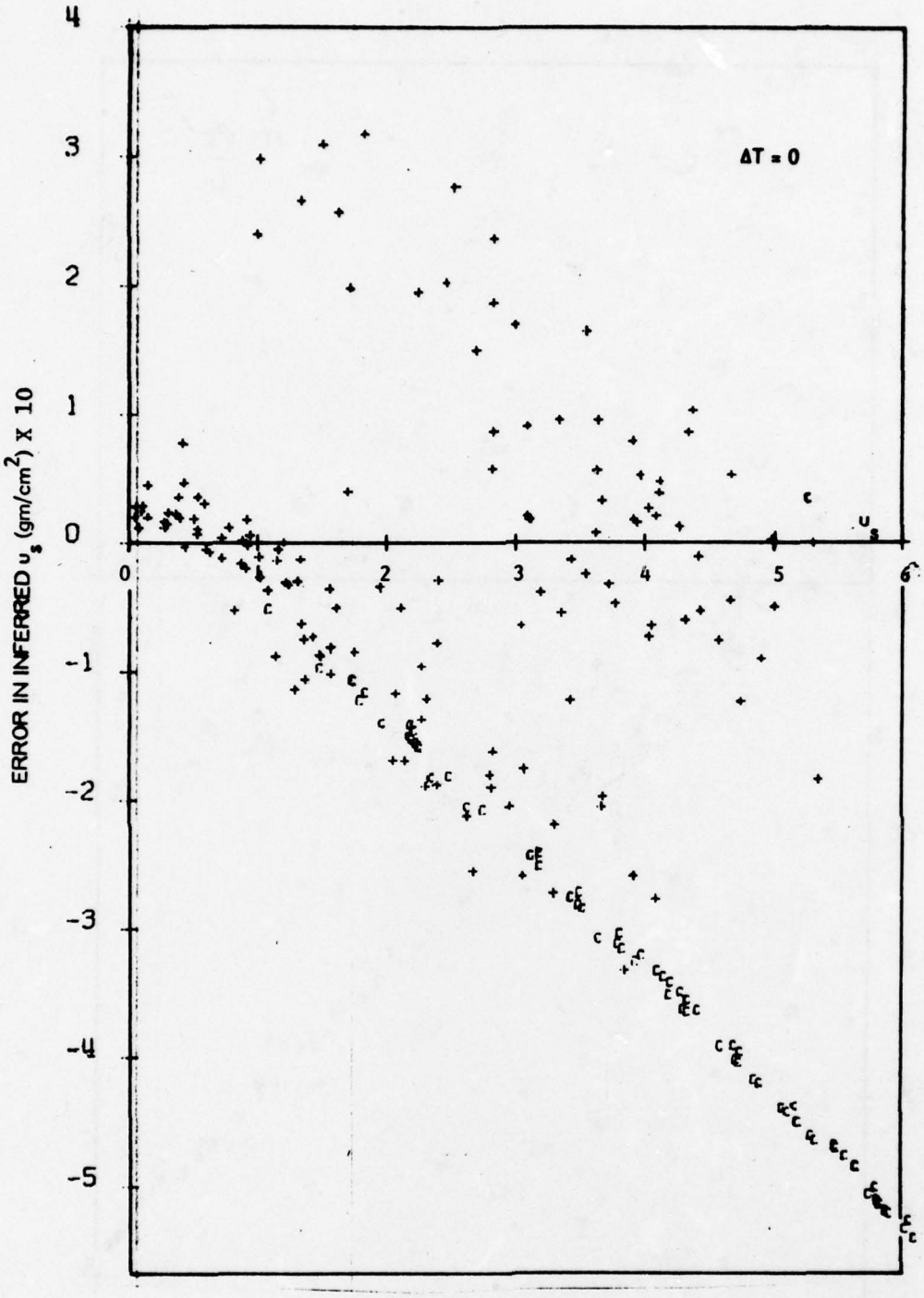

Figure 75b Error in Inferred Precipitable Water u_s for $T_s = T_1$

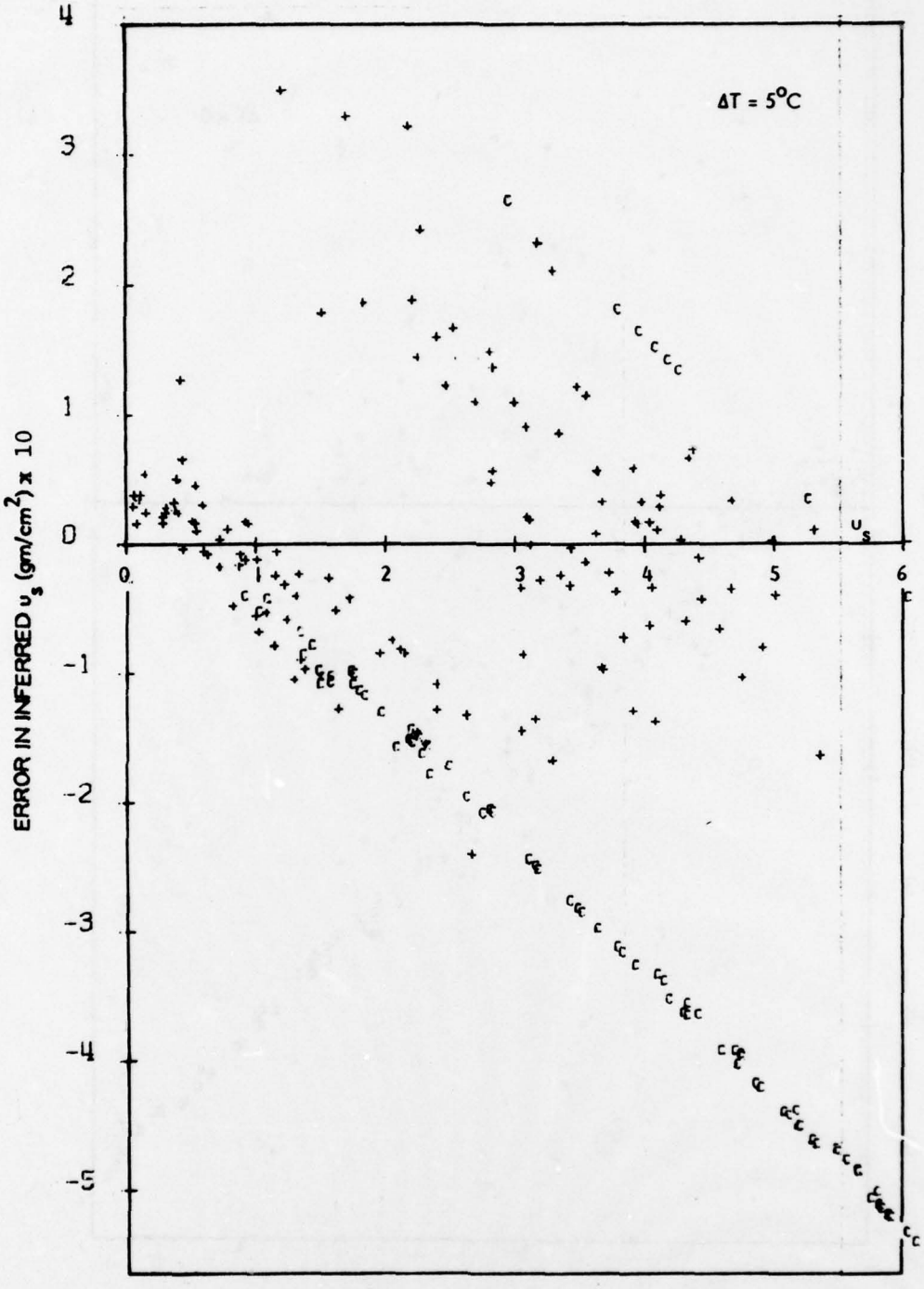

Figure 75c Error in Inferred Precipitable Water u_s When $T_s = T_l + 5^oC$

Table 7 MEAN AND STANDARD DEVIATIONS (STD) OF ERRORS IN T_s AND u_s INFERRED FROM WINDOW CHANNEL RADIANCES

	u_s	0-1	1-2	2-3	3-4	4-5	0-6 (gm/cm^2)
$\Delta T = -5^oC$	No. of Cases*	35	38	33	41	20	171
	Mean T_s Error	-0.23	-0.23	0.05	0.44	1.11	0.19
	STD of Error	0.14	0.52	0.44	0.62	0.75	0.71
	Mean u_s Error	0.10	-0.18	-0.84	-1.61	-0.87	-0.71
	STD of Error	0.21	0.74	0.92	1.55	1.50	1.27
$\Delta T = 0$	No. of Cases*	35	32	27	32	19	148
	Mean T_s Error	-0.22	-0.24	-0.22	0.41	1.10	0.09
	STD of Error	0.14	0.37	0.72	1.15	0.86	0.86
	Mean u_s Error	0.14	0.19	-0.42	-0.64	-0.26	-0.19
	STD of Error	0.22	1.38	1.64	1.33	0.85	1.23
$\Delta T = +5^oC$	No. of Cases*	34	23	22	33	19	134
	Mean T_s Error	-0.20	-0.26	0.61	0.64	0.83	0.27
	STD of Error	0.14	0.72	1.12	1.22	1.05	1.04
	Mean u_s Error	0.21	-0.01	-0.01	-0.20	-0.65	-0.09
	STD of Error	0.30	1.29	1.46	0.92	0.56	0.99

* Number of Cases for which the Actual Precipitable Water is in the Range 0-1 gm/cm^2, 1-2 gm/cm^2, etc. The Table does not include cases for which Eqs. (59) had no solution.

SECTION 4
CONCLUSIONS AND RECOMMENDATIONS

4.1 TEMPERATURE RETRIEVAL CAPABILITY

The study compared the direct, nonlinear, nonstatistical techniques of Smith[1], Chow[2], Fleming[3], a modified version of Twomey's method[4], and two variants of these techniques. Smith's iterative method was judged to give the best temperature retrievals, for this class of retrieval technique.

Smith's method was then compared to the Fleming statistical[3] direct method and two linear inverse methods: the minimum-information method of Foster[6] and Twomey[7], and the full-statistics method of Foster[6] and Strand and Westwater[8]. This four-way comparison produced the following conclusions:

1. The most accurate of the four methods is usually either the full-statistics method or the Fleming statistical method, depending on the climatology represented by the actual profile and assumptions made as to the degree of correlation between the surface temperature and low-level air temperature. From the data available it was not possible to determine the air-surface temperature correlation.

2. When sensitivity to the use of inappropriate statistics and ability to retrieve anomalous profiles are included as factors in the evaluation, the full-statistics method emerges as the best retrieval technique. We refer here to statistics defining the temperature covariances between all atmospheric levels, not just the air-surface covariance.

3. Quite satisfactory temperature retrievals are obtained with either the full-statistics or Fleming statistical methods using only two sets of statistics, one for the tropics and one for extratropical latitudes.

4. For the two best methods, maximum errors in the temperature retrievals below the 70 mb level at extratropical latitudes are approximately 3 to 4 degrees C, when noise in the data is negligible (or effectively suppressed by the regularization parameter values adopted in the study). For the tropics the maximum error below 70 mb is 4 to 5°C and occurs near the tropopause. However, when the tropopause is unusually high or low errors up to 8 or 10 degrees will occur.

4.2 HUMIDITY RETRIEVAL CAPABILITY

The conclusions relative to the capability of DMSP-H to retrieve precipitable water overburden profiles are:

1. Three of the six channels are essentially redundant. The use of channels 1, 2 and 4, at 353 cm^{-1}, 347 cm^{-1} and 408 cm^{-1} yields as much information as all six channels.

2. The channels are too strongly absorbing to infer low-level moisture. Channel 4, the most transparent, becomes opaque when the precipitable water exceeds approximately 1.3 gm/cm^2, which is a typical value for the total water at middle latitudes. In the tropics the total water nearly always exceeds 1.3 gm/cm^2.

3. None of the channels is sufficiently opaque to infer moisture above the 300 mb level in dry artic cases.

4. The full-statistics method appears to give better solutions for the log of the integrated water profile (ln u versus p) than the minimum-information method. The former method is at least able to retrieve ln u values different from the guess at altitudes where the actual u is greater than 1.3 gm/cm^2; this "information" is not really retrieved but comes from the statistics represented by the covariance matrix and the mean profile used for the guess.

5. The ln u profiles retrieved by the full-statistics method retain much of the general shape characteristics of the guess ln u profile. Thus, large errors occur in the retrieved profile when the actual profile differs significantly in shape from the guess profile. However, the retrieved profile is unaffected by simple scaling of the guess profile. Errors in retrieved u below the 300 mb level were less than 30 percent in the best of the cases tested, and of the order of 100 percent in the worst case. It is possible that these errors can be reduced by using mean (guess) profiles and covariance matrices representative of different seasons and climate region as well as latitude.

6. The relative humidity profile corresponding to the retrieved ln u profile tends in many cases to have a large oscillatory component, and bears little resemblance to the actual humidity profile. This is probably due to the fact that the retrievable information is contained in only three channels.

7. The bands at 795 cm^{-1} and 900 cm^{-1} (each of width 20 cm^{-1}) are not sufficiently transparent to be used for accurately determining total precipitable water, although they yield good estimates of surface temperature for middle and high latitudes ($u \leq 2$ gm/cm^2). These bands would be good candidates as sounding channels to replace the redundant DMSP channels.

4.3 RECOMMENDATIONS

The results of this effort suggest that the following study tasks should be pursued in future research aimed at improving the humidity-sensing performance of DMSP:

1. Analyze the performance of DMSP with redefined humidity sensing channels, consisting of the present 353 cm^{-1}, 347 cm^{-1} and 408 cm^{-1} channels in combination with bands of width 5 cm^{-1} or 10 cm^{-1} at 795 cm^{-1} and 900 cm^{-1}, and a sixth band somewhat more opaque than the 353 cm^{-1} channel. The weighting function $-d\tau/d \ln u^*$ of this sixth channel should have a maximum at $u^* \simeq 5 \times 10^{-4}$ gm/cm^2. Consider other proposed combinations of channels in the H_2O rotational band.

2. Analyze humidity sensing performance when the primary sensing channels are selected in the 6.3 μm water band rather than the rotational band. The weaker H_2O continuum in the 6.3 μm region should result in sharper weighting functions.

3. Investigate the use of the two most transparent humidity channels for determining surface temperature. If these bands can determine surface temperature more accurately than the six CO_2 channels, low-level errors in the retrieved temperature profile and corresponding errors in the retrieved ln u profile would be reduced.

4. Study the climatological statistics of water vapor profiles to determine whether distinctly different means and covariances can be constructed according to season, latitude and climate type. More accurate initial guesses and covariance matrices would lead to improved retrieval solutions. If sufficient data is available, determine whether there is a significant correlation between surface temperature and low-level air temperature.

5. Study the statistics of H_2O retrieval errors, with instrument noise effects included, and determine the distribution of errors according to climatological category.

6. Study in detail the relationship between temperature retrieval errors and humidity retrieval (ln u) errors.

7. Study the effects of possible errors in the CO_2 and H_2O transmittance functions.

8. Study the effectiveness of proposed techniques for correcting for partial cloud cover.

REFERENCES

1 W.L. Smith, Appl. Opt. 9, 1993 (1970).

2 M. Halem and M. Chow, J. Appl. Met. 15, 394 (1976).

3 H.E. Fleming, "Status of Mathematical Inversion Techniques", Spring Conference of the Optical Society of America, March 1975, Anaheim, Calif.

4 S. Twomey, J. Computational Phys. 18, 188 (1975) (see Eq. 7, pg 196).

5 J.I.F. King, J. Atmos. Sci. 21, 324 (1964).

6 M.R. Foster, J. Soc. for Industrial and Appl. Math. 9, 387 (1961).

7 S. Twomey, J. Assoc. Comp. Mach. 10, 97 (1963); J. Franklin Inst. 279, 95 (1965).

8 O.N. Straud and E.R. Westwater, J. Assoc. Comp. Mach. 15, 100 (1968).

9 C.D. Rodgers, Quart, J. Roy, Met. Soc. 96, 654 (1970)

10 W.L. Smith, H.M. Woolf and H.E. Fleming, J. Appl. Met. 11, 113 (1972).

11 R.A. McClatchey, Satellite Temperature Sounding of the Atmosphere: Ground Truth Analysis, AFGL-TR-76-0279, November 1976.

12 A.S. Zachor, J. Quant. Spectrosc. Radiat. Transfer 8, 771 (1968)

13 R.A. McClatchey, Personnal Communication

14 R.M. Goody, Atmospheric Radiation, Vol. I (Theoretical Basis), Oxford University Press, London (1964)

15) W.L. Godson, J. Met. 12, 272 and 533 (1955)

APPENDIX A
DERIVATION OF EQUATION 22

We seek the J x M matrix C which best fits the relation

$$\underset{\sim}{\Delta B} = C\underset{\sim}{\Delta I} \quad (\underset{\sim}{B} \equiv \underset{\sim r}{B} ; \underset{\sim}{I} \equiv \underset{\sim r}{I}) \tag{A.1}$$

in the sense of least squares. That is, C should minimize the error

$$\xi(C) = \sum_{j=1}^{J} \sum_{k=1}^{K} \left(\Delta B_{jk} - \sum_{i=1}^{M} C_{ji} \Delta I_{ik} \right)^2 , \tag{A.2}$$

in Eq A.1 when it is applied to the data ensembles $\Delta B_{jk} = B_{jk} - \langle B_j \rangle$, $\Delta I_{ik} = I_{ik} - \langle I_i \rangle$. The k^{th} columns of the matrices ΔB and ΔI correspond to a particular ensemble member, and represent the departure from a mean Planck radiance profile (at the reference frequency r) and the corresponding departures from the mean channel radiances.

The solution for C is obtained from the normal equations $d\xi/dC_{nm} = 0$:

$$0 = \frac{d\xi}{dC_{nm}} = 2 \sum_{k=1}^{K} \Delta I_{mk} \left(\Delta B_{nk} - \sum_{i=1}^{M} C_{ni} \Delta I_{ik} \right)$$

or,

$$0 = \sum_{k=1}^{K} \Delta B_{nk} \Delta I_{mk} - \sum_{i=1}^{M} C_{ni} \left(\sum_{k=1}^{K} \Delta I_{ik} \Delta I_{mk} \right)$$

$$= \Delta B(\Delta I)^T - C(\Delta I)(\Delta I)^T . \tag{A.3}$$

Solving for C we obtain

$$C = \Delta B(\Delta I)^T \left[\Delta I(\Delta I)^T \right]^{-1} \tag{A.4}$$

Equations A.1 and A.4 represent a linear regression solution for $\underset{\sim}{\Delta B}$. Note that the radiative transfer equation has not been used if both ΔI and ΔB are measured data.

The vectors $\underset{\sim}{\Delta I}$ and $\underset{\sim}{\Delta B}$ are related by the radiative transfer equation, as are the data ensembles ΔI and ΔB. If we acknowledge that the elements ΔI_{ik} contain noise E_{ik}, the relationship is

$$\Delta I = W(\Delta B) + E \ . \qquad \text{(A.5)}$$

Thus,

$$[\Delta I(\Delta I)^T]_{im} = \sum_{k=1}^{K}\left(\sum_{j=1}^{J} W_{ij}\,\Delta B_{jk} + E_{ik}\right)\left(\sum_{j=1}^{J} W_{mj}\,\Delta B_{jk} + E_{mk}\right)$$

$$= \sum_{\ell} W_{i\ell} \sum_{j}\left(\sum_{k} \Delta B_{\ell k}\,\Delta B_{jk}\right) W_{mj} + \sum_{k} E_{ik}\,E_{mk} \ , \qquad \text{(A.6)}$$

from which

$$\Delta I(\Delta I)^T = W[\Delta B(\Delta B)^T]W^T + EE^T \ . \qquad \text{(A.7)}$$

Equations A.6 and A.7 assume that E is uncorrelated with $\underset{\sim}{\Delta B}$, and that the E_{ik} are random with zero mean. We can show similarly that

$$\Delta B(\Delta I)^T = [\Delta B(\Delta B)^T]W^T . \qquad \text{(A.8)}$$

According to the second assumption stated above, EE^T is $(K-1)S_E$, where S_E is the covariance matrix of E. Also, $\Delta B(\Delta B)^T$ is $(K-1)S$, where S is the covariance matrix of B. Using these definitions, and substituting A.7 and A.8 into A.4, we find that

$$C = SW^T\left[WSW^T + S_E\right]^{-1} \qquad \text{(A.9)}$$

Equations A.9 and A.1 yield Equation 22 in Section 2.2.2.

APPENDIX B

AVERAGE WEIGHTING FUNCTIONS FOR THE DMSP TEMPERATURE SENSING CHANNELS, AND EMPIRICAL FUNCTIONS $\tilde{\tau}(\upsilon_s)$, $\tilde{N}(\upsilon_s)$ FOR THE WINDOW CHANNELS AT 795 AND 900 cm^{-1}

Table B-1 CHANNEL WEIGHTING FUNCTIONS*

Pressure (mb)	Channel 1 (668)	2 (676)	3 (695)	4 (707)	5 (727)	6 (747 cm^{-1})
.100	0.	0.	0.	0.	0.	0.
.154	.4083E-02	.1520E-02	.4486E-03	.6295E-04	.1857E-04	.1065E-03
.225	.9827E-02	.1957E-02	.6519E-03	.9733E-04	.3692E-04	.1339E-03
.317	.1176E-01	.2104E-02	.8407E-03	.1334E-03	.5376E-04	.1599E-03
.434	.1268E-01	.1974E-02	.1114E-02	.2046E-03	.6673E-04	.1688E-03
.579	.1382E-01	.2034E-02	.1508E-02	.3222E-03	.9046E-04	.1694E-03
.755	.1521E-01	.2552E-02	.2096E-02	.5141E-03	.1615E-03	.1670E-03
.966	.1641E-01	.3289E-02	.2693E-02	.7428E-03	.2531E-03	.1770E-03
1.217	.1714E-01	.4007E-02	.3117E-02	.9575E-03	.3667E-03	.2028E-03
1.511	.1768E-01	.4701E-02	.3467E-02	.1199E-02	.5046E-03	.2316E-03
1.852	.1799E-01	.5408E-02	.3677E-02	.1404E-02	.6751E-03	.2680E-03
2.246	.1814E-01	.6181E-02	.3802E-02	.1581E-02	.8658E-03	.3076E-03
2.696	.1821E-01	.7003E-02	.3903E-02	.1706E-02	.1055E-02	.3533E-03
3.206	.1829E-01	.7867E-02	.4032E-02	.1809E-02	.1247E-02	.4016E-03
3.782	.1849E-01	.8849E-02	.4256E-02	.1917E-02	.1449E-02	.4585E-03
4.429	.1880E-01	.9853E-02	.4524E-02	.2034E-02	.1644E-02	.5112E-03
5.151	.1918E-01	.1084E-01	.4814E-02	.2163E-02	.1811E-02	.5527E-03
5.954	.1969E-01	.1191E-01	.5170E-02	.2338E-02	.1988E-02	.5990E-03
6.842	.2022E-01	.1293E-01	.5539E-02	.2530E-02	.2154E-02	.6421E-03
7.821	.2083E-01	.1409E-01	.5949E-02	.2765E-02	.2325E-02	.6837E-03
8.896	.2140E-01	.1518E-01	.6357E-02	.2997E-02	.2483E-02	.7155E-03
10.073	.2190E-01	.1623E-01	.6744E-02	.3212E-02	.2630E-02	.7396E-03
11.346	.2228E-01	.1741E-01	.7231E-02	.3455E-02	.2807E-02	.7581E-03
12.753	.2254E-01	.1859E-01	.7747E-02	.3700E-02	.2994E-02	.7727E-03
14.268	.2264E-01	.1980E-01	.8310E-02	.3947E-02	.3192E-02	.7843E-03
15.908	.2268E-01	.2106E-01	.8931E-02	.4212E-02	.3403E-02	.7992E-03
17.678	.2260E-01	.2211E-01	.9557E-02	.4451E-02	.3591E-02	.8216E-03
19.584	.2249E-01	.2312E-01	.1020E-01	.4689E-02	.3778E-02	.8486E-03
21.633	.2231E-01	.2411E-01	.1090E-01	.4935E-02	.3961E-02	.8816E-03
23.831	.2208E-01	.2509E-01	.1168E-01	.5187E-02	.4143E-02	.9223E-03
26.184	.2184E-01	.2601E-01	.1248E-01	.5435E-02	.4316E-02	.9646E-03
28.698	.2153E-01	.2686E-01	.1332E-01	.5665E-02	.4465E-02	.1015E-02
31.380	.2116E-01	.2757E-01	.1416E-01	.5865E-02	.4584E-02	.1069E-02
34.236	.2077E-01	.2810E-01	.1492E-01	.6034E-02	.4676E-02	.1122E-02
37.273	.2038E-01	.2851E-01	.1561E-01	.6184E-02	.4755E-02	.1174E-02
40.499	.1996E-01	.2878E-01	.1624E-01	.6319E-02	.4821E-02	.1228E-02
43.918	.1953E-01	.2890E-01	.1673E-01	.6411E-02	.4858E-02	.1267E-02
47.540	.1910E-01	.2899E-01	.1721E-01	.6505E-02	.4895E-02	.1306E-02
51.369	.1858E-01	.2890E-01	.1766E-01	.6623E-02	.4939E-02	.1353E-02
55.414	.1796E-01	.2852E-01	.1801E-01	.6753E-02	.4982E-02	.1400E-02
59.682	.1732E-01	.2804E-01	.1825E-01	.6867E-02	.5015E-02	.1441E-02
64.179	.1669E-01	.2754E-01	.1850E-01	.6974E-02	.5044E-02	.1481E-02
68.913	.1606E-01	.2703E-01	.1873E-01	.7080E-02	.5074E-02	.1520E-02
73.892	.1530E-01	.2624E-01	.1900E-01	.7303E-02	.5161E-02	.1595E-02
79.122	.1447E-01	.2530E-01	.1929E-01	.7581E-02	.5275E-02	.1688E-02
84.612	.1359E-01	.2422E-01	.1962E-01	.7936E-02	.5432E-02	.1803E-02
90.369	.1272E-01	.2315E-01	.1996E-01	.8291E-02	.5590E-02	.1917E-02
96.399	.1187E-01	.2210E-01	.2029E-01	.8644E-02	.5747E-02	.2031E-02

* Entries are $[(\tau(p_{j+1}) - \tau(p_{j-1}))]/2$; Last row is total transmittance $\tau(p_o)$.

Table B-1 CHANNEL WEIGHTING FUNCTIONS (Continued)

Pressure (mb)	Channel 1 (668)	2 (676)	3 (695)	4 (707)	5 (727)	6 (747 cm^{-1})
102.713	.1101E-01	.2094E-01	.2065E-01	.9135E-02	.5965E-02	.2198E-02
109.315	.1013E-01	.1958E-01	.2099E-01	.9823E-02	.6267E-02	.2442E-02
116.216	.9249E-02	.1817E-01	.2133E-01	.1055E-01	.6585E-02	.2703E-02
123.423	.8374E-02	.1674E-01	.2166E-01	.1131E-01	.6913E-02	.2974E-02
130.943	.7537E-02	.1537E-01	.2197E-01	.1204E-01	.7230E-02	.3242E-02
138.785	.6768E-02	.1409E-01	.2222E-01	.1277E-01	.7535E-02	.3514E-02
146.956	.6022E-02	.1282E-01	.2243E-01	.1349E-01	.7838E-02	.3791E-02
155.466	.5261E-02	.1139E-01	.2249E-01	.1442E-01	.8226E-02	.4173E-02
164.322	.4526E-02	.9897E-02	.2237E-01	.1552E-01	.8678E-02	.4648E-02
173.532	.3810E-02	.8429E-02	.2224E-01	.1661E-01	.9127E-02	.5125E-02
183.106	.3244E-02	.7218E-02	.2196E-01	.1759E-01	.9552E-02	.5596E-02
193.051	.2738E-02	.6099E-02	.2158E-01	.1855E-01	.9982E-02	.6089E-02
203.376	.2313E-02	.5117E-02	.2112E-01	.1949E-01	.1041E-01	.6603E-02
214.089	.1984E-02	.4309E-02	.2050E-01	.2041E-01	.1085E-01	.7164E-02
225.200	.1702E-02	.3583E-02	.1979E-01	.2129E-01	.1129E-01	.7734E-02
236.717	.1431E-02	.2883E-02	.1907E-01	.2214E-01	.1173E-01	.8298E-02
248.648	.1195E-02	.2263E-02	.1831E-01	.2289E-01	.1214E-01	.8834E-02
261.002	.1022E-02	.1798E-02	.1739E-01	.2353E-01	.1260E-01	.9432E-02
273.789	.8672E-03	.1373E-02	.1644E-01	.2417E-01	.1308E-01	.1005E-01
287.018	.7306E-03	.9898E-03	.1546E-01	.2483E-01	.1361E-01	.1072E-01
300.697	.6247E-03	.6879E-03	.1442E-01	.2539E-01	.1418E-01	.1142E-01
314.835	.5722E-03	.5281E-03	.1325E-01	.2554E-01	.1474E-01	.1214E-01
329.441	.5346E-03	.4099E-03	.1209E-01	.2567E-01	.1532E-01	.1287E-01
344.526	.4998E-03	.3033E-03	.1092E-01	.2569E-01	.1588E-01	.1358E-01
360.097	.4690E-03	.2104E-03	.9786E-02	.2562E-01	.1643E-01	.1427E-01
376.165	.4415E-03	.1297E-03	.8676E-02	.2545E-01	.1695E-01	.1495E-01
392.738	.4209E-03	.7409E-04	.7613E-02	.2506E-01	.1742E-01	.1561E-01
409.827	.4055E-03	.3749E-04	.6586E-02	.2442E-01	.1787E-01	.1629E-01
427.440	.3974E-03	.2753E-04	.5634E-02	.2349E-01	.1824E-01	.1694E-01
445.587	.3894E-03	.1922E-04	.4715E-02	.2251E-01	.1859E-01	.1757E-01
464.279	.3814E-03	.1176E-04	.3853E-02	.2145E-01	.1892E-01	.1817E-01
483.523	.3738E-03	.5686E-05	.3062E-02	.2032E-01	.1923E-01	.1873E-01
503.331	.3666E-03	.1487E-05	.2386E-02	.1911E-01	.1953E-01	.1924E-01
523.711	.3616E-03	.9076E-06	.1947E-02	.1785E-01	.1973E-01	.1971E-01
544.675	.3569E-03	.5923E-06	.1545E-02	.1659E-01	.1993E-01	.2019E-01
566.231	.3526E-03	.4138E-06	.1221E-02	.1531E-01	.2008E-01	.2065E-01
588.389	.3488E-03	.2744E-06	.9364E-03	.1401E-01	.2022E-01	.2115E-01
611.160	.3447E-03	.1412E-06	.6679E-03	.1270E-01	.2032E-01	.2162E-01
634.554	.3403E-03	.3823E-07	.4793E-03	.1149E-01	.2028E-01	.2196E-01
658.580	.3429E-03	.2584E-07	.3581E-03	.1034E-01	.2038E-01	.2271E-01
683.250	.3462E-03	.1392E-07	.2505E-03	.9258E-02	.2049E-01	.2348E-01
708.572	.3540E-03	.3968E-08	.1542E-03	.8212E-02	.2070E-01	.2455E-01
734.558	.3745E-03	.1778E-08	.1051E-03	.7225E-02	.2105E-01	.2633E-01
761.217	.4029E-03	.9588E-09	.6641E-04	.6301E-02	.2158E-01	.2856E-01
788.561	.4451E-03	.4016E-09	.3693E-04	.5504E-02	.2282E-01	.3234E-01
816.598	.5048E-03	.9328E-10	.1917E-04	.4821E-02	.2375E-01	.3570E-01
845.341	.5405E-03	.6257E-10	.1332E-04	.4250E-02	.2451E-01	.3907E-01
874.800	.6215E-03	.3331E-10	.9115E-05	.3804E-02	.2470E-01	.4175E-01
904.984	.6388E-03	.5292E-11	.3544E-05	.3453E-02	.2374E-01	.4158E-01
935.905	.6230E-03	.2577E-11	.2432E-05	.2415E-02	.2190E-01	.3913E-01
967.574	.5458E-03	.1606E-11	.1663E-05	.1928E-02	.1950E-01	.3553E-01
1000.000	.5094E-03	.9240E-13	.6398E-06	.1339E-02	.1567E-01	.2932E-01
1000.000	.2116E-02	.1439E-14	.2237E-06	.2449E-02	.4499E-01	.9664E-01

Table B-2
THE EMPIRICAL FUNCTIONS $\tilde{\tau}_i(u_s)$ AND $\tilde{N}(u_s)$

0.	.500E-01	.100E+00	.150E+00	.200E+00	.250E+00	.300E+00	.350E+00
.400E+00	.450E+00	.500E+00	.550E+00	.600E+00	.650E+00	.700E+00	.750E+00
.800E+00	.900E+00	.100E+01	.110E+01	.120E+01	.130E+01	.140E+01	.150E+01
.160E+01	.170E+01	.180E+01	.190E+01	.200E+01	.210E+01	.220E+01	.230E+01
.240E+01	.250E+01	.260E+01	.270E+01	.280E+01	.290E+01	.300E+01	.310E+01
.320E+01	.330E+01	.340E+01	.350E+01	.360E+01	.370E+01	.380E+01	.390E+01
.400E+01	.410E+01	.420E+01	.430E+01	.440E+01	.450E+01	.460E+01	.470E+01
.480E+01	.490E+01	.500E+01	.510E+01	.520E+01	.530E+01	.540E+01	.550E+01
.560E+01							

u_s (gm/cm^2)

1.0000	.9860	.9720	.9585	.9450	.9315	.9180	.9050
.8925	.8800	.8680	.8560	.8443	.8325	.8210	.8096
.7980	.7750	.7510	.7280	.7070	.6850	.6630	.6410
.6200	.6000	.5800	.5600	.5420	.5230	.5050	.4880
.4700	.4540	.4380	.4210	.4060	.3900	.3750	.3590
.3450	.3300	.3150	.3020	.2890	.2760	.2630	.2510
.2390	.2280	.2175	.2070	.1980	.1890	.1800	.1730
.1650	.1590	.1520	.1460	.1400	.1350	.1300	.1260
.1220							

$\tilde{\tau}_1(u_s)$ (ν = 795 cm^{-1}, $\Delta\nu$ = 20 cm^{-1})

1.0000	.9985	.9964	.9937	.9907	.9873	.9836	.9797
.9756	.9714	.9668	.9623	.9575	.9527	.9479	.9429
.9380	.9280	.9150	.9020	.8880	.8750	.8610	.8470
.8330	.8190	.8050	.7910	.7780	.7640	.7500	.7350
.7220	.7080	.6940	.6800	.6660	.6530	.6390	.6250
.6110	.5970	.5830	.5700	.5560	.5425	.5290	.5160
.5040	.4910	.4790	.4670	.4550	.4440	.4330	.4230
.4120	.4020	.3930	.3940	.3750	.3660	.3590	.3510
.3450							

$\tilde{\tau}_2(u_s)$ (ν = 900 cm^{-1}, $\Delta\nu$ = 20 cm^{-1})

0.	.450E-07	.140E-06	.220E-06	.310E-06	.400E-06	.500E-06	.602E-06
.709E-06	.820E-06	.930E-06	.105E-05	.117E-05	.129E-05	.142E-05	.154E-05
.167E-05	.194E-05	.221E-05	.250E-05	.279E-05	.305E-05	.331E-05	.360E-05
.385E-05	.410E-05	.437E-05	.461E-05	.488E-05	.510E-05	.534E-05	.557E-05
.579E-05	.600E-05	.621E-05	.642E-05	.661E-05	.680E-05	.700E-05	.719E-05
.736E-05	.752E-05	.768E-05	.784E-05	.799E-05	.812E-05	.826E-05	.839E-05
.851E-05	.862E-05	.873E-05	.884E-05	.894E-05	.904E-05	.914E-05	.921E-05
.930E-05	.938E-05	.945E-05	.951E-05	.959E-05	.964E-05	.970E-05	.975E-05
.980E-05							

$\tilde{N}_1(u_s)$ (ν = 795 cm^{-1}, $\Delta\nu$ = 20 cm^{-1})

0.	.500E-08	.150E-07	.300E-07	.470E-07	.625E-07	.910E-07	.118E-06
.147E-06	.178E-06	.210E-06	.245E-06	.280E-06	.320E-06	.360E-06	.400E-06
.446E-06	.530E-06	.640E-06	.750E-06	.890E-06	.103E-05	.118E-05	.132E-05
.149E-05	.163E-05	.180E-05	.195E-05	.210E-05	.226E-05	.240E-05	.257E-05
.270E-05	.286E-05	.300E-05	.316E-05	.330E-05	.344E-05	.359E-05	.373E-05
.387E-05	.400E-05	.415E-05	.429E-05	.441E-05	.455E-05	.469E-05	.480E-05
.493E-05	.503E-05	.518E-05	.529E-05	.540E-05	.551E-05	.562E-05	.573E-05
.584E-05	.594E-05	.604E-05	.613E-05	.623E-05	.631E-05	.640E-05	.650E-05
.658E-05							

$\tilde{N}_2(u_s)$ (ν = 900 cm^{-1}, $\Delta\nu$ = 20 cm^{-1})